CRANFIELD UNIVERSITY

Mr Andrew Roberts

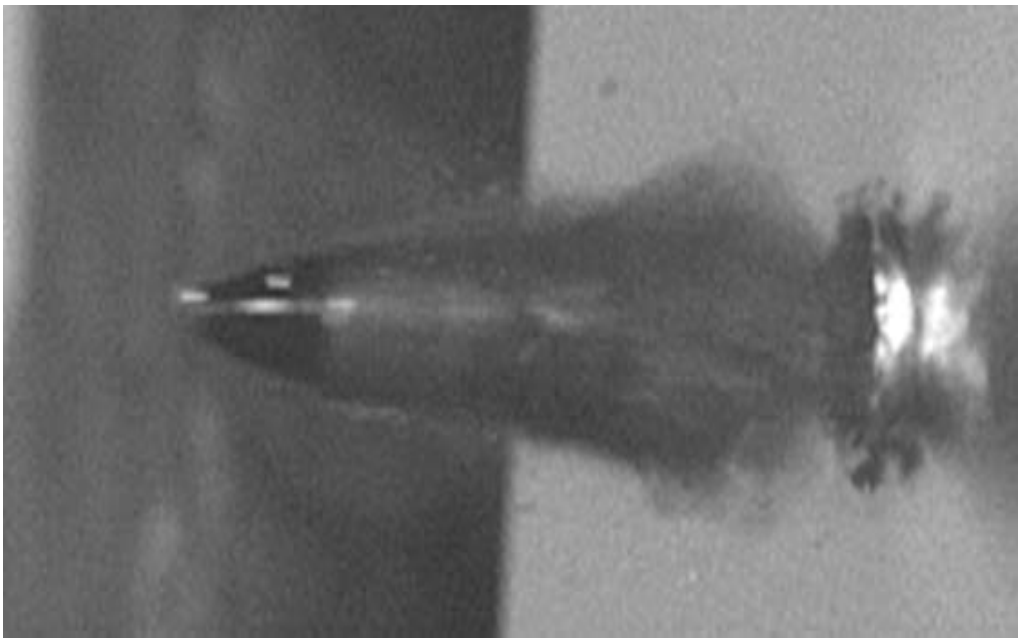

Optimisation of small arms defeat via dynamic jacket removal

Cranfield Defence and Security

Submitted in partial fulfilment of the requirement for the degree of

MSc by research

October 2014 – October 2016

Supervisor – Dr Gareth Appleby-Thomas

[Intentionally left blank]

[Intentionally left blank]

[Intentionally left blank]

Abstract

The majorities of studies into penetration by small arms have neglected the contribution of the jacket to the penetration event due to its small mass compared to the rest of the bullet. Recent research has suggested that the jacket does actually play a measurable role in the penetration of a target. This project has focused on the concept of dynamic jacket removal as an approach to optimise small arms defeat. This approach was envisaged to address the gap in current knowledge with regards to the role of the bullet jacket in the penetration of a target. Here, jacket stripping techniques were employed, elucidating underling mechanisms where armour piercing (AP) rounds were fired at target materials. Forward ballistic experiments were conducted, utilising conventional ballistic testing on an indoor small arms range as well as 30 mm and 50 mm smooth bore single stage light gas guns. To compliment this work, reverse ballistic experimentation was also undertaken on a 50 mm single stage light gas gun. Impact events were interrogated via a series of diagnostics including high speed video imaging, flash X ray radiography and depth of penetration testing. Experimental results were complimentary, providing insight into two key competing effects with regards to the jacket on penetration. These were the potential for the jacket to cushion / damp the impact, as well as the physical confinement resulting from the presence of the jacket itself around the bullet core. Further, these experiments also identified a potential optimum in terms of stripping plate design. In addition, to further investigate the role of the bullet jacket, sample cores and jacket materials were loaded both together and in isolation using a split Hopkinson pressure bar, with results in particular highlighting the cushioning effect of the jacket material. Limited numerical simulations were also produced using Ansys® Autodyn. These numerical results further elucidated the experimental work – again highlighting the importance of the jacket in terms of cushioning the impact event / reducing the subsequent pre-loading of the penetrating AP core.

Overall, both experimental and numerical results showed that the bullet jacket does indeed aid in penetration. In corollary, in practical terms, jacket removal has the potential to aid in armour performance – with the experiments conducted herein providing insight into dynamic jacket removal. In terms of such stripping mechanisms, it was demonstrated that a plate thickness comparable to the calibre of the bullet appeared optimal. Further, results have also shown the importance of hardness and other material properties when considering the final defeat of an incident projectile through spallation.

Key words

Armour piercing, FFV, bullet jacket, depth of penetration, forward ballistics, reverse ballistics, gas gun, split Hopkinson pressure bar, WC-Co core, spallation, flash X ray radiography, Copper C101, mild Steel EN3B, Aluminium AL6082 T651, CFRP

Acknowledgements

Firstly I would like to take the opportunity to thank Dr Gareth Appleby-Thomas and Dr David Wood for their help and guidance throughout this project and during the writing of this thesis. A huge ‘thanks’ goes to Brianna Fitzmaurice for the expert assistance and help with the computational modelling. Also to the rest of the staff / students of the Dynamic response group for putting up with the ‘closed door Friday’ rule I enforced during this MSc.

I would also like to thank Mike Teagle and David Miller for all of the help and support during the forward ballistic firings undertaken on the small arms range. I would also like to say thank you to Adrian Mustey for setting aside some time for me for material testing at the busiest time of year.

‘Thank you’ via air mail, also goes to Ian Crouch of RMIT (Brunswick, Australia), for collaborative work and advice during the experimental programs.

Finally I would like to thank my wife, Tina Roberts and my daughters, Paige and Keira, who have over the last two years, with many a blank face, have managed to put up with me trying to explain to them the complexities of ballistic penetration!

Table of Contents

List of Figures

List of Tables

List of Equations

List of Abbreviations

AL	Aluminium
AP	Armour piercing
CFRP	Carbon fibre reinforced plastic
CU	Copper
DOP	Depth of penetration
FFV	Forenade fabriksverken (United manufacturers)
GPa	Gigapascals
HSV	High speed video
HV	Vickers hardness
He	Helium
mm	Millimetres
SAER	Small arms experimental range
SHPB	Split Hopkinson Pressure Bar
SiC	Silicon Carbide
WC-Co	Tungsten Carbide - Cobalt

1.0 Introduction and literature review

This thesis has been split into several sections with the aim of addressing the underlying research question – namely the optimisation of dynamic jacket removal during penetration. Theses sections comprise of an initial overview of the area (a literature survey); materials employed (characterisation / rationale for choice); experimental approaches; results and discussions, and; conclusions. The current section is designed to give the reader a rounded background in the development of armour systems and threats throughout the ages, culminating with modern day solutions in both fields. A detailed survey of the literature is then presented to evaluate work (or lack there-of) in the fields of this study.

1.1 Armour systems – background

Armour systems are designed to provide protection. They fall into two categories; 1) Natural armour and; 2) Man made armour. Natural armour includes hard shells found on crustaceans and gastropods, and the toughened carapaces of insects. These structures have evolved to protect the soft tissues / organs of those creatures that live inside them.

Man-made armour protection systems date back to at least 3000 BC. For example, Laible and Barron [1] stated that the use of organic fibres such as silk, wool and cotton layered with metal plates forming a composite structure, has been traced back to 1292 – 1255 BC. Body armours have been made from materials ranging from quilted fabrics and bronze plates to armour worn by medieval knights comprising of flexible coats of chain mail rings and Steel plates. In general, armour materials have been selected to be either strong / resistant to impact (hardened) or flexible (tough) to absorb and dissipate energy from incident projectiles. Along these lines, armour systems developed in some countries have even included fabrics soaked in brine (to harden the material), crocodile skin and corselets made of wood or bamboo (figure 1.1)

Figure 1.1 – Examples of ancient armour design [2][3].

In the last 100 years personal and vehicle armour systems have developed greatly due to conflict, the occurrence of two World Wars and the development of better small arms rounds and general munitions. This process of armour evolving alongside the existential threat is a consistent theme throughout armour development.

1.1.1 Homogeneous Armour

Vehicles have traditionally employed a homogenous armour system, comprising of a single element. A wide variety of armour materials have been utilised, ranging from ceramic [4] to composite [27]. However, very-many homogeneous solutions comprise metallic materials, in particular due to their ability to also act as structural elements. Aluminium alloys have come to the fore in this area, for example, Al 5083 H32 [5] which is used on the M113 APC (armoured personnel carrier), with the solution employed possessing a single armour layer that varies between 12 mm to 38 mm thick (see figure 1.2 below).

Figure 1.2 – M113 APC [6].

Aluminium alloys are also widely used in the transport and aerospace industries. Their application in these roles is largely due to the fact that they offer a combination of lightness, stiffness and strength (e.g. high specific strength), along with good corrosion resistance. Given the costs inherent in heavier armour solutions in terms of logistics (e.g. higher fuel / transportation costs), as well as the inevitable drive to defeat more effective modern munitions, there is an increasing need for these properties to be apparent in modern day armour solutions.

In an example of recent research using an armour-relevant alloy, Manes *et al*. [7] used a 6061 – T6 Aluminium alloy for ballistic testing, employing armour piercing (AP) projectiles with Steel and Tungsten Carbide cores, respectively. These were fired from a conventional gun using a laser system to record the velocity and a high speed video (HSV) camera to interrogate the impact event. The researchers tested Al plates of 3 different thicknesses; 25 mm, 101.6 mm (4 inches), and finally; 76.2 mm (3 inches), recording depth-of-penetration (DOP).

The authors found that recorded DOPs matched with the modelled data and concluded that, when a hard bullet impacts a ductile material like Al, the extra mass of the sabot arrests the whole bullet in the penetration path. This issue arose because sub-calibre bullets were employed which therefore required sabots which constrained the round during the initial stages of the penetration process, reducing the ability of the bullet to penetrate the target. While they also highlighted the relative paucity of data in this area, they did suggest that Al could be employed as a first layer in a multi-layer system where jacket removal is necessary – a conclusion which is in-line with the aims of this study. Radin *et al*. [8] also used Al plates in a series of tests, but in thin layers, combined with thin plates of Polycarbonate (PC) – something closer to a composite solution – as opposed to the thicker plates used in Ref. [7]. These constructs were impacted with hardened Steel projectiles fired from a light gas gun [9]. They found that by having the PC filling the gap between the layers of Al, the ballistic performance of the system was increased by 10%. They also noted the importance of a multi-layer sequence, finding that if the system was fronted with the Al plate its performance improved. They postulated that this was due to the way the Al deforms under impact, e.g. as to whether it craters or petals.

High strength Steels are also commonly employed as homogeneous armour solutions. During and just after WWII, Steel armour was used to protect heavy fighting vehicles. Among these

the Soviet KV tank of 1941 employed Steel armour plates 75-mm thick, while in 1944 the German King Tiger tank had armour plates of 150-mm thickness on its hull. Interestingly, these plates were flame hardened, forming Martensite on the outer layers and giving a dual hardness characteristic to the armour, making it less a single hardness homogeneous armour [10]. The King Tiger tank (see figure 1.3) also had plates of 185-mm thickness on the front of the turret [11], with the position of this thicker armour indicative of the perceived orientation of likely threats (consistent with approaches such as Whittaker's threat assessment for armoured vehicles [4]). In contrast, in the modern day environment, off-route threats such as explosively formed projectiles (EFPs) make it more challenging to choose which areas of a vehicle to up-armour.

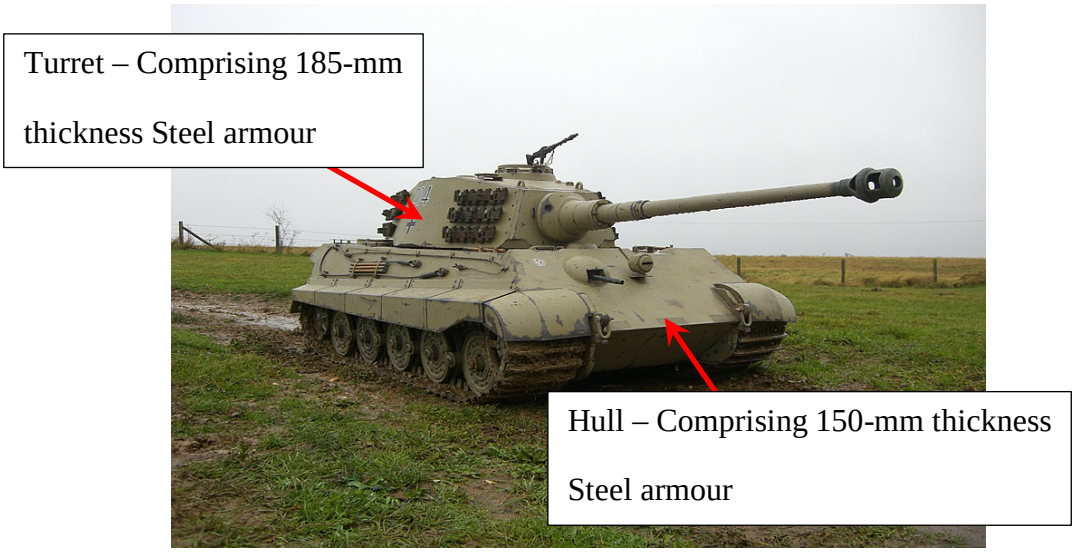

Figure 1.3 – World War 2 German King Tiger tank [12].

In a recent study, Kilic *et al*. [13] used AP projectiles to test the ballistic resistance of high hardness Steel. The projectiles employed had hardened Steel cores and were of type 7.62 mm 54R B32 API; these were fired at a velocity of 854 m/s ± 20 m/s from an experimental gun on an indoor range. The velocity was recorded on a HSV camera. Penetration depth into the Steel target had been predicted using three-dimensional numerical simulation. To be able to successfully model the materials behaviour (e.g. to provide baseline materials information), Kilic *et al*. ran a series of tests on the Steel targets and the hardened core

material which included hardness testing, tensile testing, stress and strain tests. Usefully, they found that the depth of penetration results matched that of the modelled data.

This corresponds with work by Borvic *et al*. [14] where 7.62 mm Ball and 7.62 mm Armour piercing ammunition was fired at five different high strength Steel plates. A linear increase in perforation resistance with yield stress for both projectile types was noted.

As demonstrated by the studies reviewed above, it is apparent that Steel makes a good armour material in greater thicknesses due to its higher tensile strengths. This works well on powerful vehicles that are able to move the excess weight around, such as tanks. For smaller vehicles or indeed personal armour, where lower mass solutions are required, layered Steel plates combined with other materials have been used.

1.1.2 Milne de Marre

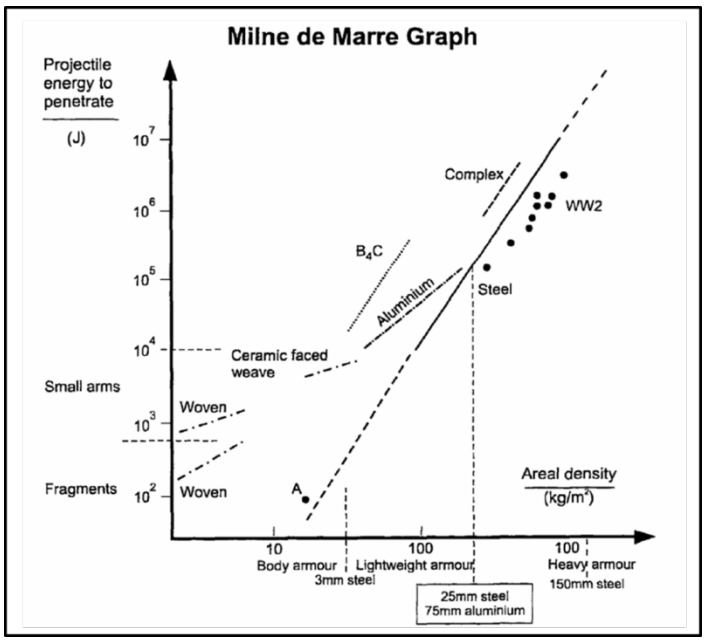

Figure 1.4 – Milne de Marre graph [10].

The performance of Steel armours against Aluminium armours can be examined via the Milne de Marre relationship, shown graphically in figure 1.4. For reference, the Milne de

Marre equation takes the general form shown below for a cylindrical impactor (e.g. neglecting a bullets ogive nose) of diameter ‘d’ and mass ‘m’ impacting a target of thickness ‘t’ at ‘v’ m/s.

$$\frac{mv^2}{d^3} = k\left[\frac{t}{d}\right]^n$$

Equation 1.1 – The Milne de Marre equation.

Where ‘n’ represents an index which ranges from 1 to 2 dependant on whether the armour in question fails under pure plastic flow, shear, or (in-between these two values) a combination of both, and ‘k’ is a constant for a given material which is a function of its yield strength.

As well as presenting a plot of the Milne de Marre equation, figure 1.4 also includes empirical data for a selection of armour systems from both Agincourt (point ‘A’) and WWII systems. The graph compares the kinetic energy at perforation of various armour materials by plotting the projectile energy needed to fully penetrate (synonymous with perforation) versus the corresponding armour thickness. The scales are logarithmic to negate the power law dependency on velocity of KE and the thickness scale is expressed in terms of areal density – mass / unit area, e.g. the mass of 1 square meter of armour material (this approach is favoured by armour designers who prefer the mass rather than the thickness of an armour material). The Milne de Marre plot can also be used by armour designers to directly compare the ballistic performance of armour materials against one another. For example, the plot indicates that 25 mm of Steel armour is the equivalent of 75 mm of Aluminium armour. Above this threshold, Steel armour would be used; essentially, within this region Steel provides a better protection to weight ratio than Aluminium. Below this point it is interesting to note that Aluminium armour is superior to Steel on a weight-to-weight basis. This can be seen by the lower gradient of the corresponding curve.

Modern body armour materials, such as Kevlar™, which can be found in ‘flak jackets’, are also included on the graph presented in Figure 1.4. These will sometimes have a ceramic insert layered with the Kevlar™ creating a composite armour structure. Unsurprisingly, these materials sit higher than point ‘A’ for a given armour areal density, and therefore provide greater protection per-unit-mass than the chainmail of Agincourt. If the lines were extended upwards, it would show that these materials are also more ballistic efficient than Aluminium

up to 9 mm thickness (12 mm of Kevlar™) and Steel up to 12 mm thickness (50 mm Kevlar™).

The superiority of high grade ceramic armours, such as Boron Carbide (B_4C) can also be ascertained on the graph, as well as more complex multi layered or composite armour solutions [10].

1.1.3 Ceramic armours

Ceramics represent another type of homogenous armour used in modern day armour systems. Although described here as a monolithic armour, some may class a ceramic as a composite as it is made of a granular material that is sintered under heat and pressure; e.g. the underlying material structure is arguably closer to a multi-phase system than, for example, a (by comparison relatively) course-grained metal.

Use of ceramics in armour systems is a relatively recent occurrence, as late as the 1960's, compared to the use of Steel armours which has occurred over many hundreds of years. During the 1990's ceramics started to become widely used as an add-on armour to existing solutions such as disrupting plates within body armour employed by the Police and military forces. Previous to that ceramics were used by the Americans during the Vietnam conflict, for example air crews would line the hulls of helicopters to protect the crew from small arms attack [4]. Since then adoption of ceramic armour solutions has grown as munitions have advanced and lighter, more mobile vehicles are needed for modern warfare. Ceramic armours are now used to defeat threats ranging from small arms attack right up to large, long rod penetrating tank rounds.

Understanding how ceramic armour works is the key to optimisation of their role as an armour solution. Firstly the material properties of (appropriate armour-grade) ceramics include high compressive strength, as compared to that of Steels, Aluminium, Titanium, and also importantly the cores of typical AP projectiles (e.g. hardened Steel or Tungsten Carbide Cobalt). This means that under ballistic attack, the ceramic – as long as it is in compression – will outperform the penetrating projectile, leading to erosion / projectile defeat. Under such loading conditions the ceramic will fail via a combination of different processes. The primary failure mode within the ceramic will comprise formation of a 'Hertzian' cone due to

a formation of a combination of radial and hoop stresses on impact. This cone can be seen in the 'Florence' model below (figure 1.5) [15]. The size of the cone is dependent on the hardness of the ceramic and the size of the penetrator. Ahead of the impact, if the impact velocity is sufficiently high, a compressive 'failure wave' comprising of an elastic precursor may comminute the ceramic. However, if this does occur, this pre-fractured material will still be locally confined during the penetration event, maintaining the ability to defeat the incident round. Of particular note, is the fact that for penetration events happening at extreme velocities (generally around 1,500 m/s, such as 'long rod' attack), and as long as the ceramic stays under compression during the attack, it will retain its strength and cause the threat to 'flow' or behave hydro-dynamically, on the surface of the ceramic. This phenomenon is known as 'interface defeat' or 'dwell'. While it typically occurs at elevated velocities, it can also occur at ballistic velocities (e.g. ahead of an impacting small arms round) if the ceramic armour sufficiently overmatches the strength of the round. However, as soon as the ceramic starts to go into tension, the armour will fail [4].

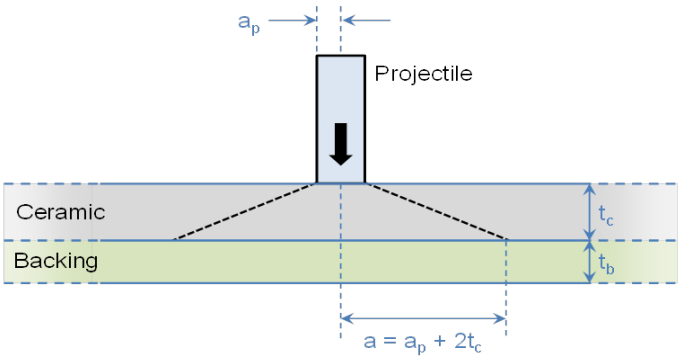

$$V_{50} = \sqrt{\frac{\epsilon \sigma t_b}{0.91 M f(a)}}$$

Where, ε and σ are the tensile strain/stress in the backing plates, M = projectile mass and given that ρ_c and ρ_b are the ceramic/backing densities respectively,

$$f(\alpha) = \frac{M}{\pi\alpha^2[M + \pi\alpha^2(t_c \rho_c + t_b \rho_b)]}$$

Figure 1.5 – The 'Florence' model and calculation of V_{50} – The velocity required for a round to penetrate a target 50% of the time (Equation 1.2).

In addition to a high compressive strength, ceramics also possess low bulk densities, so greater thicknesses can be used whilst still keeping the weight of the solution to a minimum. Although ceramics make very good armour solutions there are some drawbacks to their use. In particular, they can be very costly and they are very brittle (low toughness / tensile strength), meaning that they may not be appropriate for some systems, e.g. where either cost or the potential for accidental damage while in-service are primary drivers.

Ceramics commonly used for ballistic protection include, amongst others – Alumina (Al_2O_3) for body armour and, Silicon Carbide (SC) and Boron Carbide (B_4C) (with Young's modulus values up to 390 GPa, 430 GPa and 460 GPa, respectively [4]) for protection against high velocity threats or vehicle systems.

Recent research has shown the effectiveness of ceramic as an armour against small arms attack. In 2010 Medvedovski [16] tested the ballistic performance of many modern ceramics to try and influence future design and structure. The researcher used several types of ceramic including Alumina and non-oxide ceramics (such as Carbides, nitrides, borides and their combinations). The ceramics tested also varied in their manufacturing process, ranging from material sintered in a pressure-less manner to targets hot sintered under varying pressures. The ceramics were formed into composite structures – including a layer of ballistic nylon (such as Kevlar™) and a layer of a laminated or layered polyethylene, such as Dyneema™, placed on the back. This allowed the ceramics to be tested in a 'real life' situation, as such the layups employed nominally replicated core elements of most modern day personal armour solutions. Samples were tested on a shooting range using an M16 rifle and a varying selection of projectiles, including: NATO ball; Russian ball; Winchester 7.62, and; AP M2 FMJ WC core rounds. It was found that not only the dense homogenous ceramics but also the heterogeneous ceramics had exceptional ballistic performance. It was also shown that light weight inexpensive armour solutions can be obtained, with multi hit performance. Useful approaches in this regards include the use of smaller tiles so that on average any ballistic impacts will occur on a single tile, allowing for that single tile to be replaced and not the entire armour, while still utilizing the optimal properties / performance of the ceramic under ballistic impact. The properties of the ceramic were characterised after manufacture by using X-Ray diffraction (XRD) and Scanning electron microscopy (SEM). The Young's modulus (elasticity) was measured as was the density and Vickers hardness of each sample.

This work corresponds with earlier research undertaken by Hazell *et al*. [17] where a series of well characterised silicon Carbide ceramic tiles with differing properties (such as manufacturing processes, grain structure, etc) were impacted using 7.62 x 51 mm Tungsten Carbide (WC) cored FFV projectiles fired from an experimental gun on an indoor range. The targets were mounted to 25-mm thick Al plates, with 3 more plates added to create a semi-infinite backing. The DOP technique was used as a chief diagnostic. Post-impact, samples were analysed via flash X-ray to ascertain the resultant DOP. The results corresponded with the information found by Medvedovski [16] in that the ceramics provided an excellent

resistance to ballistic impact. Hazell *et al*. found that the harder ceramics performed better, with increased performance coming from a relatively small increase (typically just 1.5 to 2.0 mm) in thickness. This small increase in target thickness resulted in a transition from rigid body penetration of the WC core to total fragmentation and consequent broken body penetration. It was postulated that the increased thickness in the ceramic gave the crack appearance in the core time to spread until total fragmentation of the core occurred. It should be emphasised that this increase in thickness was minimal to achieve such results, highlighting the importance of understanding underlying penetration / defeat mechanisms in ceramic armour systems.

1.1.4 Transparent armour

An important niche area for armour systems is that of transparent armour. Situational awareness (windows, ballistic goggles, etc), as well as the growing requirement for optical sensors on military platforms, all contribute to a requirement for optically transparent armour solutions. By definition this requirement substantially limits material choice [18]. Solutions are typically composite in nature, combining both hard and tough elements. Hard, disrupting layers typically comprise ceramics (glass, sapphire/spinel), designed to disrupt an incident projectile – with softer, tougher polymeric materials (polycarbonate) being employed as energy-absorbing backings [18,19,20]. Additional constraints include weight and manufacturing limitations, meaning that interlayer properties are often crucial to armour performance.

In a comprehensive study focused on window-type solutions, Appleby-Thomas *et al*. [21] conducted ballistic experiments on various materials used in composite transparent armour systems. Glass laminate fronted cylinders containing a polyurethane replacement resin (PRR) were impacted using lead antimony cored 7.62 x 51 mm NATO ball rounds. In these cases, the backing resin was designed to represent a semi-infinite layer – with the primary focus on the disrupting outer layer. The penetration event was recorded using high-speed video. It was noted that the PRRs elastomeric properties helped to arrest the projectile during penetration – interestingly, with quasi-hydrodynamic behaviour (nominally constant velocity) observed behind the disrupting outer layer. It was also found that the glass laminate failed in a similar manner to typical armour ceramic in that a Hertzian cone was formed [15]. Understanding of

these failure modes led to use of asymmetric float glass laminate disruptors to further reduce the DOP. All of these factors must be considered when designing an armour system where thickness and weight need to be addressed whilst still keeping the structure transparent.

This work also corresponded with results shown by Hazell *et al*. [22]. In this study the researchers used lead-antimony-cored bullets to fire into glass fronted polymer resin targets. The bullets were fired from an experimental gun on an indoor range. High speed video imaging showed the resin interacting with the porous lead-antimony core and helping arrest penetration. It was also shown that the added layer of a float glass disruptor on the front of the resin targets help reduce penetration as shown by the work of Appleby-Thomas *et al*. [21]. Numerical simulation was also employed by the authors to further enhance and support experimental results.

Overall, these studies show that using a hard disrupting layer to start to interact with the bullets jacket causes a reduction in penetration. This corresponds with the aim of this research project; e.g. if a projectiles vulnerability to such a disrupting layer can be optimised (for example by removing an encasing jacket), then penetration resistance could be enhanced.

1.1.5 Composite materials and systems

In the context of armour systems, the word ‘composite’ can be used to describe a system that comprises layers of different materials with different properties, that when brought together form a complex system designed to do several tasks. An example of this would be a modern day body armour which comprises of a top layer of an aramide fabric, such as Kevlar™, designed to start to disrupt the bullet jacket, followed by a hard ceramic, such as Boron Carbide, to stop the core of the bullet and finally a thin layer of a Dyneema™ type material to help dissipate the incident energy / shock. Another example of a composite armour system is the transparent armour mentioned previously in Section 1.1.3. These materials all have different properties that when brought together make an effective armour system.

While a generic term for systems comprising multiple elements, the term ‘composite’ is often specifically used to describe a specific class material, often comprising fibre reinforced polymeric structures. Examples of such composite materials include carbon fibre, glass fibre, Kevlar ™, Dyneema™, etc.

The composite materials mentioned above are made from fibres which have been set in a matrix and then impregnated with a curing resin. The fibres can be orientated to lie in specified directions to ensure strength is retained within the material and the fibre direction can be altered from layer to layer. In such systems the fibres typically have a high tensile strength, with the matrix being characterised by lower strength, but enhanced elasticity / toughness. High strength matrices have been considered in the past – however, in such systems the comparable stiffness of the fibres and matrix leads to micro-crack evolution during everyday service and fast failure once the strength of the system is exceeded.

Carbon fibre reinforced polymers / plastics (CFRP) are a widely used composite employed in a huge variety of industries from aerospace and motor racing to the frames of expensive bicycles and chassis of supercars. They are used for many purposes because of their lightness and strength (high specific strength), as well as their ability to be moulded to practically any shape. Despite the relative lack of knowledge with regards to more conventional structural materials (e.g. the use of metals for thousands of years), composite use is expanding exponentially. For example the newly manufactured Boeing 787 Dreamliner comprises of 70% by volume and 50% by weight CFRP [23].

In 1990, Cantwell and Morton [24] researched the impact perforation of CFRP in both the low and high velocity regimes, defined by the authors as the free fall of a drop tower as low velocity and speeds of 700 m/s as high velocity. They studied the effectiveness of CFRP for applications on aircraft and other aerospace vehicles and the possibility of impact in those situations. Low velocity impacts were undertaken on a drop tower where a 680 g load was allowed to drop freely from heights up to 2 m. A 6-mm diameter hemispherical-nosed impactor was fixed to the carriage. Damaged panels were inspected via optical microscopes. The low velocity impacts showed that damage occurred in three forms, through delamination, fibre cracking and, matrix fracture. It was found that the damaged area where the impactor did not penetrate was far greater than the area if the impactor had penetrated. This was primarily attributed to the delamination of the panel between the various layers. Such damage is consequently often not immediately apparent after an impact (and is typically termed Barely Visible Impact (BVI) damage).

High velocity impact experiments were undertaken on a single-stage light gas-gun. Where perforation occurred, damage extent was again observed to be smaller overall as compared to

the low velocity impact cases, with less delamination evident but more damage through fibre breakage and matrix cracking. Both the low and high velocity results therefore highlighted the importance of projectile-target interaction time.

In similar work, Hazell *et al*. [25] investigated the penetration of a 5 harness satin weave CFRP cured with a RTM6 resin, by a high velocity Steel sphere accelerated by a light gas-gun to velocities in the range of 170 to 374 m/s. High speed video imaging was used to measure the velocity both before and after impact of the panel. The difference in velocity was due to the kinetic energy lost during the penetration event (e.g. factors such as energy loss on impact through light and sound, as well as factors such as heating, were deemed negligible). Samples of 3 and 6-mm thickness, of the aforementioned 5 harness satin weave, were tested at normal and oblique angles. It was found that panels that were impacted at normal angles at low velocity failed due to tensile failure of the rear weave. This was more apparent in the 6-mm thick samples. As the velocity was increased to above 170 m/s, the failure mode changed and it was observed that a conical mass (a 'plug') was ejected ahead of the projectile. It was also found by microscopy and ultrasonic C-scan of the 3-mm thick samples that the degree of post-impact delamination remained constant regardless of the impact energy of the projectile. A similar occurrence was observed in the 6 mm samples as well. It was postulated from these tests that the lay-up sequence of the weave had little effect on the underlying penetration mechanisms.

Interestingly, it was also observed that under impact at oblique angles, more of the kinetic energy of the projectile was transferred to the panel when compared to the same thickness panel in a 'normal' configuration. It was subsequently concluded that this response was primarily a geometric (presented material thickness) effect.

Overall, Hazell *et al*. concluded that the thicker samples showed greater energy absorption at lower velocities. This advantage was noted to disappear as impact velocities elevated. This was consistent with the findings of Ref. [24] in that the CFRP both failed under high strain conditions, in the same manner.

The studies reviewed here appear to show that CFRP does not make a good single element armour material, because of its poor reaction to impact. However it is still widely used in industry – in particular, such materials (for example, Phenolic Resin based composites [26]) have found application as ablative armour used to dissipate heat. This type of usage for CFRP

can be found in the aerospace industry and the construction of space vehicles where heat transfer can be an issue, effecting electronics etc.

Although it has been shown that – in general – CFRP has poor penetration-resistant properties, similar materials can still be found in composite armour systems. In very recent work Crouch *et al*. [27] used a Boron Carbide (B_4C) ceramic clad on the front face with an aramide fibre reinforced layer of epoxy resin (a material with similar properties to CFRP). Although this material did not contribute to the defeat of the hard Steel core round used, it was instrumental in starting to pre-strip the round of its gilding jacket. Interestingly, this is a process that is in direct partnership with the aims of this study and the reason why CFRP is chosen as a material to investigate herein.

1.1.6 Spall liners and UHMWPE

Another common type of composite material used in armour solutions is ultra-high molecular weight polyethylene (UHMWPE). This is a material whose fibres and matrix are made from the same material (a 'self-reinforced' composite). The fibres are made through a process called 'gel spinning', wherein the long chain molecules are dissolved in a solvent to form a gel. The gel is then extruded and cooled to form the fibres with a high degree of molecular alignment. This makes the fibres exceptionally strong in one direction [28].

UHMWPE materials are commonly used in armour solutions as spall liners. Spall liners are used to line the inside of tanks and other vehicles that are susceptible to attack, especially from RPG threats. The explosively formed jet can overcome the thickness of the armour and penetrate the hull with high velocity fragments. The spall liners are inherently tough and are designed to help absorb the impact and catch fragments. This material is used for this application due to the combination of its low density, its ability to catch blunt fragments and also, importantly, its formability – which allows it to be moulded to the inside contours of the vehicle or structure in question [27]. In recent years UHMWPE materials have been used in more armour solutions than just spall liners. The two most common brands used are Dyneema™ (manufactured by DSM) and Spectra™ (manufactured by Honeywell Int. Inc.). An example of the use of such a material was work by Iremonger [29] in 1999, where L2A2 lead antimony cored 7.62 mm bullets were fired at Dyneema™ targets at velocities of 870 to 900 m/s. The targets remained un-backed, as the author wished to view the effects of the

projectile on the back edge of the target material. A high speed camera was employed to measure the velocity of the incoming round and to witness the penetration of the target, as well as to check for any abnormality of the incoming round. After penetration the targets were sectioned and the DOP of the target was ascertained. The targets were also photographed. From these photographs, the mechanisms needed to stop the projectile were observed. Dyneema^{TM} targets of thicknesses which ranged from 4.2 to 32.0 mm were used. The Dyneema™ in thicknesses of 22.0 and 32.0 mm completely stopped the bullet, with this behaviour attributed to a contribution of several factors. Firstly, on impact the panel was observed to start to compress, with some fibres subjected to shear. It was observed that approximately a quarter of the way through the panel the round had started to deform and disrupt. At this stage delamination of the layers had occurred. It was believed that the most important factor needed to stop the bullet was the bending action of the rear portion of the panel. Under such loading the fibres were being placed into tension, with incident energy being absorbed / dissipated through the stretching of these fibres – with this subsequently leading to the arrest of the projectile. It was postulated that the thinner samples did not react as well as the thicker samples due to the lack of material needed to allow these mechanisms to occur to a sufficient extent under high velocity impact.

Such UHMWPE material is also used in body armour solutions as a backing membrane. In this configuration it is used in the same capacity as a spall liner. This configuration was employed in experiments undertaken by Crouch *et al*. [27] in recent reverse ballistic research into the pre-stripping of Steel-cored rounds. This work, which involved the monitoring of impact events via flash X-ray, suggested the importance of jacket removal in terms of penetration.

In addition, Dyneema^{TM}, or similar materials can also be found as the sandwiched material in non-explosive reactive armour [4].

1.1.7 Modern day armour solutions and future designs

Moving beyond passive armour systems, active systems where the armour physically interacts in a dynamic manner with an incident projectile can also be employed. One such

type of modern day armour is explosive reactive armour or ERA. This type of solution was developed and used in the 1980's as a way to defeat munitions such as anti-tank guided weapons and rocket propelled grenades or RPGs. These munitions typically form an explosively formed jet which can penetrate up to 300 mm of solid Steel armour. In its simplest form, ERA is made from sheets of explosive, sandwiched between two Steel plates [30]. The incoming explosively formed jet penetrates the outer Steel casing and rapidly compresses and heats the explosive which detonates, propelling the Steel plates apart and disrupting the jet (by imparting lateral momentum to the highly aligned jet). Such ERA systems are usually applique in nature, encased in boxes mounted on the outside surface of the tank armour. The boxes, which serve as both mounting and environmental protection systems, are also angled to an appropriate orientation to likely incoming threats (see figure 1.6).

Figure 1.6 – Modern day tank with ERA cassettes on display [31].

Even though ERA adds approximately 1,000 kg to the overall weight of a tank, it is equivalent to adding 20,000 kg of equivalent armour Steel [4]. More recently ERA has been refined by extensive experimentation and trials where the inclusion of glass or even ceramic plates into the cassette have aided in the reduction of weight and improved the armours capability [32].

Another type of a modern armour solution is non-explosive reactive armour. This works in a similar way to ERA but without the use of an explosive. The make-up of the armour is the same, composed of a filler material sandwiched between two Steels plates. When the outer

material is penetrated by an explosively formed jet, it drives a plug of the material ahead compressing the sandwiched filler material. The sandwiched material compresses against the rear Steel plate, storing elastic energy. This then expands radially away from the surface of the vehicle and disrupts the incoming threat. This type of armour is friendlier to surrounding troops as nothing leaves the added cassette, as it does with ERA and is a cheaper alternative. However, it should be emphasised that it does not perform as well as ERA due to the lower velocities that are within the armour system under impact. Performance of this armour can be improved by using it in conjunction with other armour solutions, or by using hardened Steel plates as the sandwiching material [33].

A very recent development in armour solutions is that of electric and electromagnetic armour. Electric armour was first suggested in 1973 as a way of disrupting incoming rounds and threats such as RPGs. As the jet is formed in the RPG it makes contact with an outer plate on the armour which is grounded and an inner plate which has a large electrical current passing through it [28] (see figure 1.7).

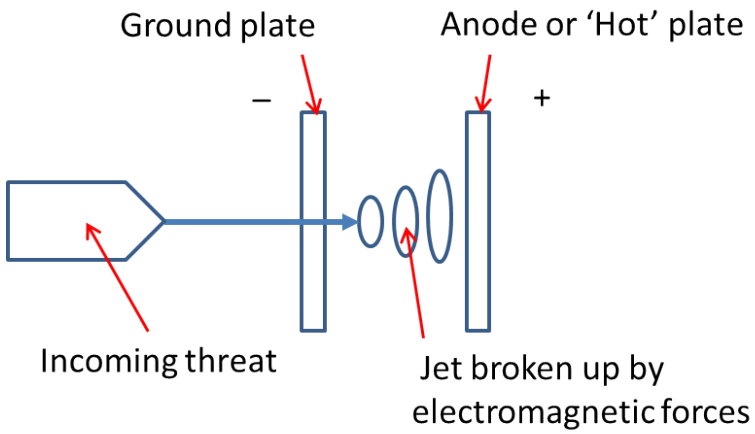

Figure 1.7 – Electric armour design.

The jet acts like a switch, connecting the two plates together electrically. The result is a powerful electromagnetic force which causes the jet to break up into rings. This process is known as magnetohydrodynamic pinch [34]. Other concepts in this field include electromagnetic armour which uses electromagnetic energy to propel flyer plates into the path

of incoming projectiles. These flyer plates are steerable and work in a similar way to ERA except instead of an explosive, they utilise electromagnetic energy [35].

Other future concepts in this field include armour systems that track an incoming round and launch a preselected projectile or defence mechanism to defeat that particular round. Such systems as these are known as 'Hard kill defensive aid suites'. Although these systems have been trialled they are still very much in their infancy. There are several factors to consider for this type of armour. Firstly any incoming threat will be travelling extremely fast, in the case of a long rod penetrator the velocity will be around 1500 m/s. So any on board computer, as the threat is moving, will have to work twice as fast to track, assess, and launch the correct type of counter measure. Having said that, systems of this type are in use in the battlefield today. Systems such as ARENA and TROPHY. Both use radar to pick up and assess in coming threats and issue countermeasures [28].

Future protection systems for vehicle / personnel armour are forever evolving. In some cases, key armour components are already being upgraded. For example, introduction of composite materials can help to reduce weight while still maintaining key ballistic and blast protection levels. Such composite materials have the potential to save a ton or more in overall weight, producing both economic and environmental benefits (e.g. as more efficient lower powered engines can be utilised). The U.S Army's Supacat SPV400 already benefits from a composite armour 'pod' which can also be supplemented with ceramic armour plates. As well as material evolution, vehicle armour design has also been revised. Modern armoured vehicles have started to incorporate a 'V' shaped hull that would direct blast waves away from the personnel inside the vehicle. The Matador MPV (Mine Protected Vehicle), as used by the South African Army, utilises this design.

The modernisation of personal armour has also been at the forefront of research in recent years. Materials such as Carbon Nano tubes are being researched for the use in such systems. Carbon Nano tubes are single sheets of carbon atoms that are rolled into tubes. Each tube is extremely strong but very light weight. Concepts behind the research suggest that if enough tubes are connected together, a material can be produced that is many times stronger than Steel but much lighter than Titanium. One such material already created this way is called Graphene. This material is in its infancy, but the overall concept is to incorporate this material into the armour systems of aircrafts, ships, vehicles and body armour, and aim to do this in the next decade. Setbacks at the moment include the ability to mass produce these

types of materials cost effectively. A concept of a future body armour design, incorporating Graphene can be seen in figure 1.8.

A similar material that is also being researched currently is cellulose. Cellulose is a natural fibre found in wood. Compressed to a single molecule thickness, cellulose polymer chains possess greater tensile strength than Steel. These polymer chains can easily be produced by feeding the cellulose to certain types of Blue Algae [36].

Figure 1.8 - The future of body armour? A concept design involving the use of Graphene [36].

1.2 Threats and projectiles – background

For as long as there have been armour solutions there have been threats that the armour protects against. Dating back thousands of years, projectiles such as simple rocks and stones have been used in warfare to defeat opponents. Throughout time these projectiles have developed with the development of armour solutions into the modern day threats we see in warfare.

The development of threats and projectiles also has heavily relied on the development of weapons that are able to propel these threats greater distances and with consequent greater force.

For the purposes of this study modern day threats will be investigated. These threats have been divided up into 5 main categories; 1) Fragmenting munitions and fragments, 2) High explosive squash head rounds, 3) Directed explosive energy threats, 4) Medium and large calibre KE ammunition and; 5) Small arms rounds.

1.2.1 Fragmenting munitions and fragments

When dealing with armour design, the designer must bear in mind that projectiles are not always a perfect size and shape to defeat. The best example of these is shell fragments caused by exploding munitions or fragmenting warheads. The formation of a fragmenting warhead is very closely related to a conventional projectile in that they rely on a high explosive filling to break up the casing material and propel it toward the target at high speed. These munitions can also be sectioned into 3 categories; 1) Natural fragmentation, 2) Pre-formed and; 3) Fire-formed fragmentation (see figure 1.9).

Natural fragmenting warheads are designed with a casing without any inclusions or fracture points manufactured into it. These are designed to fracture along natural grain boundaries and weak points, giving the fragments a varying size and weight. These munitions are effective when detonated near to a target rather than against it. The fragment patterns depend on orientation to the target and warhead shape [37, 38]. These types of fragments can also be divided up into 5 common fragment shapes. These are; 1) Copper band, 2) Box plateau, 3) Parallel piped, 4) Mountain ridge, and; 5) Wedges [39].

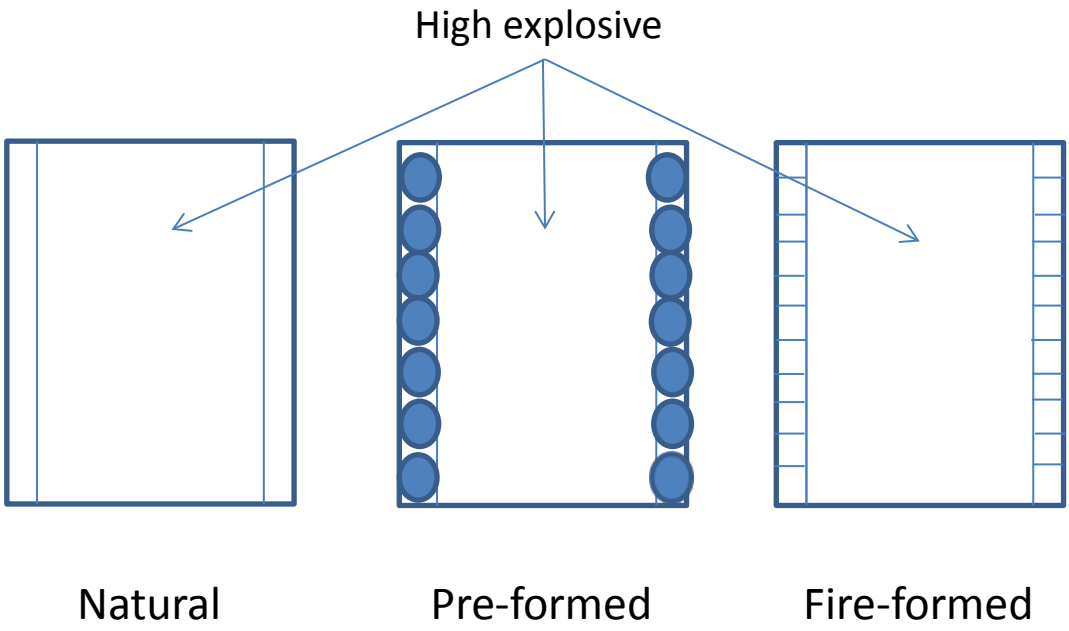

Figure 1.9 – 3 examples of fragmenting warheads.

The second type of fragmenting warhead is a Pre-formed warhead. This warhead has added fragments adhered to the lining of the case. They are (typically) either held in place with fine mesh or epoxy. The fragments can be of any material or size and shape. Common added fragments are spheres of different sizes, cubes, rods, wires, etc. These are used to generate maximum personnel casualties as fragments will cover a huge varying distance around the detonated warhead [37, 38].

The third type of fragmenting warhead is a Fire-formed warhead. This warhead has, in the manufacturing process, inclusions or weak points manufactured into the casing. The advantages of doing this is that fragment size, shape and weight can be carefully controlled and the direction the fragment is launched in can also be determined. A common type of Fire-formed fragmenting warhead is a common M67 hand grenade where even though the kill radius of the grenade is 5 meters, the casualty producing radius is 15 meters and fragments can be propelled as far as 230 meters [37, 38, 40].

1.2.2 High explosive squash head rounds (HESH) and spall

High explosive squash head or HESH rounds (see figure 1.10) work by detonating a high explosive on the surface of an armour system to create a high velocity compressive shock wave through it. When this shock wave meets the back surface of the armour the wave is reflected back through the plate; the lower density (and therefore impedance) of the rear surface leads to this reflected wave being tensile in nature [41]. This reflected tensile wave moving back into the material will eventually overrun the continuing compressive loading from the initial detonation (and potentially even combine with tensile releases resulting from reflections from the front of the target). Once the armour goes into net tension, the very high associated tensile stresses will typically exceed the strength of the impacted armour plate. This causes the material to rupture – often along grain boundaries – forming a spall plane within the armour (see figure 1.12 A to C). Once the material fails entirely, a large fragment or 'scab' will detach from the back surface of the armour with considerable velocity (up to one third the speed of sound), leading to significant behind armour effects. A well designed HESH round will produce a scab around 1 ½ times its own diameter [4, 28, 37, 38], (see figure 1.11).

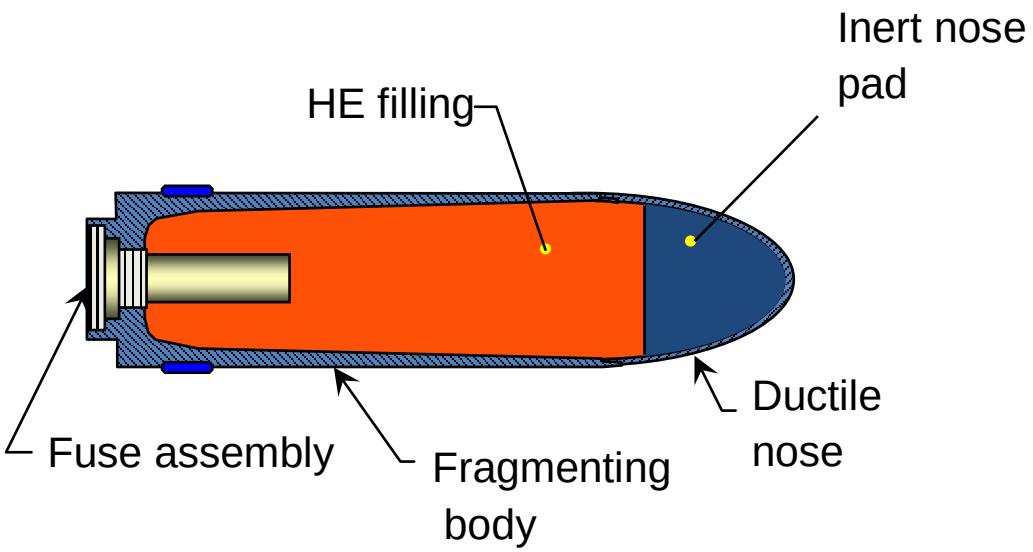

Figure 1.10 – High Explosive Squash Head (HESH) round [42].

Figure 1.11 – An example of a ‘scab’ produced by a spalled material. How a HESH round works on an armour [4].

In line with their mode of operation, HESH rounds employ the use of a fairly insensitive explosive which will not detonate on impact. When the round hits the target the soft material of the head collapses and spreads the explosive composition intimately over the surface of the armour. As the round continues to move despite contact, due to inertia, the fuse will come into contact with the surface of the armour causing the high explosive to detonate. This will then cause damage of the type seen in figure 1.11. The main casing of the HESH round will also fragment on the outside of the armour causing added damage to vehicles / personnel [37, 38]. Over recent years the use of HESH round has declined in the Western world with the development of spaced armour solutions (which capture the scab in the space between the layers).

Spall explanation

A) Impacting projectile causes compressive waves within the sample and the projectile. (Red = Compressive waves)

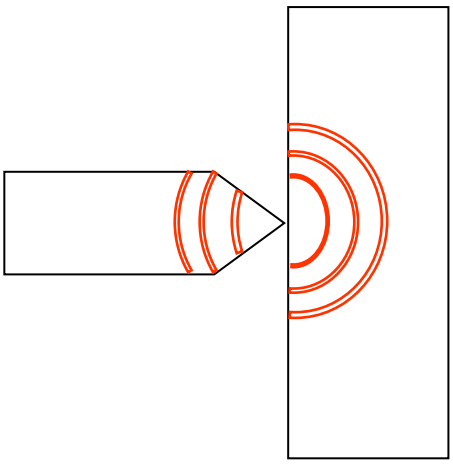

B) Compressive waves reflect off of the rear surface of the armour / projectile. The waves reflect as tensile waves due the lower impedance of the rear surfaces (Green = Tensile waves).

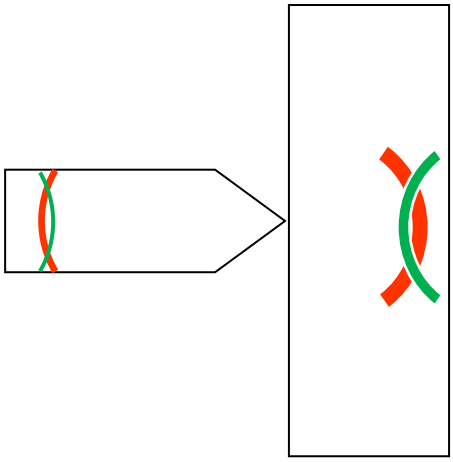

C) The continuing compressive waves clash with the tensile waves causing the material to go into tension. Failure occurs in the armour / projectile along grain boundaries or localised weaknesses in the microstructure of the armour or projectile. These then combine and grow, causing Spall to occur.

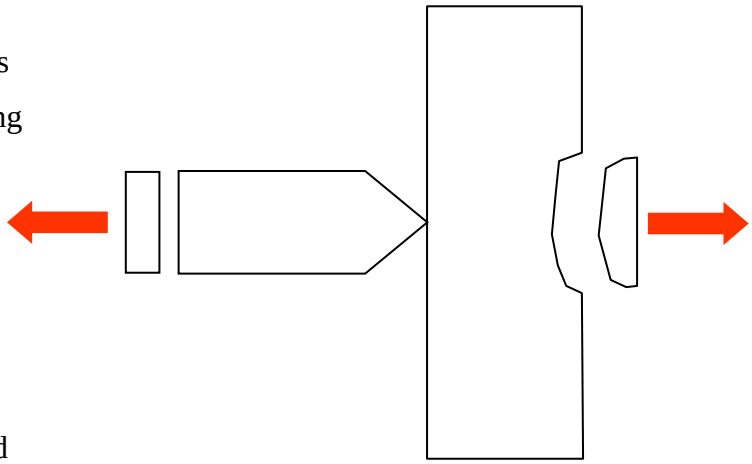

Figure 1.12 A to C - Spall explanation.

1.2.3 Directed Explosive energy threats

Directed explosive energy threats can be divided up into two main categories. These are; 1) shaped charge warheads and; 2) explosively formed projectiles (or EFPs).

Shaped charge warheads

Shaped charge warheads essentially comprise a high explosive surrounding a conically shaped material liner. The material used for the liner is typically metal, with Copper the most common due to a combination of its density and ductility (leading to maximised penetration and ease of 'jetting' respectively). The warhead also contains a detonator to initiate the explosive. This type of warhead is extremely effective against thick, heavy armour such as

tank armour. Armour used to defeat a shaped charge, or at least to minimise its effects can include spaced armour and explosive reactive armour. As an example of the effectiveness of such munitions, Figure 1.13 shows the penetration path of a relatively small (ca. 90-mm diameter) locally manufactured shaped charged jet. The jet has penetrated through 18 inches of mild Steel plate. The tapering nature of the penetration path is a function of the velocity gradient which formed across the length of the jet as the liner collapsed. The Copper slug (formed behind the jet) which subsequently embedded itself in the penetration path can be seen in figure 1.14.

Figure 1.13 – Example of the penetration path of a shaped charge jet.

Figure 1.14 – Copper slug taken from the midpoint of the penetration path seen in figure 1.12.

One of the most common threats to contain a shaped charge is a rocket propelled grenade (RPG-7, see figure 1.15). Although called a grenade, the fragmenting properties of the RPG-7 are minimal as the shaped charge jet is its main threat. Another common warhead to contain a

shaped charge is a high-explosive-anti-tank (HEAT) round. A sectioned example of such a munition can be seen in figure 1.16. Note the spigot on the front; this is designed to facilitate triggering, allowing the jet to begin to form at the optimal stand-off from the target [37]. The initiator / trigger for the explosive charge (an inert filler coloured red for the purposes of teaching in the picture) can be seen at the tip of the stand-off spigot.

Figure 1.15 – An example of a RPG-7 round (centre).

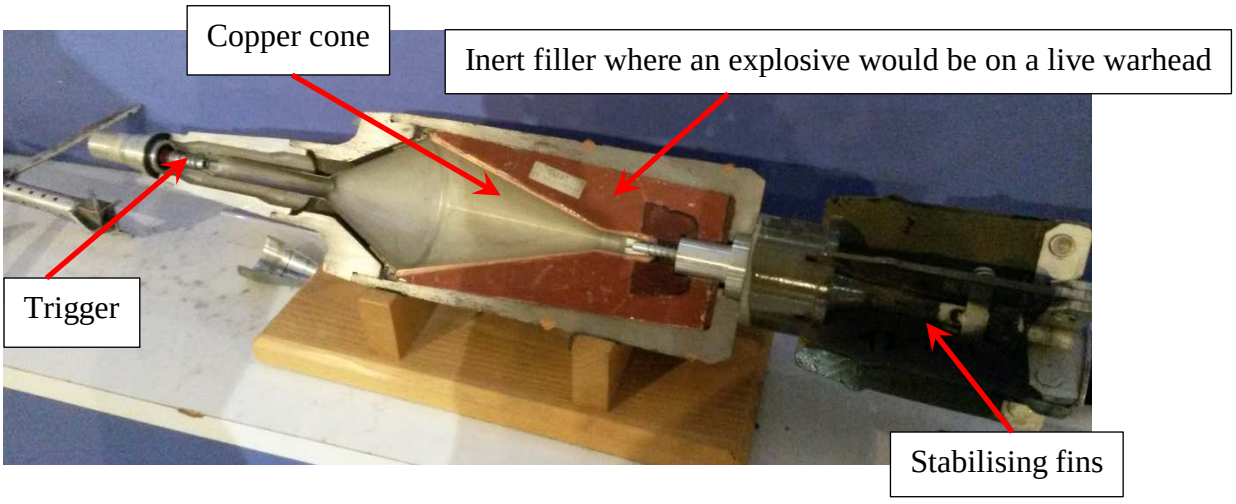

Figure 1.16 – An example of a High explosive Anti-Tank (HEAT) warhead.

The penetrating jet begins to be formed when the detonation, or chemically supported shock waves set up by the detonating explosive reach the tip of the conical liner. The liner material is driven radially both towards and away from the apex of the cone. This process, which deforms the liner material so rapidly that it flows like a fluid (hydrodynamically). This leads

to the formation of both an elongated jet (around 20 wt.% of the liner material), and slug (containing the reminder of the cores material). This process, illustrated schematically in figure 1.17, can lead to jet tip velocities of up-to 11 km/s).

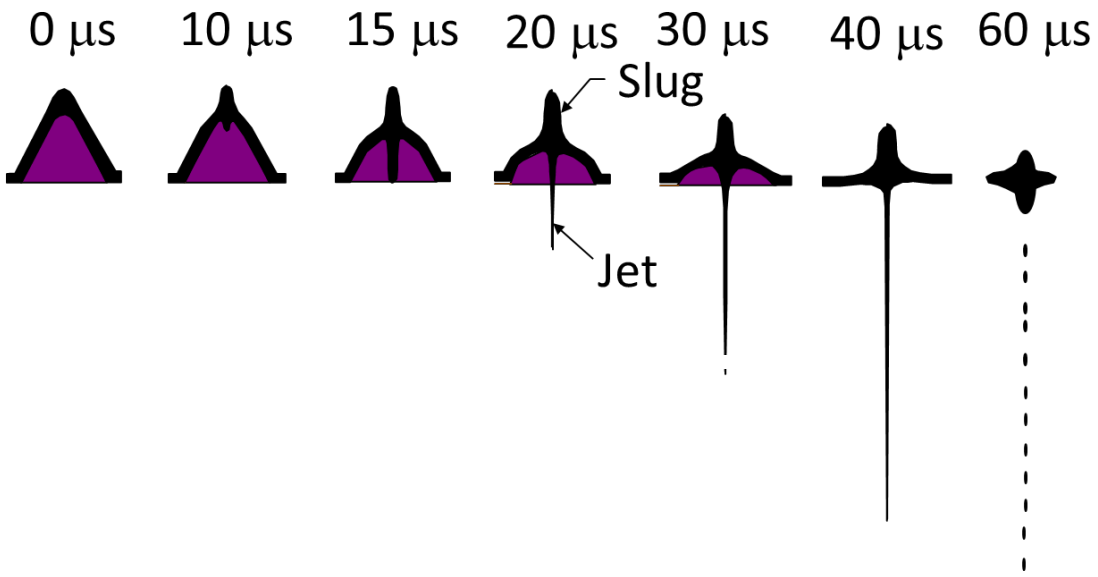

Figure 1.17 – Schematic illustration of the formation of a shaped charge jet [43].

Key variables that can be altered to influence shaped charge warhead performance include cone material as well the angle and overall shape of the cone. Typically, liner materials comprise metals such as Copper and Aluminium, although Steel, titanium and molybdenum have also been employed. In addition, some ceramics – including glass – have been shown to form jets. Differing cone shape and liner material choice combinations produce varying velocities and forms of damage. For example, an Aluminium cone might be deployed in attacks on concrete structures as the resultant jet, while less penetrative than one formed via a Cu liner (due to the lower density of Al as opposed to Cu), tends to lead to greater surface disruption. Essentially, a penetrating narrow jet would only cause minimal behind-armour effect. This is a critical issue for all munitions, ranging from shaped charges to bullets (as studied here) as the key role of a projectile is to maximise behind-armour effects, while armour should minimise or prevent these. Shaped charges – due to the aforementioned requirement for the jet to form (stretch) have an inherent additional complexity in that the stand-off distance between the cone and the face of the armour at trigger is also very important. Too close and the damage is minimal and too far away and the shape charge jet will lose its effectiveness and break up. Finally, if the cone is too wide, the threat will turn

into an EFP (explosively formed projectile) [4, 28, 37, 38]. The Bernoulli equation, see equation 1.3, can be used to calculate the depth of penetration of a shaped charge [44]. The depth of penetration (L_p) is calculated by taking the square root of the density of the liner / jet material (ρ_j) over the density of the target (ρ_T) multiplied by the length of the jet (L_j).

$$L_p = L_j \sqrt{\frac{\rho_j}{\rho_T}}$$

Equation 1.3 – The Bernoulli penetration equation.

Explosively formed projectiles (EFPs)

Explosively formed projectiles are essentially a limiting case of a shaped charge warhead, although in several ways they are more similar to kinetic energy penetrators (covered in section 1.2.4) in their effect on the target. With a shaped charge, increase cone diameter leads (very broadly) to a reduction in material in the resultant jet post-detonation and a corresponding increase in the amount of liner material which contributes to the slug following behind. To this end, whereas a shaped charge would contain a cone of a particular material to form a jet, EFPs contain a hemispherical or disc shaped liner, analogous to a cone with an angle >120º. Usefully, the design of the liner can also be altered, so that when the EFP is formed it can have added inclusions like stabilisation fins. Consequently, EFPs are relatively ballistically stable, able to fly for up-to hundreds of charge diameters (as opposed to a handful of charge diameters for a shaped charge). Collapse of a typical EFP liner is illustrated schematically in figure 1.18.

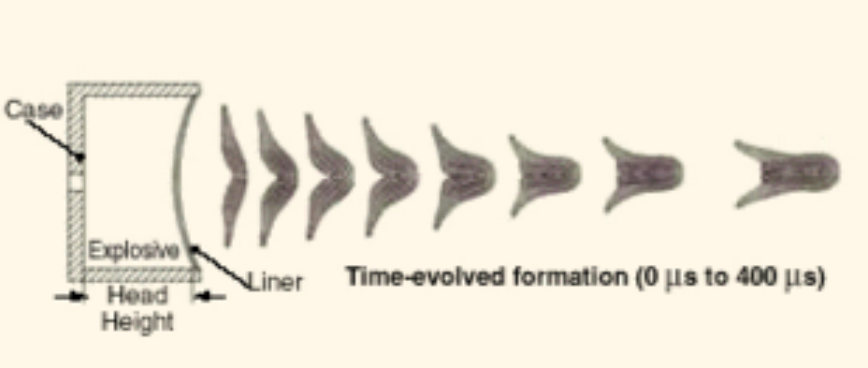

Figure 1.18 – EFP formation [45].

Common weapons featuring this type of warhead include belly-attack type mines, which target the relatively unprotected underside of tanks and other vehicles (see figure 1.19). While EFPs have poor penetration compared to shaped charge jets, if they do perforate a target they can cause huge amounts of damage. As a general rule, an EFP should be able to fully penetrate armour with a thickness comparable to the charge diameter, whereas shaped charges can perforate targets up to 5-8 charge diameters (or potentially even more with advanced designs). High density liners such as Steel, Tungsten and DU (depleted uranium) tend to be employed; further, it is worth noting that their lower KE means that – unlike shaped charges – EFPs may not set off explosive reactive armour (ERA) [37, 38].

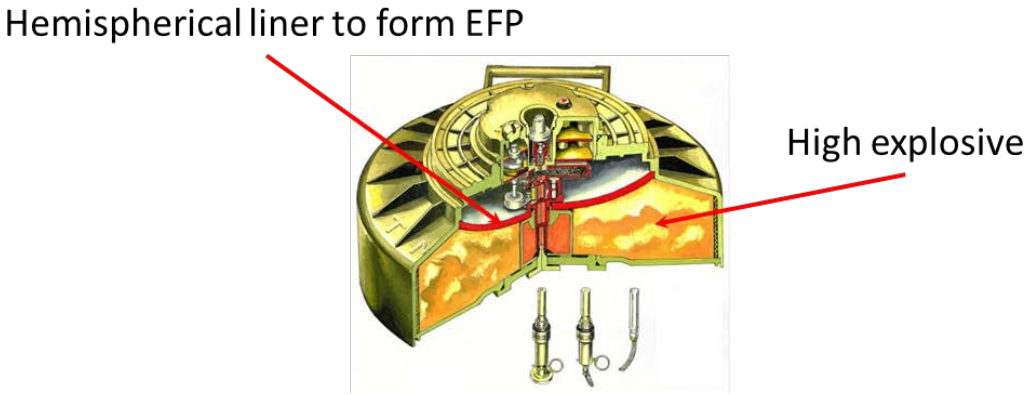

Figure 1.19 – A belly attack mine employing the use of an EFP [42].

In addition, in recent years EFPs have been used more widely in the makeup of improvised explosive devices (IEDs). Due to the ballistic stability, such systems – which can be relatively easily manufactured at a crude level (a pipe, dish and explosive packing with an appropriate detonator behind will suffice) can act as very effective off-route devices, causing immense damage to the engines and transmissions of vehicles as well as personnel.

1.2.4 Medium and large calibre kinetic energy (KE) ammunition

Kinetic energy threats – where behind-armour effects are simply a function of the incident projectile's KE – are one of the most effective ways to attack heavy armoured vehicles. Use of a dense penetrator launched at an extremely high velocity, results in a sufficiently high enough kinetic energy density at impact to punch through the armour system. These types of munitions have been used for centuries, with the earliest being heavy Steel or stone cannon balls. Behind armour effects can include spallation of armour material [28], physical damage via both trauma and heating to crew, ammunition and components and even pyrophoric effects (for example if something like DU is employed). The basic design of KE ammunition includes a heavy penetrator (usually a dense material such as Tungsten, or traditionally a heavy hardened Steel). Modern KE ammunition is then carried in a discarding sabot which can utilise a much larger, more powerful launcher. Traditionally KE penetrators were encased in standard shell casings.

Early examples of KE ammunition were developed after the initial appearance of tanks on the battlefield. In 1916 the UK started development of an armour piercing high explosive round, to be fired from a 40 mm light anti-tank gun. The round included a heavy Steel core and a high explosive tip. As the round hit the target the explosive would detonate on the armour surface and 'blast' a path for the penetrator through the armour. Burning debris from the detonation would also be dragged through the armour, causing damage to the inside of vehicles, personnel. This type of round was later succeeded by a simplified armour piercing round, where the high explosive filling was removed and the material of the penetrator was changed to more dense material such as Tungsten. During penetration, the KE within the more dense material was enough to punch through the armour systems of the time. It was during the Second World War that KE ammunition, using the same principles as weapons designed today, were developed. Designers looked more closely at different materials and

took more notice of the laws of ballistics, enabling rounds to travel faster and penetrate deeper.

It was in this period where armour piercing discarding sabot (APDS) ammunition was first developed and used. The round consisted of a smaller calibre penetrator of a hard material, encased in a discarding sabot. It enabled the round to be fired from larger, more powerful guns and upon leaving the muzzle the sabot would discard, leaving the smaller calibre penetrator with the same initial kinetic energy it was launched with – and – consequently – very high incident kinetic energy density to penetrate the targets hull. This was to remain standard KE ammunition until the 1970's where the development of armour systems caused the round to become fairly ineffective against some heavy tanks / vehicles. This lead to a redesign of the munition. Materials were kept the same, as were the types of launching mechanisms and propellants involved because no replacements for these were readily available at the time. The answer was to use long thin penetrators, also known as long rod penetrators (LRPs), which utilised high kinetic energy over a concentrated area.

Upon penetration, with the kinetic energy involved, the penetrator and the armour start to behave quasi-hydrodynamically. By having a longer, thinner penetrator the time of interaction between the penetrator and the armour is increased, therefore increasing the chances of full penetration. Due to the length of the new designed penetrators they were required to be fin stabilised. This means that most modern tank barrels are of a smooth bore variety. However, Fin stabilised projectiles can still be fired from a rifled barrel as well. In these cases the discarding sabot part of the round is fitted with a slipping band which rotates with the rifling, leaving the round fairly still. A small amount of spin is accepted, as this will in fact aid the discarding of the sabot. Once the sabot discards, the round is left with a high velocity and because of the small cross sectional area, has relatively low drag. These modern day KE rounds are known as armour piercing fin stabilised discarding sabot (APFSDS) rounds [4, 28, 37, 38]. The Bernoulli equation [44] can also be used to calculate the depth of penetration for KE rounds, however a constant (K) is placed in front of the equation to account for the velocity and non-perfect hydrodynamic penetration.

Materials commonly used for the penetrator have included Tungsten alloys and DU. Modern day armour solutions which have helped in trying to defeat these types of rounds include the use of ceramics and spaced armour [4, 28]. Figures 1.20, 1.21 and 1.22 show a modern APFSDS long rod penetrator, sabot arrangement and shell casing.

Figure 1.20 - A modern day APFSDS long rod penetrator.

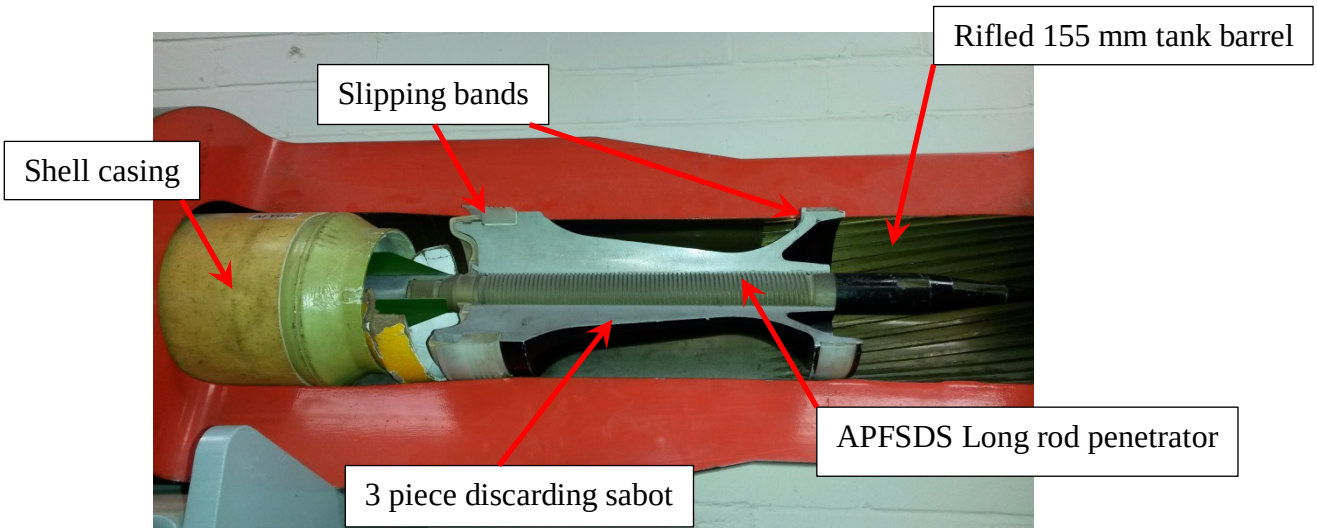

Figure 1.21 – An APFSDS long rod penetrator seen here mounted in a rifled 155 mm tank barrel. The barrel and sabot have been ‘cut away’ for instruction purposes, clearly showing how the penetrator sits within its sabot assembly. The Slipping bands can be clearly seen on the sabot. The top of the shell casing can also be seen on the left of the picture.

Figure 1.22 – A modern day APFSDS long rod penetrator, held in its sabot arrangement mounted on a 155 mm shell casing.

1.2.5 Small arms ammunition

Small arms ammunition is the name given to bullets and projectiles that are fired from weapons up to 20 mm in calibre. This includes pistols, rifles and machine guns.

Whether the round is fired from a pistol or a heavy machine gun, the makeup of the round is fundamentally the same (see figure 1.23). The round will have a casing which will hold a suitable propellant and a primer cap used to initiate the propellant when struck by the weapons firing mechanism. It will also consist of a bullet or projectile of a known calibre. There are many calibres available of small arms ammunition, common sizes include; 5.56 mm, 7.62 mm, 8 mm, 9 mm and 12.7 mm [37, 38].

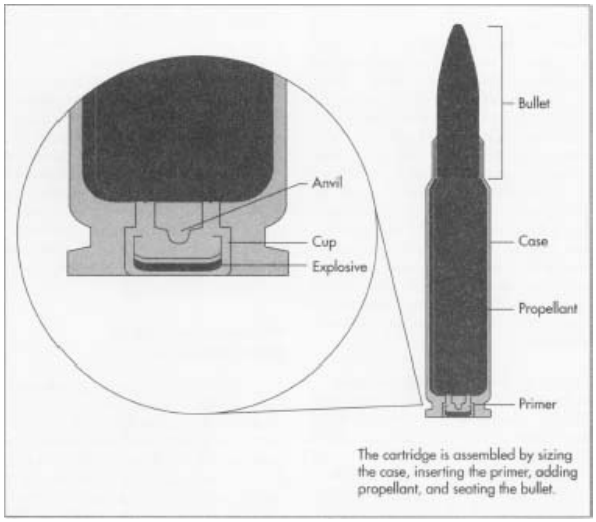

Figure 1.23 – Small arms round makeup [46].

The bullet part of the round can be one of a huge number available for use. These can be anything from soft 'ball' rounds to hardened Steel or Tungsten Carbide armour piercing (AP) rounds. Short range, pistol bullets have a low velocity and do not need to be overly stable during flight as great distances do not need to be achieved; consequently, ballistic shape is less important. A common low velocity bullet shape is the 9 mm parabellum bullet, which is short and snub nosed. Another design feature of hand gun bullets is their ability to cause maximum damage. Due to the shape of most low velocity bullets, they naturally tumble when penetrating. Types of low velocity bullet include; Hollow points, soft nosed and semi-jacketed amongst others. These low velocity bullets are not considered further in this thesis and the reader is directed to Ref. [37, 38] for any further information.

Long range bullets fired at higher velocities, such as the 7.62 x 51 mm AP FFV (used in the experiments for this study) are long and thin and have pointed tips [37, 38]. Most modern day rounds employ the use of a 'jacket'. Jacketed bullets were first used in the late nineteenth century, where it was found that solid lead bullets were breaking apart in the barrel and causing huge amounts of damage. Another type of bullet jacket, or shell casing, was used in the late 1890's. Developed by Russian admiral Stepen Makarov, sheets of Steel were used to encase the tips of large 15 inch projectiles fired from heavy naval guns. The Steel tip added to the projectile was there to help cushion the hard Steel round from initial impact. These became known as 'Makarov tips'.

The first jacket materials were made of cupro-nickel. A cheaper gilding metal (10% Zinc and 90% Copper) is used in modern small arms ammunition. Mild Steel coated with a cupro-nickel or gilding metal is also sometimes used on modern rounds – such as the 7.62 x 51 mm AP FFV round employed in this study.

The bullets jacket is there to serve several purposes, some of which include to engage with the rifling in the barrel to create spin and a gas tight seal and to give confinement or cushioning to the core material to aid penetration, as the theme of this study aims to prove. The jacket also helps to provide an optimum aerodynamic shape to reduce drag during flight.

1.2.6 Incendiary and Tracer rounds

Other bullets available for use include incendiary rounds and tracer rounds. Modern day incendiary rounds, as their name suggests, contain a small amount of high explosive in the tip of the bullet. As the bullet hits the target and starts to penetrate, the explosive charge is initiated. Incendiary rounds are commonly used against light armoured vehicles and aircraft. Traditionally the inclusion was a highly flammable compound such as phosphorous.

Tracer rounds are similar in construction to incendiary rounds, but instead of having an explosive filler, they will quite often have a layer of a reactive metal within them. This metal is usually Zirconium or Magnesium. The employment of a tracer round is designed to provide a gunner with correct aim and to highlight the target area in question to other firers (although this also gives away the source of fire, effecting survivability). Upon initiation of the propellant within the bullets case, the heat produced causes the added metal to burn. The metals included are chosen because they burn with a bright light, therefore showing a visual path of where the bullet is aimed. Tracer rounds are usually fired alongside other rounds, so they must be ballistically matched to the rounds they are fired with [37, 38].

Figure 1.24 – A range of rounds with varying calibres and shapes, from handgun at the extreme left to rifle and shot gun to the right [47].

1.2.6 Armour-piercing (AP) rounds

Solid bullets are known as ‘Ball’ rounds. This name comes from the use of lead balls as musket rounds. Lead or lead antimony is still used as the basis of solid cored soft, deforming rounds because of its high density. The higher density imparts more kinetic energy into the round, without increasing its volume. The greater the kinetic energy a round has the greater the energy it can impart into a target during penetration. An example of a soft cored modern day round is the Soviet M67 7.62 x 39 mm round, which comprises of a soft lead antimony core and a Copper gilding jacket. The idea of having a soft core is that the core will deform and yaw during penetration, causing cavitation within the target. This will then cause maximum damage to flesh and internal organs. Soft lead cored bullets are commonly used against un-armoured targets [37, 38, 48].

Where penetration of an armour system is required, armour piercing (AP) ammunition is used. As their names suggests, AP rounds are designed to defeat amour systems. The same as other small arms ammunition, their makeup comprises of a jacket and a central core, pressed into a case containing propellant. In order to defeat protection systems the core is comprised of a hard (strong) material – typically Steel or Tungsten Carbide – Cobalt (WC-Co) e.g. M43 7.62 x 39 mm and Forenade fabriksverken (FFV) AP 7.62 x 51 mm [49] rounds respectively. As harder armour solutions have developed (e.g. Boron Carbide – B_4C rather than Alumina - Al_2O_3), use of WC-Co cores is becoming slowly more prevalent due to its

higher hardness (1320 Hv / 750Hv for WC-Co / Steel respectively). An example of a common Steel-cored armour piercing round is the Soviet M43, comprising of a Steel core surrounded by a lead antimony filling. This is then encased in a Copper gilding jacket approximately 0.75 mm thick. The nose of the penetrator is flattened (see figure 1.25). This is designed to cause maximum damage once penetrated, as the penetrator will yaw within the target causing cavitation. The inclusion of ceramics into personal armour has greatly reduced the casualty rate against this round [28].

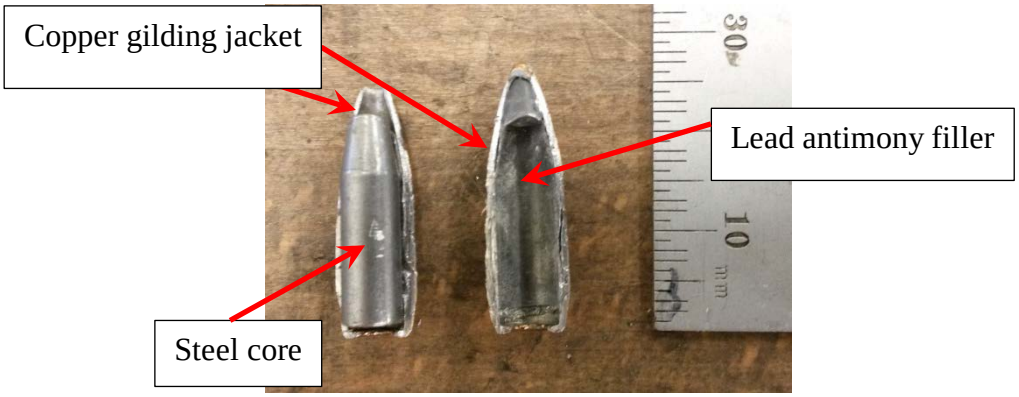

Figure 1.25 – A sectioned M43 soviet round, showing the core and lead filling.

Another common AP round is the FFV AP 7.62 x 51 mm round. This round is one of only a few rounds that employ the use of a WC-Co penetrator. This coincidently was the round selected for the aims of this study. The round has a fairly simple makeup compared to the M43, pictured in figure 1.25. This comprises of a Copper gilding jacket, approx. 0.60 mm thick, a WC-Co penetrator, and a small Al cup that the penetrator sits in. As can be seen in figure 1.26, the penetrator has a conical nose which comes to a point, for maximum penetration into the target. Another round which employs the use of a WC-Co penetrator is the 7.62 x 51 mm Sniper 9 round (see figure 1.27 for core comparison). This resembles a FFV, but the penetrator has a double angled nose cone, allowing for the bullet to have an overall more streamlined appearance, to cope with the higher velocities and greater distances needed for this application.

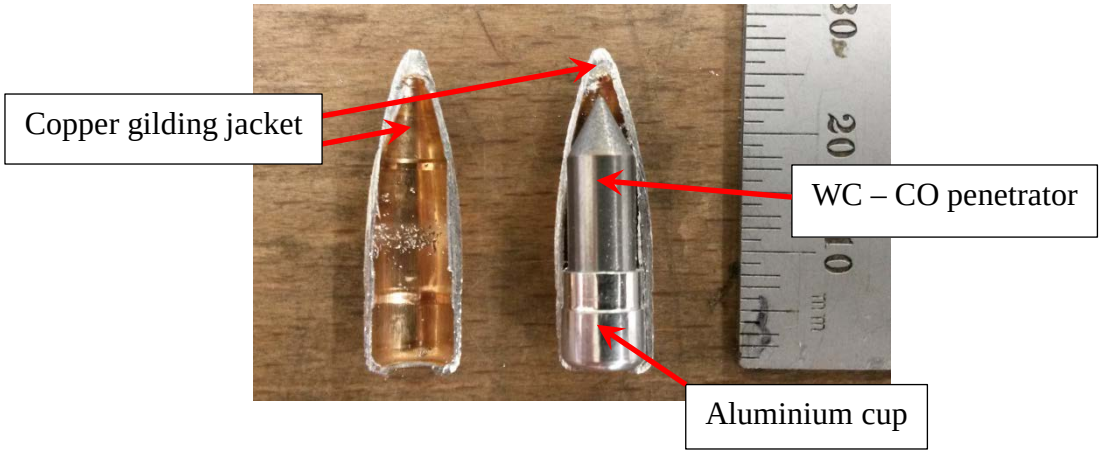

Figure 1.26 – A sectioned 7.62 mm AP FFV round, showing the core and Al cup.

Figure 1.27 – WC-Co core comparison. Left of the image is a core from a FFV round (employed for use within this study). Right of the image is a WC-Co core from a Sniper 9 round. Note the double angled penetrator and the longer length.

As WC-Co makes such a good armour penetrator, a significant number of studies have focused on the properties of this material. For example, Martineau *et al.* [50] looked at penetration of naval armour-relevant high-strength low-alloy (HSLA) 100 Steel using simplified geometry saboted 6.40-mm diameter WC-Co spheres launched at 0.8-2.5 km/s using a powder gun. The effects of impact on the 51-mm thick targets were analysed post-

impact by measuring the properties (depth, volume and diameter) of the resultant crater, with residual strains / stresses monitored via analysis of deformation when target specimens were sectioned. It was noted that the maximum stresses, above the yield stress of the material, were found at least one crater diameter under the resultant crater's floor. This was present on all targets impacted. It was postulated that if further stresses were to be added to this area it would lead to cracking and total failure of the material. It was recommended further work was examined around this concept. The experimental results were also compared to numerical simulations produced by the investigators. The models showed that the increase in velocity of the projectile had a direct comparison to the increase of crater size. This was found to be a linear increase. However, when analysing the experimental data the increase in velocity didn't correspond with the resultant crater. This inconsistency was also backed up by experimental findings of others. The differences were thought to be down to the slight differences in the structures of the material tested.

In similar tests conducted by Hazell *et al*. [51], 12-mm diameter WC-Co spheres were accelerated into WC-Co targets (symmetric impacts) at velocities ranging from 28 to 484 m/s to investigate the failure mechanisms of materials used to make hard armour piercing projectiles, such as the penetrator of the 7.62 x 51 mm FFV round used in this study. The projectiles were accelerated using a gas gun with Helium and compressed air as the driving gases. A Phantom V12 high speed camera was used to record the impact event.

The WC-Co targets were observed to cause the projectile material to flow radially out from the point of impact, the characteristics of interface defeat. As with the work produced by Martineau *et al*. [50], an increase in impact velocity showed a non-linear increase in depth of the resultant crater. The authors also used numerical simulations to model these phenomena and found that it was due to the cracks forming in between the grains of the target material. The modelled data matched the experiment data produced.

After experiments were conducted fragmented target material was recovered from the target chamber and the impact was re-created by piecing together the debris found. From this the authors were able to deduce that the WC-Co targets failed the same way as conventionally indented ceramic. A Hertzian cone [15] was formed in front of the penetrating projectile. It was also found that a 6.35-mm thick target of the same material as the projectile would defeat that projectile up to velocities of 280 m/s, where interface defeat was witnessed. Above these velocities the projectile would penetrate with minimal interface defeat. Using the data and

numerical modelling the authors were able to simplify the information needed for future simulations required to understand the penetration mechanisms of WC-Co projectiles.

To compliment the work produced in Ref. [50], a series of experiments were conducted by Herlaar *et al*. [52] investigating symmetric impact of WC-Co penetrators. The target penetrator was held in a clamp with the back of the penetrator (the flat end) facing the muzzle of the barrel. A saboted penetrator of identical material, e.g. also comprising the core of a 7.62 x 51 mm FFV, was launched down the barrel of a powder gun backwards, so the flat faces of the penetrators impacted. Tests were conducted from 250 to 500 m/s. The resultant impact was recorded using high speed video (HSV).

It was observed that the projectile rapidly eroded, crushing the target core. Material from both cores was ejected. It was postulated that a compressive wave was initially moving into the target core from the projectile and both the projectile and target fractured along their lengths. As the velocity increased the fracture behaviour changed with fragments from the impact faces becoming smaller.

The authors concluded that the defeat of the core lies with brittle fracture with no plastic deformation witnessed.

Scanning Electron Microscopy (SEM) was also used to view the cores after impact. It was seen in many cases that cracking had occurred between grain structures, a finding consistent with the simulations conducted by Hazell *et al*. [51].

The results from Ref. [50] are of direct relevance to this project. It is clear that, un-protected, hard AP cores are prone to failing in a brittle manner – something which would reduce their ability to penetrate the target. In this way, we can immediately see how the jacket of a bullet must play a role in the penetration process by protecting the core, or cushioning it, from the compressive waves produced on impact. This is a role hinted at, but not sufficiently elucidated in some elements of the literature Ref. [27, 48, 61], and which this study aims to further investigate.

1.3 Computational simulation

The use of computational modelling / simulation, can in some cases reduce the need for experimental programs and, therefore, increase the efficiency of subsequent (armour) system development. Having said this, computational modelling does have its disadvantages too. Such models cannot account for 'real life' situations that affect an experiment, such as experimental and human error, weather factors and unexplained material behaviour. Computational modelling, as used by the authors of Ref. [7, 13, 22, 48, 50, 51], is usually employed to help evaluate and support the results gained through experimental data. Ansys® Autodyn is a common computer simulation program – a hydrocode – which can help model blast, impact and penetration events [53]. Hydrocodes are computer codes which can model fluid behaviour by monitoring the external and internal effects of a pre-defined mesh of cells (a common mesh used in modelling is the Lagrangian mesh), which represents the system being simulated [54]. Hydrocodes simulate motion of a system by solving mass, momentum and energy conservation relations subject to pre-defined boundary conditions [53]. To be able to successfully simulate a system operation, three basic components must be considered: 1) an equation of state (EOS) for materials being simulated; 2) a strength model and; 3) a failure model [55]. Stresses within the material are considered by separating the stress in question, into the hydrostatic (fluid-like / pressure) and differential / deviatoric (strength-related / stress) components. Essentially, strength modelling governs the stresses which are developed within the modelled material, while the equation of state relates (hydrostatic) pressure to the volumetric strain and internal energies. In essence, the strength model relates differential stresses to differential strains, which then enables modelling of shear distortions within the modelled materials. The failure model governs the failure modes of the modelled materials. An erosion model is another numerical mechanism that is employed during modelling that allows for the deletion of elements, removing highly distorted elements of the model before they become degenerated. Erosion models are employed when using Lagrangian models. With Lagrangian models the cell size will get comparatively smaller as the model runs; erosion models therefore allow for cells to be discarded when overly distorted. As an added benefit, removing information from the model can also help the model run significantly faster.

While computational simulation has only been employed in a supporting manner in the current study, it is worth briefly highlighting the extent of its use – and thus its important role

in ballistic studies more generally. As an example, in recent work, Hazell *et al*. [22] employed Ansys® Autodyn to study the ballistic impact of lead-cored rounds on glass faced, resin targets (previously addressed in section 1.1.4). For these experiments a two dimensional (2D) model was produced using a Lagrangian mesh. The same approach was adopted by Zhang *et al*. [56] when modelling hypervelocity impacts into laminated glass. Both authors employed the use of the Johnson-Holmquist (JH) ceramic model [57]. This model has been shown to provide the user with good results when modelling the failure modes of ceramics, such as laminated glass, when under ballistic impact. The JH model was applied to the laminated glass in both Refs. [22, 56] and a Smooth particle Hydrodynamics (SPH) processor was applied to the bullet used. A SPH processor is an addition to the numerical simulation which allows for the successful modelling of brittle materials due to the avoidance of erosion and ability to accommodate separation of the modelled material due to cracking. Applying it to the bull*et al*lowed simulation of the extensive deformation and material separation that was observed experimentally. The bullets jacket was also modelled using a Lagrangian mesh. This would allow for the modelled jacket to flow and deform as witnessed, again, during experimentation. Both authors, Ref. [22, 56], found similarities between the modelled data and the experimental data in the way the laminated glass performed under ballistic impact and what was witnessed experimentally. The authors also concluded that the use of the numerical simulations helped to glean evidence of the deformation and defeat of the incoming round at various time intervals, something which experimentally, would be difficult to capture. The models also showed the deformation and stripping of the bullet jacket during penetration. These studies highlight the potential applications of numerical simulations – in no small part as, given good agreement with experiment / consequent confidence in the models, the authors were able to extend their studies while minimising (expensive) experimental work. Importantly, although sometimes not the main thrust of an experimental programme, these authors also showed that, under the right conditions, even relatively simple models can help to support and evaluate conclusions derived.

1.4 Bullet jacket effectiveness

The behaviour (underlying mechanisms, optimisation, etc) of armour materials and threats has been extensively investigated for many years. However, the study into the role of a bullet's jacket during penetration has had relatively little attention. One potential explanation for this is the bullet jacket material being very thin (typically 0.6 to 0.7 mm) and relatively soft compared to armour materials, leading to an underlying assumption that relatively few gains are available from its investigation / optimisation. To this end, only a limited amount of work has been undertaken in this field.

In 2010 a study was undertaken by Forrestal *et al*. [58] into the perforation of 7075 T-651 Aluminium using armour piercing 7.62 mm APM2 projectiles. The projectiles were fired from a rifle on an experimental range at velocities ranging from 600 to 1,100 m/s. The APM2 projectiles employed are made up from a hardened Steel, ogive nosed core surrounded by lead filler and then the gilding jacket. The study was undertaken to better the understanding of penetration mechanisms of this type of projectile perforating Aluminium targets (with the hardness of the cores greatly exceeding that of the target). The targets employed possessed thicknesses of 20 and 40 mm. The 40 mm targets were made up of two 20 mm targets adhered together using a 12 hour setting epoxy. The initial firings against the 40 mm targets showed that the gilding jacket and lead filler were completely removed from the Steel core during penetration. Based on this, the authors decided to remove the gilding jacket and lead filler from some projectiles and just fire the core into the Aluminium. From the experimental results, the authors concluded that the jacket had very little or no effect on the penetration of the Aluminium targets.

The authors concluded that their work matched previous work they had done on perforation of 5083-H116 Aluminium armour plates using ogive nosed rods and 7.62 mm APM2 bullets [59]. The perforation of the armour plates by the ogive nosed rods was intended to produce experimental data to back up numerical simulations produced on the penetration mechanics of this type of Aluminium armour plate. The same set up was employed as mentioned in Ref. [58], with only the target material choice changed. The authors also decided to fire the plain Steel core and match it to plates that had been perforated with a full jacketed, unmodified bullet. Analysis of results drew them to the same conclusions as in Ref. [58], in that the gilding jacket had little-or-no effect in the penetration of the Aluminium plates. Conclusions in both cases were derived by the authors measuring the ballistic limit velocities (the velocity

required for a projectile to reliably penetrate a material more than 50% of the time, as found in the NATO STANAG 2920[*]) of the armour plates. They found there was only a 1% to 8% change in the limits between the full jacketed rounds and core-only rounds on the 20 mm and 40 mm targets, respectively.

Corresponding to the assumption made by the authors of Ref. [58, 59], Hazell *et al*. [60] also concluded from their experimental work that the bullet jacket played a limited role in the penetration of a ceramic based target. The authors fired 7.62 x 51 mm FFV AP WC-CO cored rounds at explosively pre-loaded and intact ceramic (Alumina and Silicon Carbide) targets from an experimental gun on an indoor range. The rounds were fired with velocities up to 900 m/s. The work was undertaken to investigate the resisting stresses offered to a penetrating projectile from ceramic targets. It was concluded from this study that ignoring the bullet's jacket during penetration means that the penetration is from the kinetic energy of the core alone and that the tip of the jacket does not cause damage to the ceramic target.

However, in more recent work an MSc research project by Philbey. [48], the role of the bullets jacket is far more important than previously thought. Building on this research project, Hazell *et al*. [61] have produced one of the most complete works in this area to-date. This paper, using both data from the MSc and new research, used results from reverse ballistic experiments undertaken on a single stage light gas gun, forward ballistic experiments undertaken on an indoor range using an experimental gun and computational modelling, to start to interrogate the effects of the bullet jacket on penetration in more detail.

Reverse ballistic experiments were carried out, where a ceramic faced projectile (Alumina and Silicon Carbide in thicknesses of 5 and 10 mm) was accelerated into a stationary bullet at velocities up to 850 m/s. The bullet was a 7.62 x 51 mm FFV AP round mounted on a framework to ensure the bullet was held on the centreline of the gun and in the centre of the field of view of the X ray heads. Upon impact, four X ray heads were triggered with each head being delayed to ensure a flow of images were taken for one experiment. For some of these reverse ballistic experiments, the bullets jacket was completely removed and the tests were undertaken on just the cores. The resultant images showed that damage occurring on the nose of the penetrator was far greater on the cores that had the jacket removed than the fully jacketed rounds. This led to a drop in penetration of the core and also a greater amount of

[*] NATO STANAG (North Atlantic Treaty Organisation Standardisation Agency) 2920 – Ballistic test method for armour materials and combat clothing.

surface defeat was witnessed on the X ray images of these un-jacketed rounds. Building on these results, it was also postulated that the tip of the jacket did actually start to pre-stress the ceramic in front of the penetrator.

Forward ballistic experiments, conducted on an indoor range with an experimental gun, were designed to complement the reverse ballistic work and showed similar results. The DOP technique was used as the main diagnostic for these experiments. Again, 7.62 x 51 mm FFV AP bullets were employed – with these accelerated into similar ceramics – but in this case with the targets backed by Aluminium and over a slightly higher velocity range of up to 900 m/s. The resultant depth of penetration was measured. Once again, some rounds used in these experiments were modified by having the nose of the jacket removed to reveal the WC-Co core. The results showed that targets impacted with a full jacket penetrated deeper than those without.

Computational simulations were also produced which backed up the experimental results found in the forward and reverse ballistic experiments. The modelling also showed evidence of the ceramic being pre-stressed and damaged by the tip of the bullet jacket.

The results of this paper concluded by suggesting the jacket plays one or several of the roles the experimental studies showed. The authors believed that the removal of the bullets jacket enabled the cores to be damaged earlier on in the penetration process, and allowing for a greater amount of dwell to occur on the surface of the ceramic. Dwell of an incoming round or munition is where the penetration is paused or resisted by the armour material. During this time the round is behaving hydrodynamically and is ‘flowing’ on the surface of the armour. If the kinetic energy of the round is great enough it will eventually start to penetrate the armour material. This is known as the dwell-to-penetration transition. All of the cores recovered from the reverse ballistic experiments, along with the associated X rays, showed greater damage to the nose of the core where the jacket had been previously removed. It was also stated that if the bullets jacket could be removed prior to encountering an armour material, the effectiveness of that armour material could be enhanced. This conclusion sits in line with the aims of this study. Overall, this paper and that of Philbey [48] – and its contrast to previous studies, serve to emphasise the relatively limited body of knowledge currently existing in this area.

The ability to pre-stress the armour material was also evident in work carried out by Gooch *et al*. [62]. The authors used reverse ballistics on a 100 mm single stage light gas gun to image

the penetration of Boron Carbide ceramics using a flash X ray system. The results of these experiments also concluded that the tip of the bullets jacket with the lead filler used on an APM2 round, played a considerable role in the interaction between the penetrator and the ceramic.

The other major conclusion from the results of Ref. [61] was that the bullet jacket acts as a buffer or shock absorber between the target and the hard WC-Co core. Other work has shown that the inclusion of a buffer material helps to extend the dwell time of a projectile against silicon Carbide targets. In particular, it has been demonstrated that the inclusion of a Copper (Cu) buffer plate on the surface of a target can lead to an increase in terms of the impact velocity needed for the dwell-to-penetration transition to occur. It is postulated that the buffer works by attenuating the shock from the projectile, therefore leading to a gradual loading of the target face [63, 64, 65].

More recent work conducted by Crouch *et al*. [27] also shows the importance of the role of the bullet jacket. For these experiments a 7.62 x 39 mm M43 Steel core round was used in the reverse ballistic configuration. Experiments were conducted on a single stage light gas gun, employing the use of a flash X ray system to monitor the impact event. The target materials were accelerated into the stationary bullet at velocities ranging from 697 to 739 m/s, encompassing the typical muzzle velocity of this type of round. The targets were comprised of a mixture of plain Boron Carbide (B_4C) targets, B_4C targets that were clad with an aramid fibre set with epoxy, B_4C targets backed with UHMWPE and finally B_4C targets that had an aramid cladding and a UHMWPE backing. Some experiments were also conducted with CFRP and UHMWPE targets, to investigate jacket stripping materials.

Rounds used were either fully jacketed or just the Steel core. A baseline was set by impacting fully jacketed rounds and cores with plain B_4C. As an additional diagnostic, after each firing the damaged core was recovered post shot and the final length was ascertained after dwell had occurred. Even against the plain B_4C a difference was noted in the X ray images and in the resultant length of the core, where the unjacketed rounds were notably shorter (20 mm to 14 mm for a jacketed round and a core only round, respectively against 3.1 mm of plain B_4C). The addition of a material on the front of the B_4C acted as a stripper material to help to strip the jacket away to leave the core more vulnerable to defeat. The resultant length of the damaged core each time would give an indication to the effectiveness of the stripper material introduced to the ceramic target. Essentially, the closer the final length to the baseline, the

better the material was at removing the jacket. The UHMWPE backing was in place to catch any debris that penetrated through the ceramic.

A set of experiments were also conducted that had the inclusion of a Copper buffer plate on the front of the ceramic target, in line with the approach described in Ref. [61, 62, 63] above. The Cu fronted ceramic targets were accelerated into core only projectiles. While only a very limited number of experiments were conducted, the results gained from these experiments showed the exact same results as the plain B_4C targets accelerated into jacketed projectiles. It was concluded that the buffer was having the same effect as the jacket and filler material of the fully jacketed rounds. In addition, in line with previous work, computational modelling (using Ansys® Autodyn) was also undertaken, the results of which backed up the experimental results.

This result, as with the conclusions of others, is particularly intriguing as it appears to suggest that the main role of the bullet jacket is one of protecting the bullets core through absorbing the shock that the target material imparts back into the round. As the results discussed above seem to suggest, this element of the role of the bullet jacket appears to be more apparent than that of acting to laterally restrain (confine) the core. This is the fundamental mechanism which will be investigated during this study. Similar results appear to be evident in the experiments conducted by the authors of Refs. [27, 48, 61, 62, 63, 64], all of which involved adding a Copper buffer plate to the surface of the target material. These target materials were then impacted by a modified round or a bullet core only and the same results are apparent as the fully jacketed rounds. However, as touched on above, the results presented in the recent work by Crouch *et al*. [27] were limited in extent – further such work has not been taken to the stage of trying to properly exploit this element of the penetration mechanism for penetration resistance, meaning that this avenue of research still needs to be pursued further.

1.4 Summary

This literature survey has highlighted the interplay between threats and protection (armour) over the years. In particular, the wide range of threats and counter-measures which can be deployed against the same has been identified. Within this gambit of systems, small arms present a unique threat, not least as they are often targeted directly at the most vulnerable elements on a battlefield (personnel). While ceramic armours are efficient against such threats, AP rounds (most recently with heavy WC-Co cores) are becoming more prevalent – negating the effectiveness of such protective solutions. To this end, development of enhanced ceramics (such as B_4C) is clearly an important area. However, in addition to this, if the way in which these ceramic materials are to be employed is to be optimised, a fundamental understanding of the underling mechanisms when a projectile impacts a target is clearly required. Such knowledge will open an avenue to develop new and novel techniques to optimise ceramic armour systems.

Overall, the results gained by the authors of the papers reviewed in this literature survey appear to suggest that if the bullets jacket could be pre-stripped from the bullet core, the core would very likely be more vulnerable to earlier defeat by an armour material. It is tentatively suggested that such an approach could lead to the redesign of armour systems allowing for materials used to be either ballistically more efficient or, alternatively, lighter and thinner and more cost effective while providing the same required level of protection. Numerical simulation has also been shown that it can be used to help support and evaluate experimental results and aid in the design of an armour system. This would be advantageous in the evaluation of events during experimental programs that would otherwise be extremely difficult to be viewed. To this end, in this thesis a series of iterative experimental campaigns have been undertaken with the aim of investigating both potential approaches to, and benefits of, pre-stripping the jacket from an incident round attacking a ceramic fronted target. In addition to the potential practical benefits of such an approach, it was anticipated that this investigation would provide further empirical evidence with regards to the nature and extent of the underlying influence of the jacket on the penetration process. Such information would be inherently novel and of direct application to the development of future numerical simulations / optimisation of armour systems.

2.0 Materials

A wide variety of materials was employed in this work. These broadly fell into three categories, those used for stripper plates, target materials or backing blocks (for DOP experiments) and projectile materials. Materials were selected for a variety of reasons. In particular, for stripper plates, the focus was on provision of as wide a range of properties as possible, with the aim of providing additional insight into the influence of material properties on interaction with a projectile. In this section materials employed are detailed, along with a discussion of the key material properties considered.

2.1 Material properties

The key material properties to help in the jacket stripping and round defeat process considered in this study were -

- Hardness - Young's Modulus - Hugoniot Elastic Limit (HEL)
- Density - Acoustic Impedance - Shear Strength
- Acoustic wave speeds - Yield Strength

These properties are explained in the following chapter, along with details of how each was measured. Hardness or the resistance to penetration. Vickers hardness values were employed, measured using a Highwood Indentec HWDM – 7 micro hardness machine (see figure 2.1). The machine was calibrated using a 700MHV hardened Steel block before samples were tested in order to ensure accuracy of measurements / allow for potential wear to the indenter. All samples were tested on both sides and in a variety of different places across their surfaces, with an average taken to achieve the final hardness values seen in table 2.1 and 2.2. The idea of this approach was to allow for any local variations in material properties (e.g. as a result of heat treatments, etc). To successfully record hardness values for the round employed (jacket and core), the round was encapsulated in Bakelite, allowed to cure and then polished back to reveal the jacket and core. It was anticipated that this process – which involved microstructural specimen preparation techniques – would have been relatively gentle and would have imparted minimal heat into the sample (as lubrication was employed), thereby negating any potential thermal effects. Hardness measurements were then taken from the polished surfaces (see figure 2.2).

Another key property considered was material density (ρ). Density was measured using a Mettler Toledo XS105 Dual range immersion density machine (see figure 2.3). The machine was left to settle and calibrated before use. The equipment initially required the original mass of the sample to be ascertained by placing it on a flat plate, above the basket. The temperature was then taken of the de-ionised water in the beaker and the materials were then loaded into the sample basket for testing. The rationale for noting the water temperature – which was inputted into the machine – is that the volume of the water changes slightly with a change in temperature. The machine works on Archimedes' principle – where a sample suspended in a fluid is buoyed by a force equal to the weight of the fluid displaced by the sample. The machine calculates the density by measuring the mass of the sample in the air against the mass of the sample in the water. While density can also be calculated by mass divided by volume, for simple geometry samples where the volume can be calculated easily, the use of this balance-based system ensured a high degree of repeatability and accuracy (for example, measurements were not allowed until the mass being measured in grams was stable to 5 d.p.). Density measurements for the samples considered here can be seen in table 2.1 and 2.2.

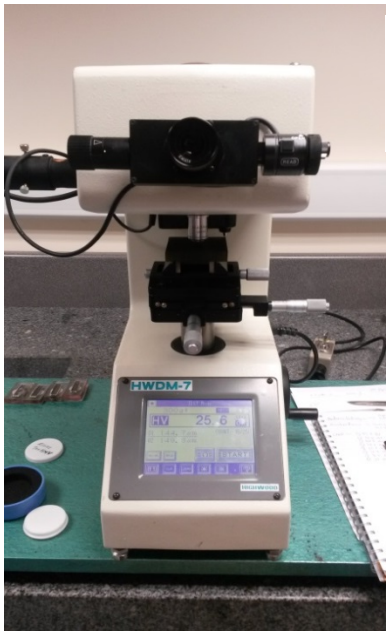

Figure 2.1 – Highwood Indentec HWDM-7 micro hardness machine.

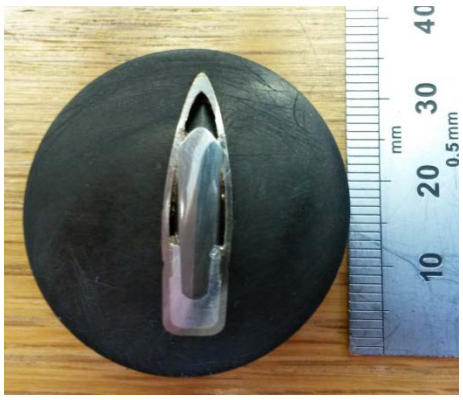

Figure 2.2 – Mounted and polished FFV.

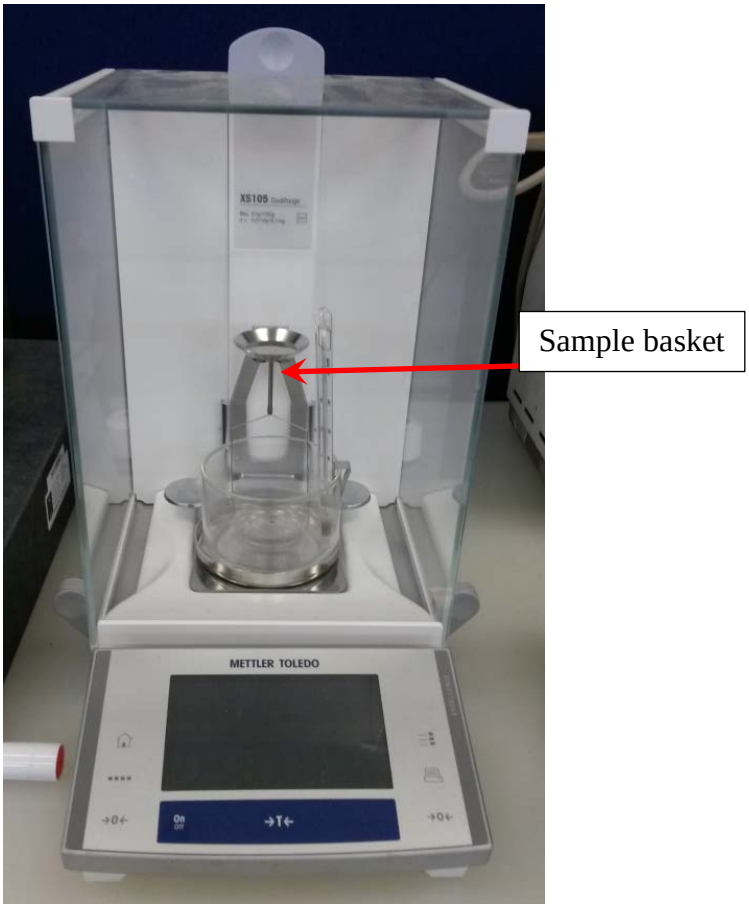

Figure 2.3 – Mettler Toledo XS105 Dual range immersion density machine.

Acoustic wave speeds (C_0, C_l and C_s → *bulk, longitudinal and shear sound speeds respectively*), were also measured and recorded. These were determined via ultrasonic testing, using Panametrics ultrasonic transducers operating in the pulse echo configuration at 1-5 MHz (for longitudinal sound speed, C_l values) and in the transmit and receive configuration also at 1-5 MHz (for shear sound speed, C_s values). In the former configuration a single transducer both transmits and receives the ultrasonic pulse, while in the latter pulse-receive setup, useful for either attenuating samples or (as in this case) harder to couple shear waves, a separate transducer was used at each side of the sample under test. Time of flight data combined with knowledge of sample thicknesses (determined using a micrometer) allowed C_l and C_s values to be calculated. These were then used to calculate bulk C_0 values as detailed in equation 2.1. Acoustic wave speeds, representing the average of a series of measurements, can be found in in tables 2.1 and 2.2 for the materials considered here.

$$c_0 = \sqrt{c_l^2 - \frac{4}{3}c_s^2}$$

Equation 2.1 – Equation for bulk sound speed (C_0)

C_0 values were also then used to calculate Young's modulus (resistance to flexure), (*E)*, for the materials selected for use. Moduli values were calculated (using equation 2.2) from the measured acoustic wave speeds (C_0) and density (ρ). In addition, some Young's moduli were calculated via tensile testing (e.g. taking the gradient from the linear region of the recorded stress-strain curves). Calculated values of *E* for the materials considered in this study can be found in tables 2.1 and 2.2.

$$E = \rho_0 c_0^2$$

Equation 2.2 – Equation for the calculation of Young's Modulus (*E*).

Acoustic impedance (a measure of the ability to couple an incident shock wave), (*Z)* was another material property that was decided would help in aiding to strip the bullet jacket and in the defeat of the round. Values of Z were calculated using equation 2.3, from measured densities (ρ) and Young's modulus values (*E*). Results are presented in tables 2.1 and 2.2 for the materials considered here.

$$Z = \sqrt{\rho_0 E}$$

Equation 2.3 – Equation for the acoustic impedance of a material (*Z*).

Yield strength (σ_y; where a materials properties change from elastic deformation, this is the stress at which a material beings to plastically deform due to an applied force): yield strength values taken from appropriate sources in the literature, Refs [4, 70, 71, 72, 73, 74, 75] and from tensile testing as-appropriate. Yield strength can be directly related to hardness, as the

two properties are measuring similar material conditions. When hardness measurements are taken, the indenter measures the resistance the material gives to the penetration of the indenter. The measurement of yield strength is similar, involving measurement of the point at which a material starts to deforms plastically, such as the point at which plastic material deformation results ahead of a penetrating hardness indenter. As a general 'rule of thumb' hardness is approximately three times the yield strength of a material. Where values were determined experimentally, samples were tested on a Houndsfield universal testing machine (see figure 2.5), with an applied force of 25 kN. The samples were pulled at a rate of 5 mm / min. Samples of each material tested were first machined to comply with testing standards and then mounted in the machine (see figure 2.6). Values seen in table 2.1 were calculated / taken from the resultant graphs. Tensile testing was also used in some cases to produce Young's modulus and calculated shear strength values (see tables 2.1 and 2.2). Force applied (Newtons) against elongation (mm) graphs were produced by the testing machine; see figure 2.4, for a typical Steel tensile test graph. From the graph not only is the position of the yield strength apparent (labelled), but that of the ultimate tensile strength (UTS) of the material, as well as the point where the material failed. Graphs showing the tensile tests for the other materials used can be found in appendix 1.

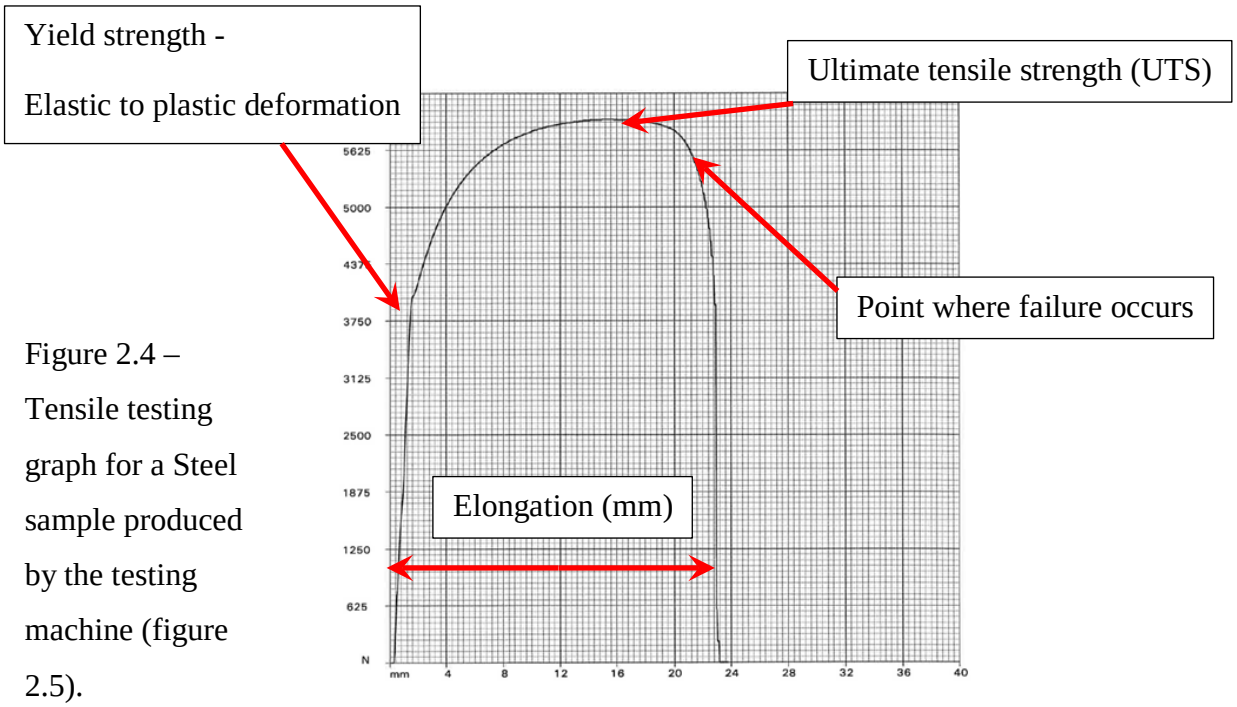

Figure 2.4 – Tensile testing graph for a Steel sample produced by the testing machine (figure 2.5).

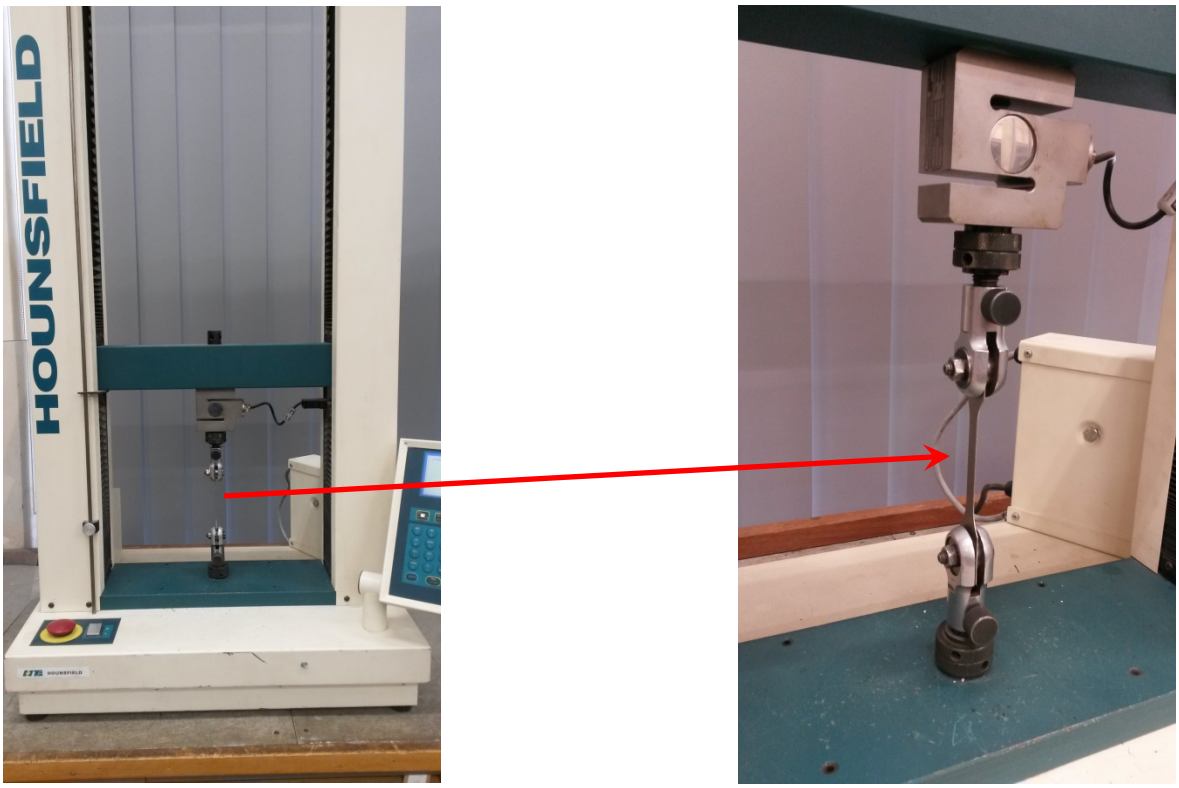

Figure 2.5 – The Houndsfield universal testing machine employed for tensile testing in this project (left) and, figure 2.6 – a Steel sample mounted ready for testing (right).

Hugoniot Elastic Limits (σ_{HEL} – HEL) or dynamic yield strengths were also ascertained for the stripper materials tested. The HEL is defined as the point where a material changes from elastic deformation to plastic deformation under loading from an introduced shock wave. If the introduced shock wave is below the HEL limit, one wave will propagate through the material; this will be elastic in nature. If the applied shock is higher than the HEL (assuming the system is not 'overdriven' – e.g. shocked so hard that the elastic wave is no longer apparent), two waves will propagate through the material, one will be elastic in nature and the other will be plastic. This plastic wave will deform the material, making it act in a fluid like manner. Above the elastic limit the wave velocity increases with increased pressures [41]. HEL values were taken from a combination of in-house plate-impact experiments and appropriate literature sources. Values for the differing materials considered are presented in tables 2.1 and 2.2.

The last property considered was the shear strength (τ) of the chosen stripper plate materials. The shear strength of a material can be described by the *strength* of a material or component against the type of yield or structural failure where the material fails in *shear* – namely a

sliding failure that occurs on a plane that is parallel to the applied force. In terms of ballistic shear failure it is the difference between the target material failing on the surface and 'tearing' as the projectile penetrates or the failure occurring through the target material; further, a 'plug' of material will then form and be pushed ahead of the projectile. Shear strengths were calculated from measured / referenced yield strengths using the measured or determined yield strengths multiplied by 6/10 – in line with an approach determined in Ref. [66]. Resultant yield strengths can be viewed alongside other material data in tables 2.1 and 2.2.

2.2 Stripper plate Materials

Four materials were considered that would have the appropriate properties associated with this study. These materials were -

- **Copper** – Copper C101 (99.9% pure Copper) was selected because it is a well characterised material with properties that were anticipated to be advantageous in this study. Some of these properties include good ductile strength, malleability, and the fact that it is relatively inexpensive. However, a significant disadvantage of Copper from the perspective of a stripper pate is its high density.

- **Aluminium** – Aluminium AL6082 (an alloy of Aluminium, Manganese, Magnesium and Silicon) with a temper of T651 (solution heat treated, stress relieved by stretching and then artificially aged) was selected due to Aluminium's existing application as an armour solution, Ref [6] (figure 1.2). Further, Aluminium has several potentially advantageous properties for use as an applique armour element such as a stripper plate – namely, low density and expense, the fact that it is already well characterised and its ready availability in a wide selection of hardness's and tempers.

- **Steel** – Steel is available in a huge variety of alloys and compositions as well as configurations where properties change from one type to the next. For this study a standard Steel of EN3B (bright mild Steel bar) was selected. This Steel is readily available and has a wide range of suitable properties. Some of these include relatively high hardness compared to the other materials tested, the fact that it is inexpensive, its

wide range of existing uses (which helps ensure a ready supply), and its availability in several different forms (bar, plate, flat bar, sheet). Steel can also be used in thinner samples, therefore reducing the mass of the stripper employed. Further, Steels have been used for many years as vehicle armour on larger heavy fighting vehicles, Ref [14].

- **Carbon fibre reinforced plastic (CFRP)** – This material is available in an almost endless variety of forms. These can include different numbers and configurations of layers, type, volume fraction and weave of reinforcing fibres employed, the type, volume fraction and (set) density of the resin used, sample thickness, etc. The CFRP material selected for this study was a Biaxial 10 ply carbon fibre manufactured by Hexcel. The layup comprised a total of 5 x 45° and 5 x 90° orientated fibres, laid alternately in an RTM-6 resin matrix [26]. The CFRP utilised high tensile strength Tenax HTS 5361 aero grade fibres. This material was supplied by Short Brothers, Ireland, for impact work previously conducted by researchers in the Dynamic Response group at Cranfield University. Such CFRP material, although not used as an armour, has previously been used for impact testing and has been used as part of a composite armour solution [24, 27].

Material properties for the materials outlined above which have been employed in this study can be found in table 2.1 for literature values and again in table 2.2, for measured and calculated values.

2.3 Backing plate and projectile materials

The forward ballistic experiments employed in this study to investigate depth of penetration data used a semi-infinite backing material that comprised of several blocks of Aluminium Al6082 T651. The blocks were 100 x 100 x 25-mm thick. This material was primarily chosen because of its relative softness so that penetration would occur to a reasonable depth, in order to ensure that subsequent DOP measurements were as accurate as possible. It is also widely used in the research laboratory as a backing material for ballistic experiments due to cost and availability and has been employed in a similar way in previous studies [60, 61]. The size of

the backing blocks was determined because of availability and it gives a reasonable sized target to aim at on the small arms range at 10 m. Face dimensions of 100 x 100 mm also ensured (assuming a central impact) that any reflected shock waves moving in from the outside edges did not influence the penetration process of incident projectiles (e.g. the targets appeared semi-infinite in extent for the duration of the penetration process due to their much greater width than depth). This mechanism (e.g. premature tensile release arrival) could occur with smaller targets and may affect the nature of projectile penetration into the backing, giving a false indication of depth. Several blocks were placed together and secured with tape to ensure the round was captured. Initial DOP firings were undertaken with no armour / stripper plate present to both provide a baseline for subsequent calculations and to determine the total depth of backing material required in a worst-case scenario. Table 2.3 shows the material properties measured for the backing blocks.

The rounds employed for this study were 7.62 x 51 mm AP (Armour Piercing) FFV (Forenede Fabriksverken) rounds, with a Tungsten Carbide (WC-Co) core. The core is manufactured from Carbide – 5.2%, Tungsten 82.6%, Cobalt 10.5% and Iron 0.41% (percentage by weight) [67]. These rounds are otherwise known as M993 armour piercing rounds [68]. The round comprises of a hard Tungsten Carbide Cobalt (WC-Co) core sat in an Aluminium cup (see figure 2.2). This is then surrounded by a tombac (gilding material normally comprised of 90% Copper and 10% zinc) clad Steel jacket. The jacket is on average 0.6 to 0.75-mm thick. For relevant material properties for the rounds employed see table 2.3.

2.4 Material testing data

Material	Hardness (HV) [69]	Density (g / cc) [70][71]	Ultrasonic wave speeds (mm /μs)[4],[5]			Young/s modulus (GPa) [72]		Acoustic Impedance (g.mm/μs.cc) (calculated)	Yield strength (GPa) [73], [74]		Shear strength (GPa)
			c_l	c_s	c_0 (calculated)	Ultrasonic (calculated)	Tensile test		Tensile test	HEL	
Copper	100	8.92	4.70	2.33	3.85	132.48	115	34.38	0.325	0.5	0.195
Aluminium	95	2.70	6.40	3.15	5.27	74.87	69	14.22	0.295	0.4	0.177
Steel	276	7.82	5.91	3.24	4.58	163.68	207	35.78	0.350	1.7	0.210
CFRP	-	1.50	3.02	-	3.23	15.64	220	4.84	-	-	-

xx = Assumed C_0 is equal to Hugoniot intercept xx = Value for generic CFRP from ref [4]

Table 2.1 – Material properties for the stripper plate materials (literature values).

Material	Hardness (HV)	Density (g / cc)	Ultrasonic wave speeds (mm /μs)			Young/s modulus (GPa)		Acoustic Impedance (g.mm/μs.cc) (calculated)	Yield strength (GPa)		Shear strength (GPa) **
			c_l	c_s	$c_{0\ (calculated)}$	Ultrasonic (calculated)	Tensile test		Tensile test	HEL [65, 66]	
Copper	100.1	9.04	4.65	2.34	3.78	129.47	92	34.21	0.32	0.5	0.19
Aluminium	125.6	2.71	6.61	3.17	5.50	82.10	78	14.92	0.23	0.4	0.14
Steel	284.4	7.69	6.11	3.26	4.81	178.12	324	37.01	0.46	1.7	0.28
CFRP	66.1	1.32	3.24	2.34	1.79	4.22	105	2.36	*	-	

* = CFRP shows elastic behaviour up to the point of failure ** = Calculated from yield strength of material multiplied by 60% (0.6) as shear strength is usually taken as an estimation.

Table 2.2 – Material properties for the stripper plate materials (measured).

Material	Hardness (HV)	Density (g/cc)
Backing block – AL6082 T651	125.60	2.71
FFV core – WC-Co	1319.13	14.22
Bullet jacket – Tombac clad Steel	226.70	7.47

Table 2.3 – Measured material properties for backing blocks and rounds employed.

Note – In table 2.2 errors are estimated to + / - 10% where calculations and material properties have been derived from tensile testing / tensile test elongation graphs. This is due to the elongation recorded on the graph being a measurement of the elongation of the machine rather than the sample itself as an extensometer was not used in this case, directly connected to the sample. Features such as stretching of the carriage, slight bowing of the machine and the machines age are not, and in fact, cannot be accounted for.

2.5 Tensile testing

In order to investigate the core tensile (low strain-rate) properties of the key materials employed as stripper plates for the experiments described in this thesis, a series of tensile tests were conducted. These results are presented here, rather than in the materials section (section 2.0), as they provide additional context with regards to the experimental results presented previously in this section. Recorded displacement-time data (e.g. plots such as section 2.0, figure 2.5) were reduced to stress-strain graphs. Points from the displacement-time graphs were digitized and Microsoft® Excel was then used to produce the plots seen in figure 2.7 and 2.8. In this figure, all four materials are featured and can be directly compared.

- It can immediately be seen that Copper can withstand a large amount of stress and strain, indicated by the high rise and continued plateau, reflective of the high ductility of Cu. However, as has been demonstrated, ductility is not necessarily an ideal material property with regards to defeat of an incident round. Results taken from ballistic testing (section 4.1) show that Steel (a material that is hard and stiff – e.g.

with a high Young's modulus / resistance to flexure) is better at defeating an incident round. It seems that a higher resistance to bending (or flexure) *with* the incoming round is better as the material will 'push' against the round helping to strip the jacket and also, as such materials are typically harder, the stripping plate will also help to pre-stress the core. It is also worth noting that the first small plateau seen around 0.4 GPa is possibly due to the sample slipping in the jaws of the machine, as this feature is anomalous to Copper tests previously conducted by the materials department.

- The CFRP, as seen in figure 2.7 and more clearly in figure 2.8, can withstand a huge amount of stress (almost 0.35 GPa, 0.5 GPa higher than Steel) but very little strain. This is showing a typical brittle result, with the material only able to sustain minimal plastic deformation. This is due to the CFRP being made of several layers of stiff fibres in varying directions. Any small deviations seen in the results at the start are assumed to be matrix breakage and delamination of the layers. Even though CFRP can be seen to withstand a large amount of stress, it doesn't perform well on the ballistic tests (section 4.1). This shows that a suitable material must also be able to cope with strains applied to it (e.g. be tough – able to absorb a lot of energy up to the point of failure).
- The Aluminium shows a reasonable resistance to stress and strain, albeit supporting a lower stress than Steel and a lower strain than Copper. The lower strain reflects the materials higher elastic modulus, meaning the material is showing a better resistance to flexure and is thus more likely to successfully strip an incoming round.

The results taken from the forward ballistic experiments (Section 4.0) show that the Steel stripper plates outperformed the other materials in terms of successfully stripping the rounds and also helping to pre-stress and totally defeat the core. Figure 2.7 clearly shows that Steel has coped with a reasonable amount of stress (0.30 GPa) and strain before failure occurs. Consequently, it is apparent that even relatively simple tensile tests have the potential to help inform stripper plate material choice. For example, a material able to cope with larger amounts of stress than Steel, combined with the same amount or more of strain.

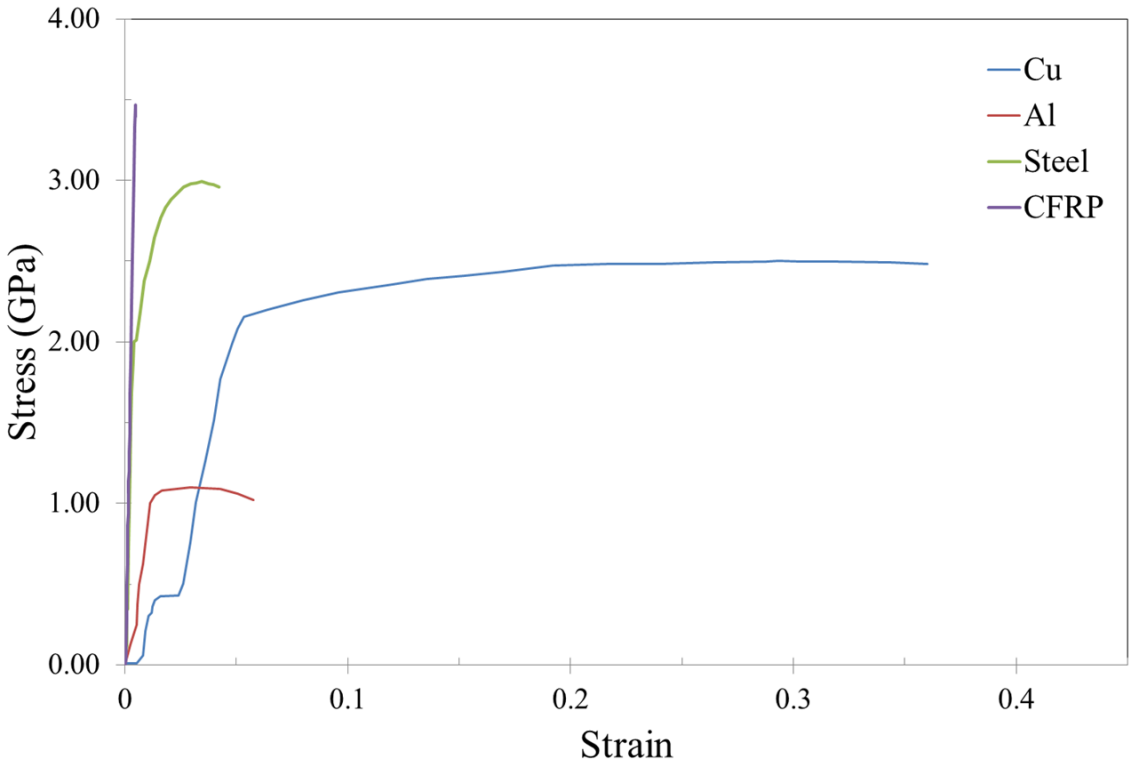

Figure 2.7 – Stress / strain graph showing all four materials used.

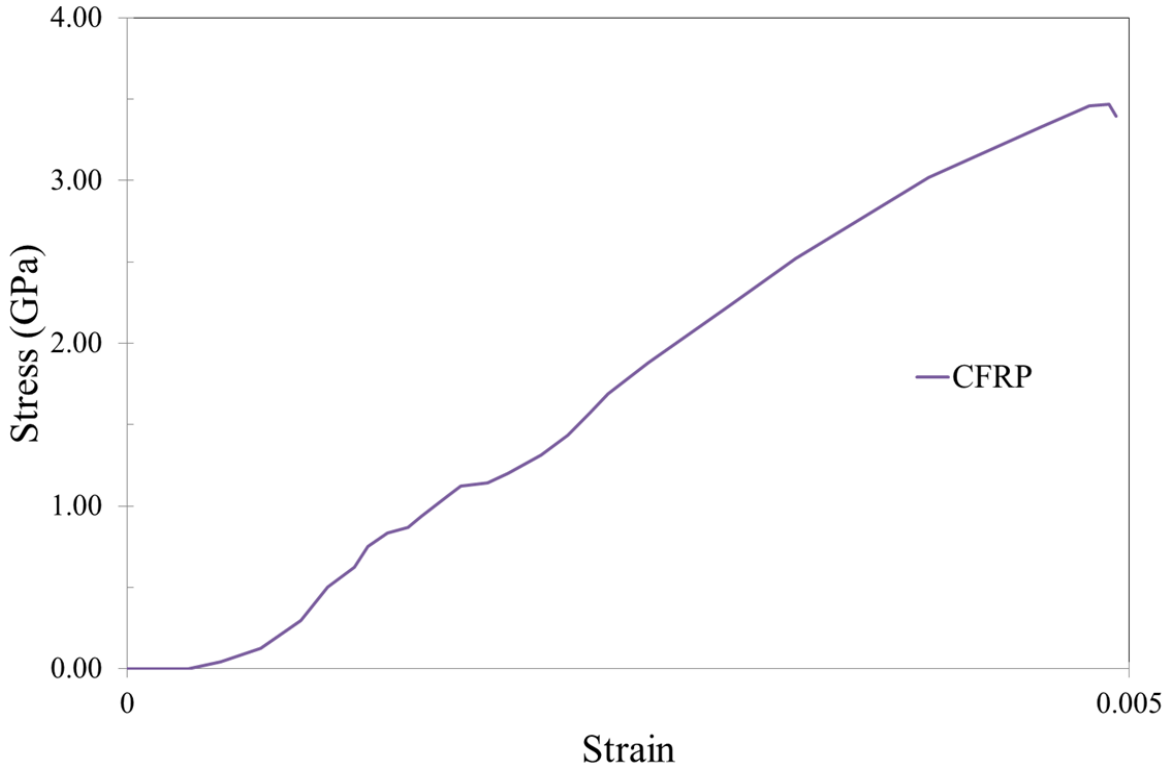

Figure 2.8 – Stress strain graph showing CFRP only, on increased X axis scale for clarity.

3.0 Experimental Set-up

In this project two forms of ballistic trials were employed. The first approach involved forward or conventional ballistic trials, where the projectile was accelerated into a stationary target. Whereas with the second approach, known as reverse ballistic tests, the target material was accelerated into a stationary projectile, in this case a bullet.

The forward ballistic trials can also be further broken down into two categories, namely: 1) standard ballistic trials using a rifled proof barrel mounted to an experimental gun and fired on an indoor range and; 2) forward ballistic trials using a single stage light gas gun. All the methods used have their own advantages and disadvantages, listed in the sections below.

3.1 Ballistic experiments

Forward ballistic experiments were conducted to ascertain material reaction to impact with an incident projectile. In this forward configuration depth of penetration (DOP) was the core diagnostic employed. In addition, reverse ballistic experiments were also carried out using one of the experimental arrangements detailed below (a 50-mm bore single stage gas gun). In this latter case, recovery of cores and flash X ray were the primary methods used to interrogate the impact events, as touched on in Section 3.0 previously. The ballistic experiments conducted can be divided into three groups whose setup is discussed in detail over the following pages.

Section 3.1.1: this concentrates on experiments conducted on the small arms range using conventional forward ballistic methods.

Section 3.1.2: this element of the thesis is focused on the experimental equipment used on a 30 mm bore single stage light gas gun and the experimental set up thereof.

Section 3.1.3: here describes the arrangements employed to conduct forward ballistic experiments utilising a 50 mm single stage light gas gun and associated diagnostics are presented. This section also details the use of the same gas gun for reverse ballistic experimentation.

3.1.1 Small arms experimental range (SAER)

A remotely fired 7.62mm experimental gun on an indoor range was used for these forward ballistics experiments as shown in figure 3.1. A proof barrel, fired from a remote station, was employed for all tests. The targets, comprising of a stripper plate of a given material, the armour (used in the Copper experiments) plus a number of backing blocks of Aluminium (used to catch the penetrated round and give a measure of depth of penetration (DOP) as described by Rosenberg *et al*. [75]), were clamped to an angle bracket 10 m from the muzzle. This distance was sufficient to ensure that the round was properly stabilised and flying true by the time it impacted the target. The material being tested was adhered to the front of a spacing ring made from acrylic. This ring was nominally 25mm in depth. This stand-off distance for the stripping plate from the Al backing / witness plates was chosen as it is greater than the overall length of the bullets core, meaning that if jacket removal were to begin at the stripper plate than there would be a reasonable distance for it to continue before penetration into the backing began. This ring and associated stripping plate material were adhered to the front of the Al backing blocks using a fast setting epoxy; for reference, a side view of a typical experimental arrangement is shown in figure 3.2 (for full material data, see the materials data presented in Section 2.0).

.

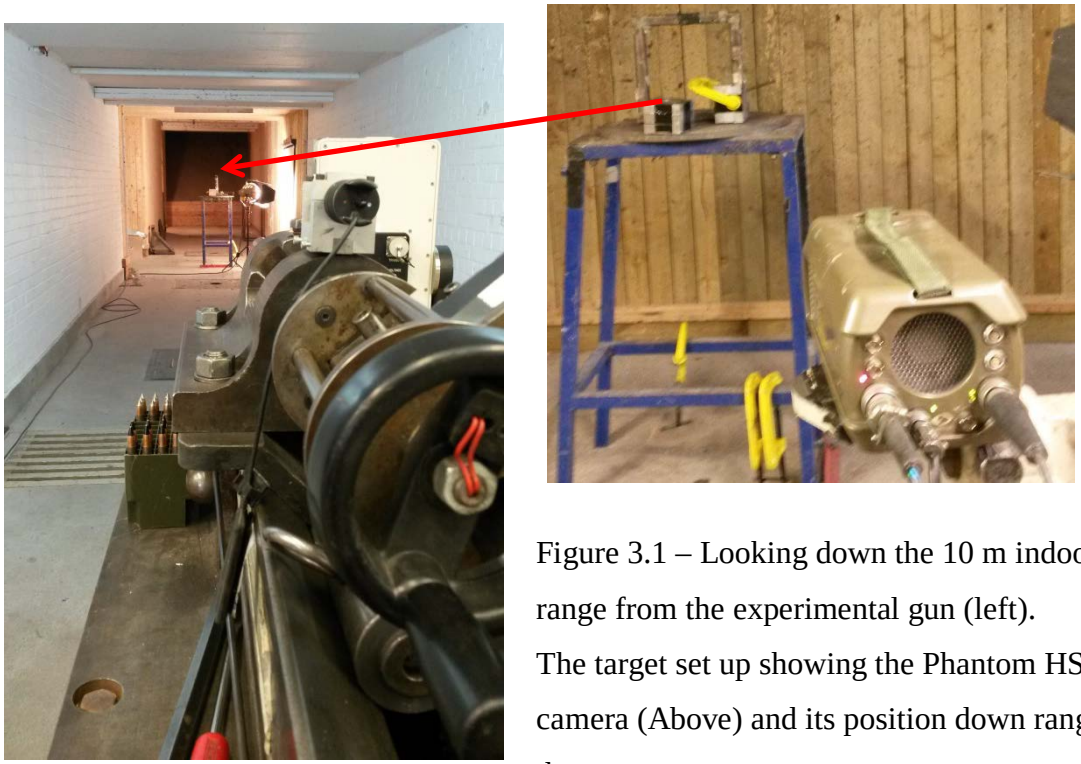

Figure 3.1 – Looking down the 10 m indoor range from the experimental gun (left).
The target set up showing the Phantom HSV camera (Above) and its position down range of the gun.

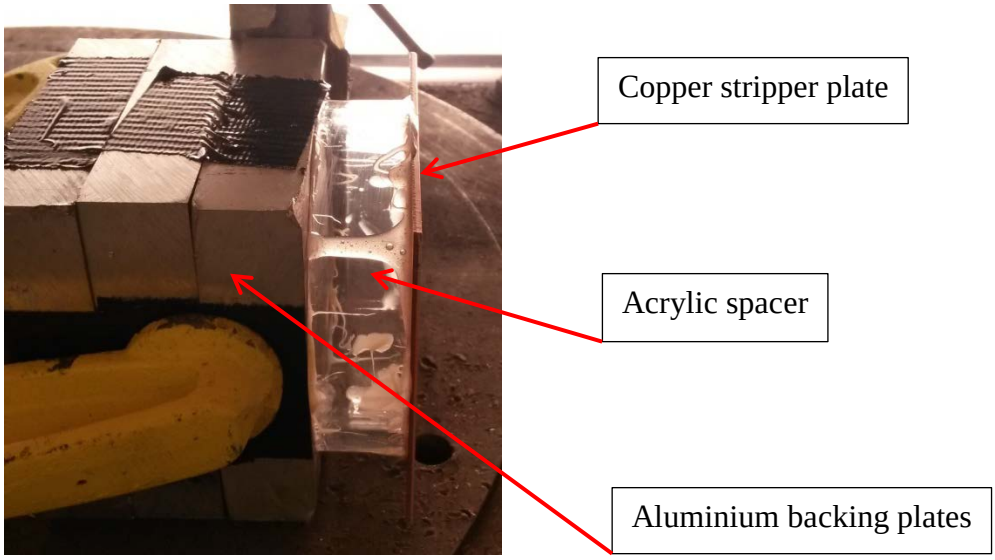

Figure 3.2 – An example of Copper fronted target used.

In all experiments a Doppler radar system was used to record the velocity of the round after firing. A Phantom V12 high speed video camera was also employed, both to check the incoming round for yaw and also to give a secondary (backup) velocity measurement. The impact itself could unfortunately not be viewed due a flash effect that occurs on penetration of the round.

The rounds used for the experiments in this set of tests were the aforementioned 7.62 x 51 mm AP (Armour piercing) FFV (Forenede Fabriksverken) rounds, with a Tungsten Carbide (WC-Co) core. These FFV rounds were used for several reasons. Firstly, the hard core resulted in a greater depth of penetration into the backing material than would have been obtained with a softer material, thereby providing a better quality and spread of final data as penetration paths were more easily measured. Secondly, as touched on previously, WC-Co cores represent the highest level of threat which a body armour system is likely to practically face at present / in the near future. To that end, the FFV rounds represented a realistic 'worst case' scenario. Half of the rounds employed were pulled before firing and had the tip machined to reveal the tip of the core. They were then re-made ready for the experiment (see figure 3.3).

Figure 3.3 – A pulled tip of a FFV round showing the revealed core.

The reason for machining the jacket to reveal the front part of the core for around half of the experiments was to ensure that the jacket completely stripped away on those particular firings, enabling a clear distinction to be drawn between completely stripped rounds and rounds that didn't strip at all or partially stripped. Careful observation of captured high speed video footage captured using a Phantom HSV camera demonstrated that removing this front section of the jacket didn't affect the bullets trajectory in any discernible way. Usefully, it can be seen from the forward ballistic firings undertaken on the 'Blue' gas gun (see Section 3.1.3) that the rounds that had the core exposed completely stripped even against the thinner thickness materials, validating the pre-stripping approach.

3.1.2 Forward ballistic trials using the 30mm light gas gun

Some forward ballistic trials were also conducted using a single stage light gas gun. The gun in question is situated within the Dynamic Response group laboratory, Cranfield University, and is shown schematically / pictorially in figures 3.4 and 3.5 respectively.

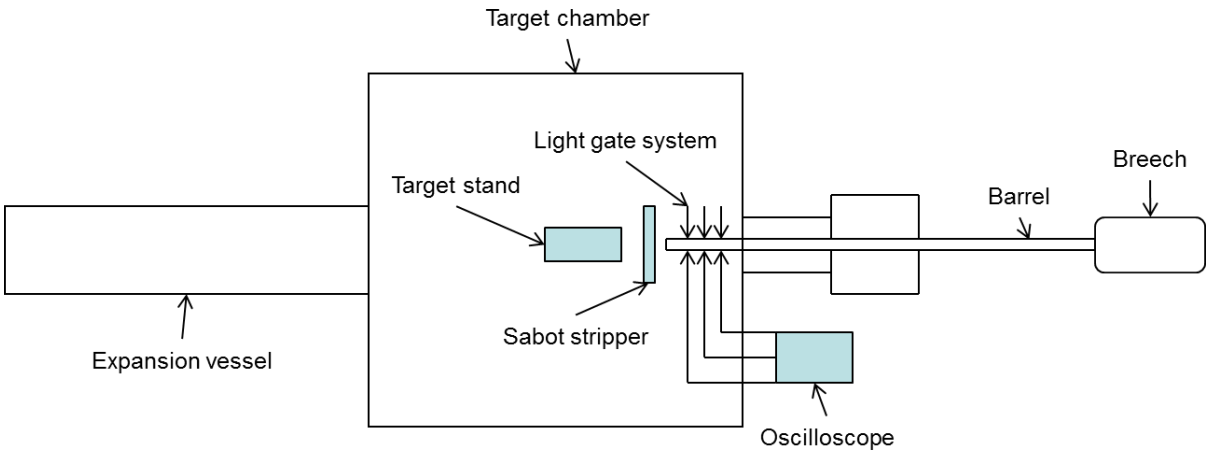

Figure 3.4 – The 30 mm single stage light gas gun (schematic).

Figure 3.5 – The 30 mm single stage light gas gun.

The gun has a 30-mm calibre, 5-m long smooth bore barrel. In order to fire 7.62 mm rounds it was necessary to encase them in an acetal sabot which was mechanically stripped just prior to impact. The saboted rounds were accelerated along the barrel by a driving gas, in this case Helium (He). The gas was released from a pressure vessel via a fast acting valve (shown in figure 3.6), which until triggered keeps the mechanism from firing. The key advantages of employing a gas gun system over a conventional range were the ability to fire in a very controlled laboratory environment (facilitating the use of different diagnostics), the ability to select velocities relatively simply by simply altering propelling gas pressure and, importantly,

enhanced safety as until the projectile was loaded and the breech (gas tank) filled from an external reservoir it was impossible to physically fire the gun.

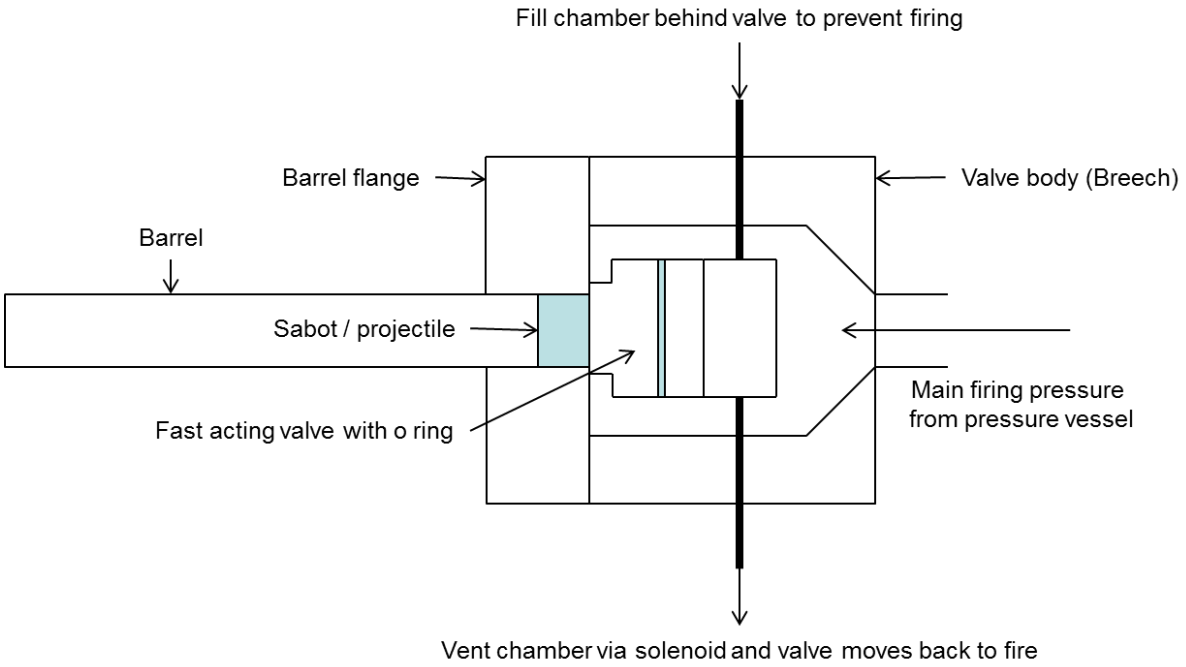

Figure 3.6 – Diagram of fast acting valve system on the 30 mm gas gun.

The use of a smooth bore barrel is, however, an area which leads to a slight disadvantage over a rifled barrel on a conventional gun. Bullets are designed to be spun to provide stability to the flying round. Consequently, such rounds when fired in a saboted configuration are inherently unstable. In this instance, this issue was overcome by reducing the distance between the sabot stripper (see figure 3.7) and the target.

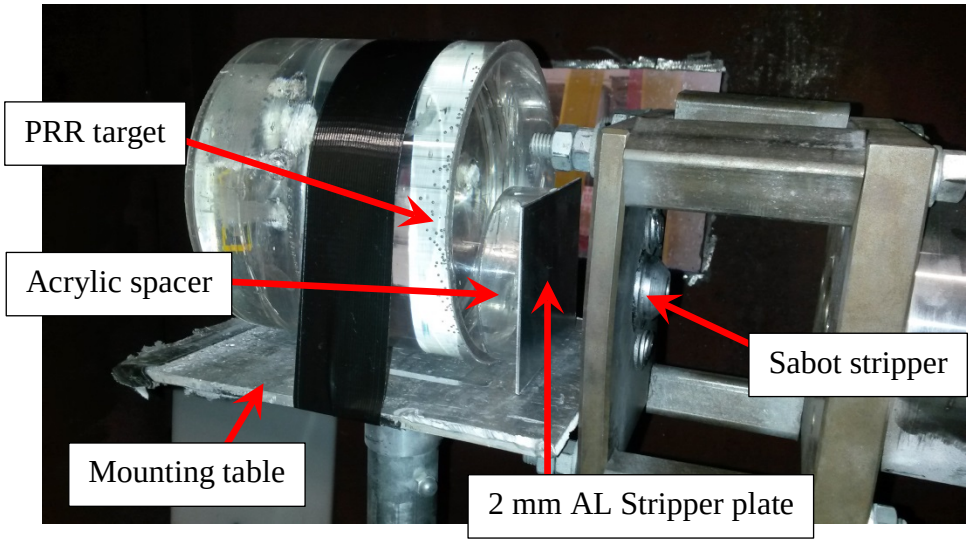

Figure 3.7 – The target set-up within the 30 mm gas gun target chamber.

In the experiments conducted here the target was mounted on an adjustable plate 25 mm from the sabot stripper (employed to remove the sabot from the bullet tip used, see figures 3.7 and 3.8 which illustrate the sabot stripping arrangement at the muzzle and a saboted round respectively) with in the target chamber. Before firing occurred, the whole target chamber was taken down to a vacuum of <400 mbar. This vacuum served two main purposes. Firstly, it gave the driving gas room to expand into without compromising the structure of the target chamber, and secondly by removing the air, the medium which transmits the majority of the sound from the impact, it significantly cut down on the noise created by the gun firing. The target, in the case of figure 3.7, a PRR (polyurethane replacement resin) with an Aluminium stripper plate mounted to the front surface. These particular experiments were conducted to further investigate results shown from the Aluminium depth of penetration data at 2 mm stripper plate thickness (see section 4.1.3, figure 4.3 (C)) where, essentially it had been noted that there appeared to have been an unusual discontinuity in the data. It was postulated that by firing a round into the PRR resin, the resin could then be sectioned and the bullet and penetration path could be analysed.

Figure 3.8 – The FFV bullet tip inserted into a 30 mm acetal sabot.

The velocity of the projectile was calculated based on traces recorded on a digital oscilloscope generated as the projectile passed an infra-red light gate system developed by the author. The passing of the projectile causes the light to turn off and a reading of this event is recorded on the oscilloscope. The time taken for obscuration of each of three successive beams led to a signal; the duration between these signals combined with knowledge of gate separation (25 mm) was then used to calculate the projectile velocity just prior to impact. Where possible velocities were taken using the time differential between gates 1 and 3 to maximise the sampling region / minimise subsequent errors. However, the use of three successive gates in this system was of particular importance as any discrepancies between successive gates indicating, for example, premature separation of the projectile and sabot, would have led to discrepancies across the two different gates.

3.1.3 Forward and Reverse Ballistic Trials using the 50 mm Light Gas Gun

Reverse ballistic experiments were also conducted with the aim of investigating the impact event in detail. These experiments employed the 50-mm bore, 6-m barrel single stage gun shown in figure 3.9. Reverse ballistics, as the name suggests, is a reverse of the standard ballistic arrangement; in this case, the projectile is the target material, which is accelerated into a stationary bullet. This type of experiment was first used by Anderson and Gooch [76]

to enable accurate X ray imaging of a penetration event whilst removing variations in the bullets trajectory such as yaw, spin, impact location. These factors can all vary from shot to shot in traditional forward ballistics.

Conventional ballistic experiments were also conducted on this gun, using the target set up used in the forward ballistic trials. Both fully jacketed 7.62mm FFV rounds and rounds with the front of the core exposed were employed – with the rounds held in place for the forward impact experiments via a push fit into a modified sabot. The only difference between these experiments and the conventional forward ballistic trials is that the round was not spin stabilised. This proved to have little effect as the DOP for these shots was measured and little difference was found between these firings and conventional firings conducted on the small arms range (see section 4.1.5, table 4.5 and DOP data tables found in appendix 2, respectively). For these forward impact experiments, flash X rays were taken of the penetration event through the stripper material on 2 mm and 6 mm Copper plate using the stripped and unstripped rounds (see appendix 2 for full X ray images), with the aim of elucidating the stripping mechanics in a manner not possible on the conventional range.

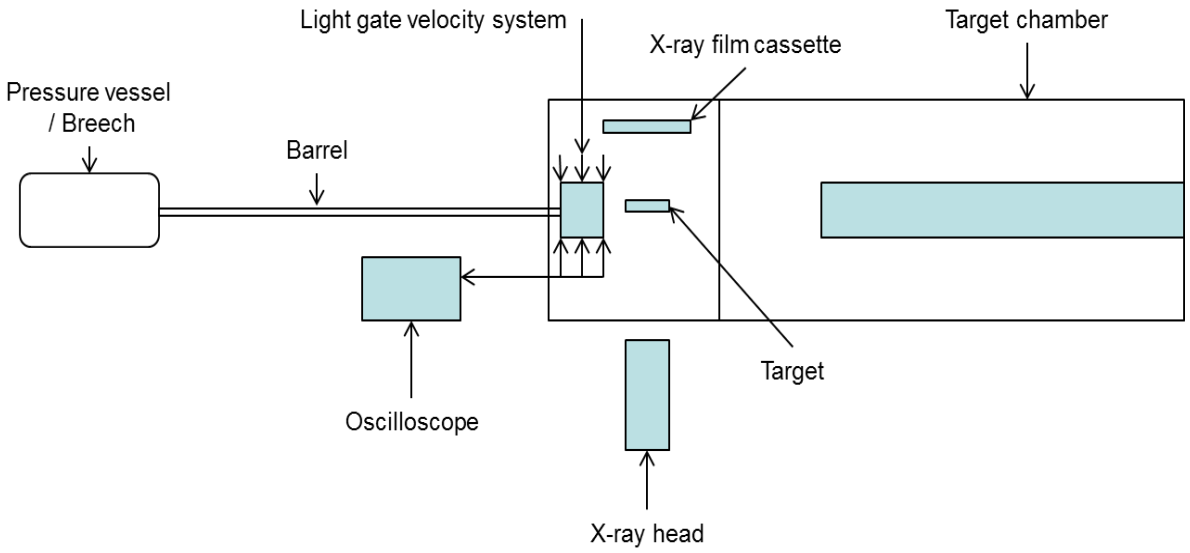

Figure 3.9 – Schematic illustration of the 50-mm bore, 6 m barrel single stage light gas gun employed for forward and reverse ballistic impact experiments (note: 4 flash x-ray heads were employed arrayed radially around the target, only one of which is illustrated here for clarity).

Before sealing the target end of the gun, the target (either a stationary bullet for reverse ballistic experiments or a standard forward ballistic target set up) was mounted on a specifically designed stand (shown in figure 3.10) within the target chamber. This arrangement was designed to hold it in the centre of the projectiles path, as well as at the centre of the arrayed flash X ray arrangement (see figure 3.12).

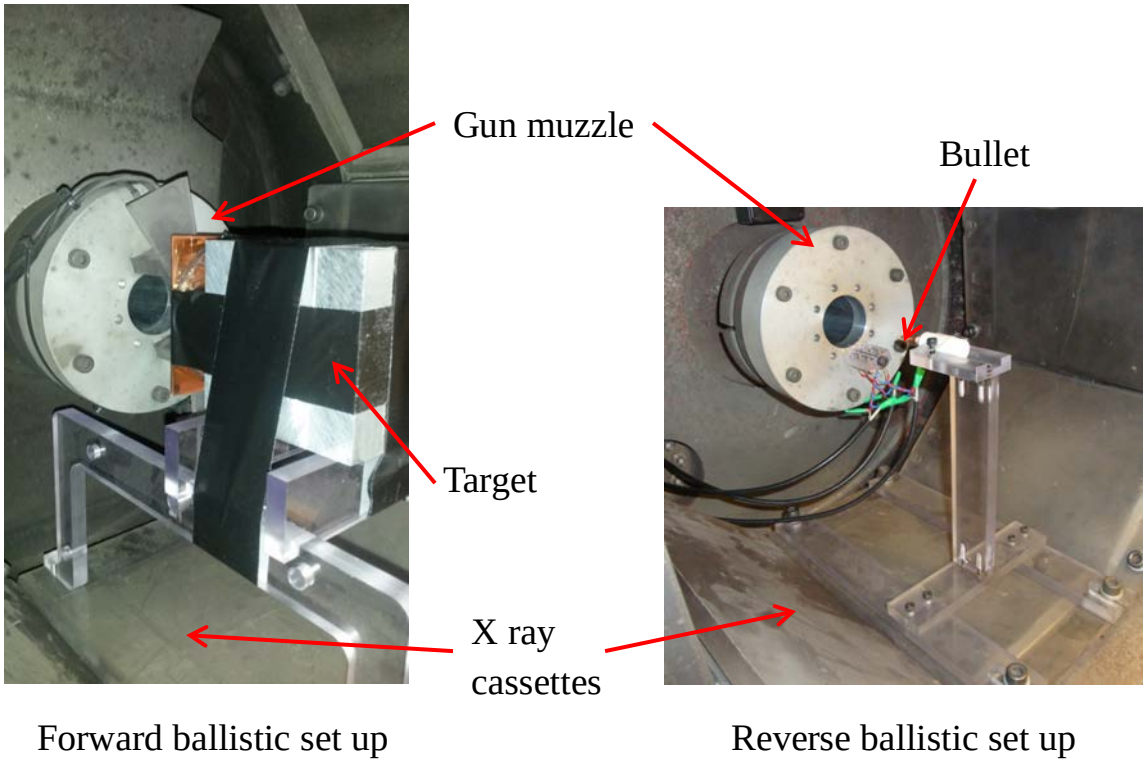

Figure 3.10 – (Left) Forward and (right) reverse ballistic set ups in the 'blue' light gas gun.

The gun was fired via a set of two Aluminium bursting discs with a predetermined depth groove machined into them, designed to burst at specific pressures of nominally 2/3 of the chosen firing pressure. The projectile (in the case of reverse ballistics, the target material or forward ballistics, the saboted round) was mounted into the barrel followed by the two bursting discs and a spacer (both with accompanying sealing o-rings), thereby creating a small chamber between the projectile and the breech (once the latter was sealed). Before firing, both the barrel and the target chamber were evacuated to <10 mbar. The main pressure vessel was then charged up to the firing pressure with the driving gas (in this case helium,

He), with the small chamber created between the bursting discs was simultaneously charged to a pressure half of that of the main firing pressure. This approach was designed to support the discs so they do not see the full firing pressure until the gas in the small chamber was vented via an electrically operated solenoid valve upon triggering (see figure 3.11). At this point, the rear-most disc would see the full firing pressure in the breech and burst, before the down-range disc burst, allowing He to accelerate the projectile towards the muzzle of the gun.

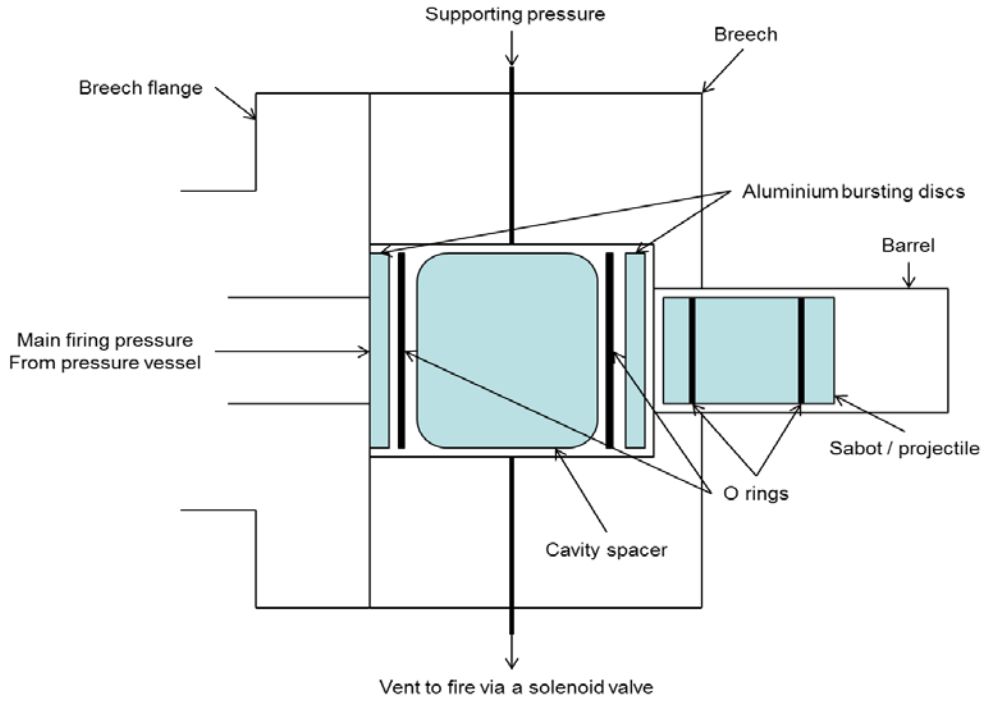

Figure 3.11 – Diagram of firing mechanism for the 50 mm gas gun (expanded for ease of interpretation).

As with the 30 mm forward ballistics experiments, the velocity of the projectile was again measured by shorting a series of sequential infra-red light gates of known spacing. In this case, the light gate system was in turn also used to trigger the flash X ray system at an appropriate point. The Scandiflash model 300 flash X ray system employed enabled each flash X ray head to be delayed to fire at any given point (following triggering by the light gate) throughout the penetration process by means of a delay generator. The set-up of the

flash X ray heads mounted on the gas gun can be seen in figure 3.12. The system comprises a control panel, high voltage generators (pulsars) and X ray tubes. The specific model details can be found in table 3.1.

Output voltage	100 – 300 kV
Output peak current	10kA
Single pulse, pulse width	20ns
Maximum dose per pulse at 1 m from tube window	90µSv
Focal spot size	1 mm
Dielectric gas	Oxygen free Nitrogen

Table 3.1 – Scandiflash X ray imager model 300 details [77].

In operation, the specific voltage required for successful X rays (determined via static tests beforehand to ensure adequate power to achieve appropriate penetration / contrast for the given target configuration), is dialled into the control panel, keeping the current amp values as low as possible. Four large capacitors situated within the pulsar units, are than charged and act to provide a rapid high voltage supply to the heads on firing. These capacitors are controlled via a dry Nitrogen dielectric; variation of the dielectric gas pressure determines the trigger voltage and is adjusted beforehand until the correct trigger breakdown voltage is achieved. Within the X ray tubes a Tungsten cathode and anode are situated, under a constant vacuum.

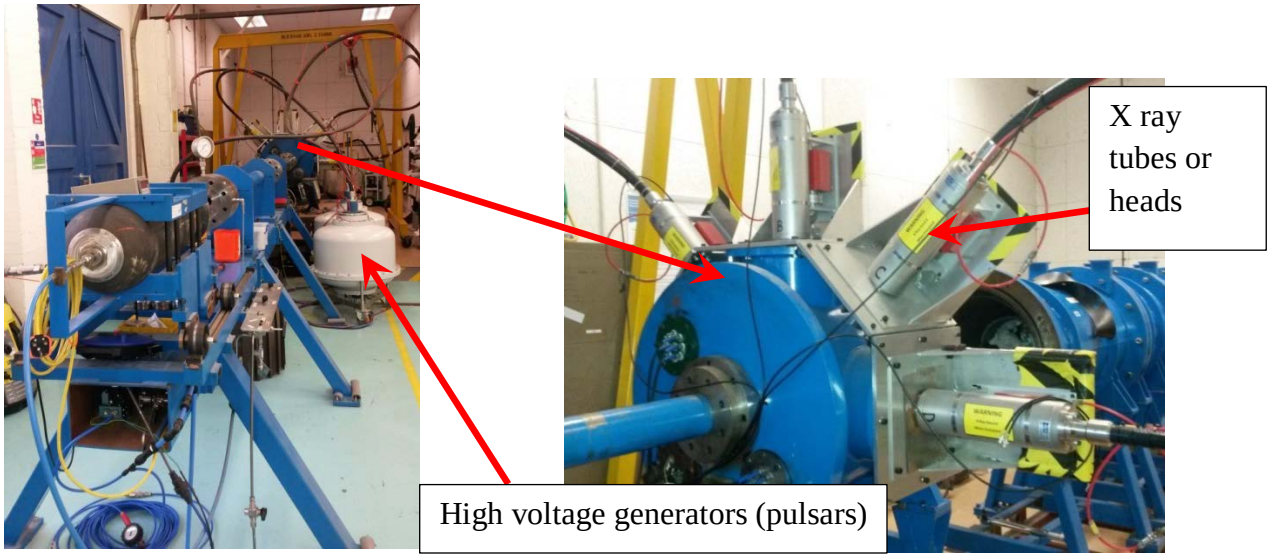

Figure 3.12 – The 4 channel flash X ray equipment situated on the 50-mm bore 'Blue' gas gun.

3.2 Bullet core removal using a hydraulic press

A hydraulic press, situated within the Dynamic Response group, Cranfield University, (see figure 3.13) was also employed to gather data concerning the pressure required punch a bullet core through its gilding jacket and through a plate. Modified versions of the 7.62 mm AP FFV (see figure 3.14) were employed for these experiments. The modified rounds consisted of a FFV WC-Co core only and a WC-Co core with the tip of an already removed jacket, back in place over the tip of the core. It was felt that this would give a better representation of what happens under full ballistic testing.

The bullet tips / cores were mounted on the ram of the press and were brought down to locate in a small indent on the surface of the stripper plate used (in this case Copper stripper plates of 2 and 4-mm thickness were employed). The stripper plate was clamped to the bed of the press to ensure no movement occurred during the pressing operation. A total of two pressings per bullet, per stripper plate were performed, where the bullet was pressed through the plate until penetration occurred. The resultant pressures were read from the pressure gauge on the press (see section 4.4, table 4.8). The difference in the pressure read between the fully jacketed and modified rounds consequently gave an indication to the pressure required to successfully strip a bullet jacket, further elucidating the role of the jacket stripping approach investigated in this thesis.

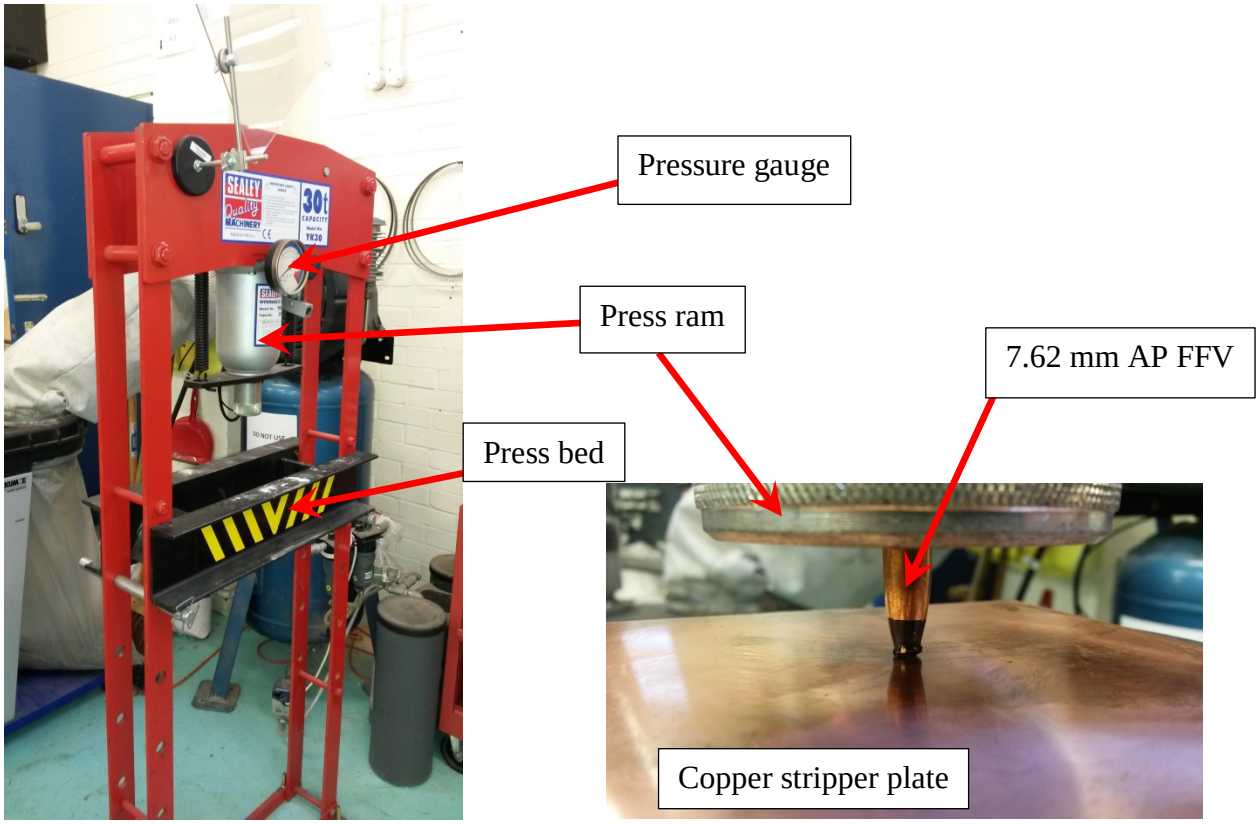

Figure 3.13 – Hydraulic press and bullet set-up.

Figure 3.14 – The modified rounds used on the pressing experiments.

3.3 Split Hopkinson Pressure Bar (SHPB)

A compressive Split Hopkinson Pressure Bar (shown schematically in figure 3.15, and pictorially in figure 3.16) was employed with the aim of measuring, and consequently better understanding, the passage of high amplitude stress / shock waves through a bullet core and jacket.

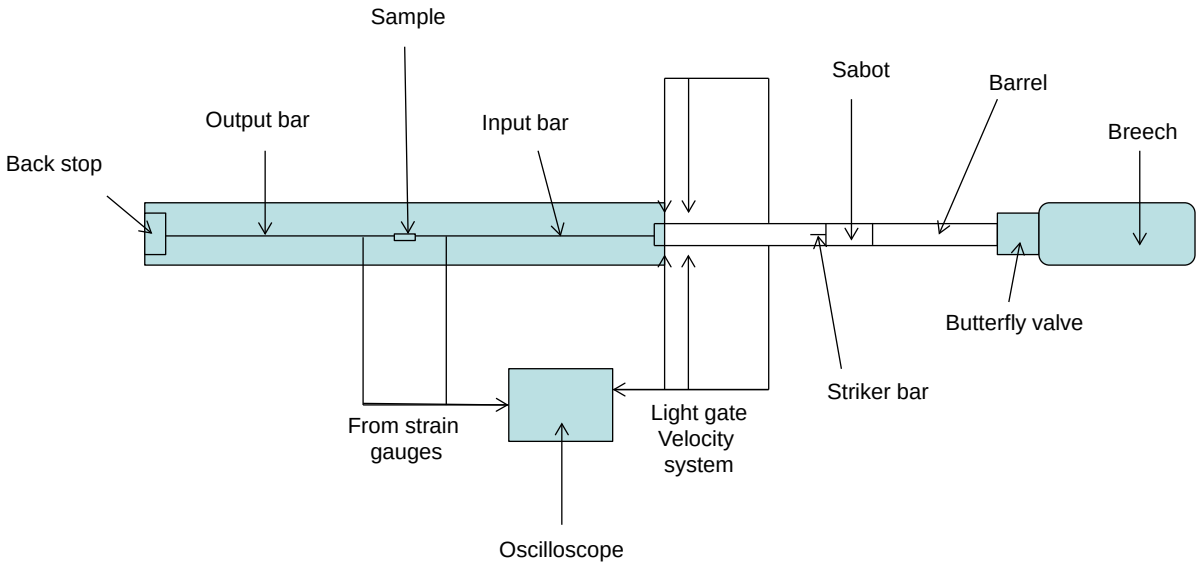

Figure 3.15 – The Split Hopkinson Pressure Bar schematic.

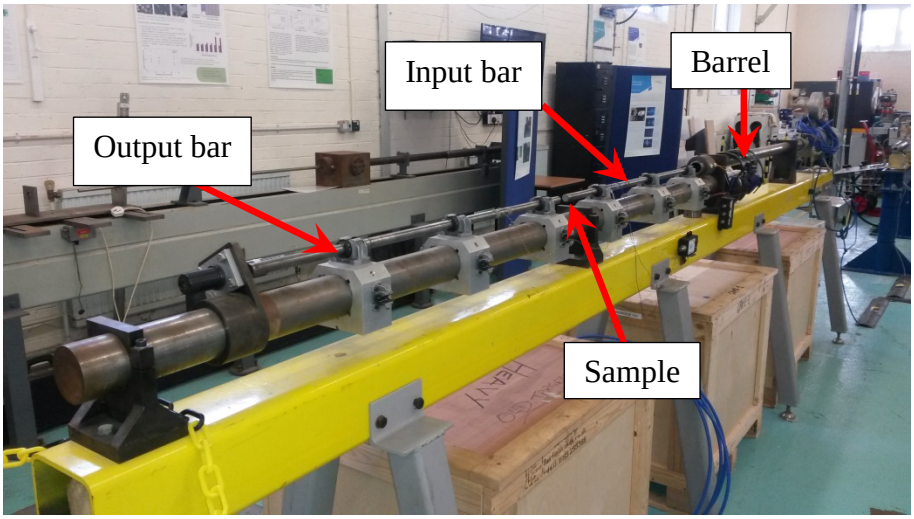

Figure 3.16 – The split Hopkinson Pressure Bar employed in this research.

Traditionally a SHPB is used to generate information concerning the elastic and inelastic strength properties of the materials being tested [78]. For these experiments the SHPB was employed to measure the passage of high amplitude stress wave through both a bullet core alone and through a bullet core with a piece of 0.75 mm Copper preceding it (see figure 3.17 and schematically in figure 3.18). The aim was to simulate the presence of the bullet jacket. From these experiments, data was generated which was subsequently used to elucidate / validate conclusions derived from the ballistic testing.

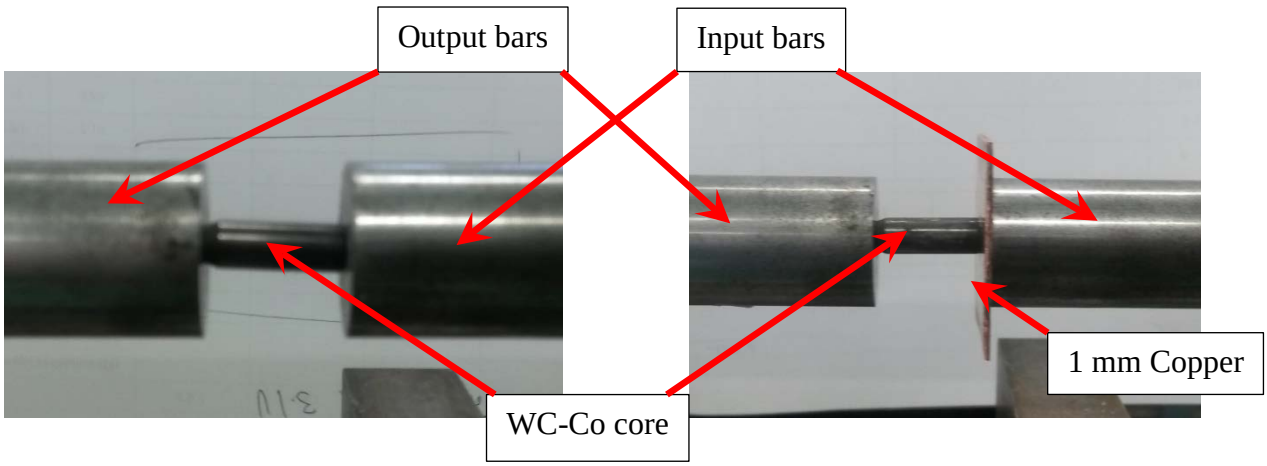

Figure 3.17 – Target set up for SHPB experiments.

The SHPB situated within the Dynamic Response group, Cranfield University, works in a similar manner to a conventional gas gun. A breech is charged with compressed air to the desired pressure to achieve the velocity required. The SHPB is fired via an electronically operated butterfly valve. When this operates, the compressed air drives a special projectile down the barrel. The projectile has an inserted metal rod known as a striker bar made from chrome Steel. The striker bar hits the first 'input' or 'incident' bar on the frame of the gun and the stress wave travels down the bar to the sample. One important caveat is that the bars should not be deformed plastically; consequently, the incident wave has to be elastic in nature and the impact velocity is limited (in this case as Chrome Steel bars were employed, this was limited to 25 m/s). The incident wave is recorded via a 350 Ohm strain gauge of type CEA-06-062UW-350 manufactured by Vishay Micromeasurements, mounted to the incident bar 250 mm from the sample. The wave then travels through the sample and into the second 'output' or 'transmitted' bar, with this transmitted wave then recorded by another 350 Ohm strain gauge mounted 250 mm downrange from the sample. Meanwhile, a reflected element of the incident wave will be picked up by the gauge on the incident bar. Further

reverberations occur, but these were ignored here. The striker impact velocity was measured via two pairs of infra-red LEDs and photodiodes of known spacing, with the obscuration of the LEDs recorded on an oscilloscope. The same oscilloscope operating at a horizontal scale of 2.0 miliseconds per sample and a recording window of 5.0 megasamples per second was then used to record the signals generated by the aforementioned strain gauges (see Section 4.3, figure 4.12). All resultant strain gauge traces can be found in appendix 3.

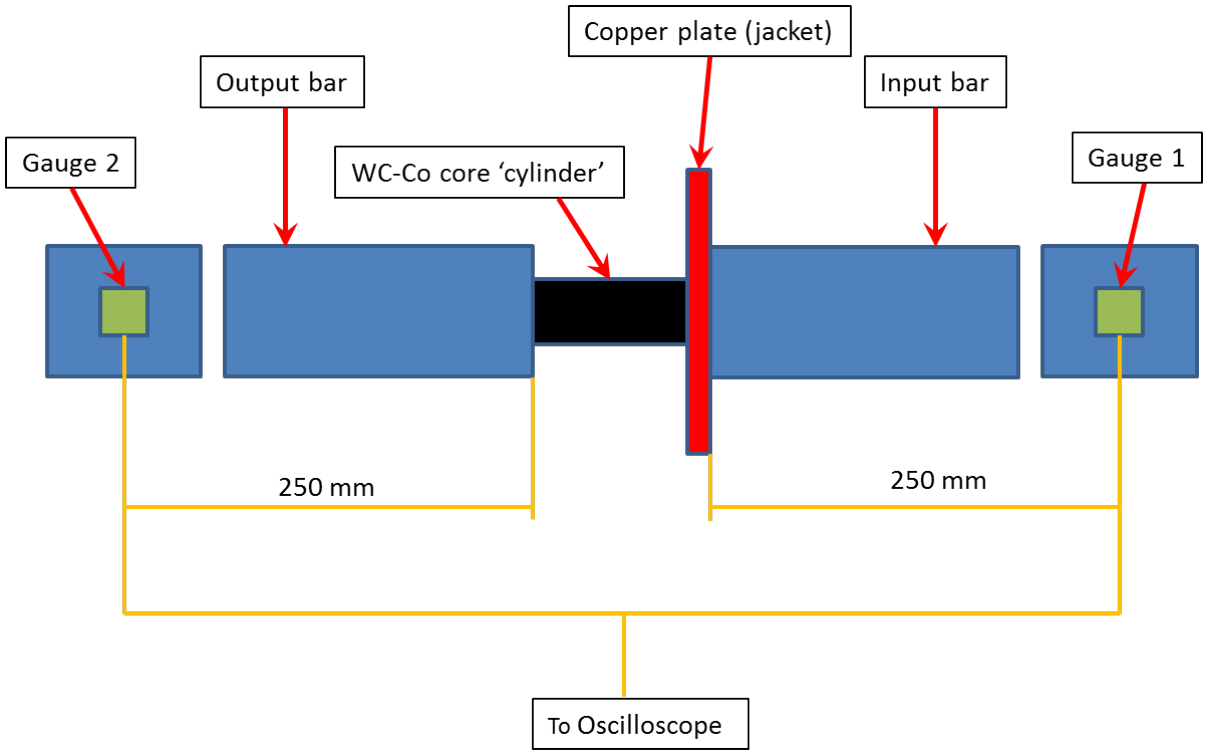

Figure 3.18 – Schematic of target set up on the SHPB and below, Table 3.2 – the lengths and sound speeds of the input / output bars and the materials tested.

Item	Core cylinder	Input bar	Output bar	'Jacket'
Material	WC-Co	Chrome Steel	Chrome Steel	Copper
Length (mm)	15	1000	1000	1
Sound speed (km/s)	6.83 [61]	5.96 [81]	5.96 [81]	4.65

4.0 Results and discussion

This section outlines the results obtained from all experiments. Forward and reverse ballistic data are presented in subsequent sub-sections, 4.1 and 4.2 respectively. Appendix 2 highlights raw data tabulated from forward ballistic experiments where a depth of penetration (DOP) was ascertained. From this DOP and other information required, mass efficiency (E_m) and ballistic efficiency (η) were derived. These calculated values are presented in the following sub-sections in this chapter (section 4.1.1 and 4.1.2, respectively) before the underlying DOP information itself (section 4.1.3). This order of presentation was adopted as E_m and η (even though both are derived from DOP data) are in-and-of themselves fundamental parameters employed when evaluating and designing an armour system. The DOP data itself is therefore subsequently presented as a series of figures in section 4.1.3. After initial evaluation it was concluded that the DOP data gave better results and better hinted at the role the bullet jacket was taking in the penetration process. Consequently, significant elements of subsequent evaluation are focused on the DOP information itself. The mass and ballistic efficiency showed similar general trends and indicated potential mechanisms, but due to differing weighting (for armour solution mass and ballistic resistance effectively) were not as definitive as the DOP results. This approach was considered reasonable both due to the similarities in underlying trends, but also importantly as the aim of these experiments was to investigate potential mechanisms underpinning dynamic jacket removal rather than designing an actual armour solution.

4.1 Forward ballistic experiments

Forward ballistic experiments carried out on an indoor ballistics range, (the Small Arms Experimental Range (SAER), Cranfield University), considered a number of different stripper plate materials. As detailed in Section 2.2, these materials were selected for several reasons, namely:

1) the fact that several of the materials are extremely well characterised in the literature (e.g. Cu, Al and Steel);
2) due to the fact that they cover a wide range of densities (from Cu at the high end to CFRP, as detailed in section 2.4, tables 2.1 and 2.2), a factor crucial to eventual

armour applications where mass (areal density) of such applique armours is a critical selection characteristic, and;

3) the current use – and therefore future applicability – of several of the classes of material considered (e.g. Steel [14], Al [5] and CFRP [25]) in real-world armour systems.

Experiments were designed with the overarching aim of investigating the importance of the bullets jacket in penetration. To this end, they were structured to not only consider stripper plate material, but also the influence of plate thickness (e.g. at a given impact velocity, projectile-plate interaction time). A Silicon Carbide (SiC) ceramic tile was also included in approximately half of the Cu plate experiments with the aim of enhancing post-stripping-plate projectile defeat, in order to further highlight any contribution caused by the jacket stripping plate. This tile was not included in subsequent (Al, CFRP and Steel stripper plate) tests as it was shown to be defeating the rounds in all cases, so trends and mechanisms could not be identified and investigated fully. In addition, in nominally half the cases the core of the bullet was exposed via machining of the jacket surrounding the projectile tip. The aim of this modification was to encourage jacket stripping, as well as to remove confinement around the core (thereby providing further insight into the role of the jacket during penetration). The different experimental configurations, together with experimental results (measured impact velocities and depths of penetration) are detailed in appendix 2. Results from these tables were subsequently used to calculate mass (section 4.1.1) and ballistic (section 4.1.2) values / to investigate the same, as well as to interrogate the influence on the various factors considered on depth of penetration DOP directly (section 4.1.3) data.

4.1.1 Forward ballistic experiments – Mass efficiency

The concept of mass efficiency (E_m) allows comparison of the ballistic efficiency of differing armours as a function of their presented mass. For a given armour, mass efficiency was calculated via a modified form of an equation from the literature [4] – e.g. equation 4.1. Here, calculated mass efficiencies based on the data presented in tables 4.1 to 4.4 are plotted as a function of stripper plate thickness, in figure 4.1(a) to (d) for Cu, Steel, Aluminium and CFRP respectively, and in figure 4.1(e) and (f) for combined data showing the core exposed and core not exposed, respectively.

$$E_m = \frac{p_\infty \rho_{Al} + (t_c \rho_c)}{t_s \rho_s + (t_c \rho_c + p_r \rho_{Al})}$$

Equation 4.1 – Equation to calculate mass efficiency (E_m).

Where t_c and ρ_c represent the thickness and density of the ceramic – Silicon Carbide (SiC) – respectively (where present), p_∞ is the depth of penetration which results with the ceramic and Al backing (of density ρ_{Al}) only, p_r is the measured depth of penetration for the complete system using both the Al backing and the stripper plate (of thickness t_s and density ρ_s).

As touched on above, Mass Efficiency (E_m) compares the ballistic efficiency of an introduced armour with that of a baseline target. The equation shows the areal density of a baseline target over the areal density of the stripper arrangement and penetration into Al or Al fronted by ceramic. By definition, larger values represent an improvement in armour efficiency, which can be seen clearly on figure 4.1 (e) and (f), with unity implying no change in relative to the baseline solution. The equation employs the calculated areal density of the materials used to give a measure of mass efficiency. The areal densities of all of the materials were calculated by multiplying the measured density (see section 2.4, tables 2.1 and 2.2) of the materials used by their thickness.

For these experiments general trends (and hence underlying armour performance / projectile defeat mechanisms) rather than absolute mass efficiency values were considered of primary importance. As shown in figure 4.1, in all cases mass efficiency is observed to trend below unity. While this general response might, at first glance, imply that stripper plates are not very mass efficient, it is worth noting that, in reality, the stripper plate thickness of 10 mm, as considered here, would be very much greater than that likely to be employed in an armour

system. In addition, the relatively low penetration and low areal density target (the backing Al), combined with the higher areal density of the stripper plate solutions, meant the configurations were inherently inefficient in terms of mass. Never-the-less, as implied above, they provided a ready approach to investigate the role of such stripper plates on penetration. To this end, it is worth highlighting a series of interesting observations from figure 4.1. First of all, it is interesting to note that the mass efficiency only decreases very slightly with stripper plate thickness for the CFRP plate as shown in figure (d), and more clearly in figure 4.1 (e) and (f), suggesting that this may be a more mass-efficient solution. In addition, comparing the different stripper plate materials it is immediately apparent that absolute mass efficiency values, unsurprisingly, scale with material density (see Section 2.4, table 2.1 and 2.2). Essentially, for a given stripper plate thickness absolute mass efficiency values are lower for Copper than Steel, with, in turn, Aluminium proving more mass efficient than Steel, but less so than CFRP. One additional point which falls out of all of the curves presented in figure 4.1 (a to d) is that the aforementioned general decrease in mass efficiency with stripper plate thickness appears to plateau at a nominal plate thickness of around 4-6 mm in all cases (with a slightly lower apparent change in thickness as this point apparent in Aluminium and CFRP). This change in material performance as stripper plate thickness crosses this threshold is tentatively attributed to a change in failure mode as the curves suggest that performance is consistent beyond this point.

One particularly interesting observation with regards to the observed plateau shown in all cases in figure 1 around 4-6 mm was that the plate thickness at this point also corresponds with the diameter of the WC-Co core used for the experiments (5.60 mm). Although no further work has been undertaken within this study to analyse this further, it may be an idea for future work to investigate this phenomena and see if the position of the plateau will change by using a different calibre of penetrator.

Overall, given that the only difference between shots in any given group was the stripper plate thickness (e.g. projectile velocities were nominally constant – see tables 4.1 – 4.4), this result, with early variation in system response being damped out around 4-6 mm, suggests that at a certain critical stripper plate thickness protection is optimised; usefully, this conclusion is backed by the corresponding ballistic efficiency data presented later in Section 4.1.2 / figures 4.2 (a) to (f).

With regards to the influence of pre-stripping the round, it was notable that both the pre-stripped and fully jacketed data presented in figure 4.1 followed broadly similar trends with stripper plate thickness. However, there was a consistent difference for a given material in absolute magnitude of E_m between the two different round types apparent across all data sets recorded. Essentially in all cases, mass efficiency was greater where a pre-stripped round was employed than a fully jacked projectile. Given the relatively small mass of jacket material removed would have had minimal effect on the projectiles momentum – but would have encouraged the jacket to begin to strip – this result, spread across all four materials, strongly emphasises the potential positive (in terms of round defeat) implications of jacket removal.

It is interesting to note, however, that an apparent anomaly in terms of recorded data occurs at a stripper plate thickness of 2 mm within the Aluminium, 4 mm for the CFRP data, and at 6 mm with the Steel data, presented in figures 4.1 (a), (d) and (b) respectively, with a fully jacketed round. The Copper stripper plates do not appear to show this anomaly, a possible explanation for this is the similarities in material properties between the Cu stripper plate and the jacket material. Such a response is also present, to a greater extent than here, on the underlying DOP data at 2 mm for Aluminium and Steel, 4 mm stripper plate thickness for the CFRP and 6 mm for the Copper, presented later in figure 4.3 (a to f). Essentially, at these points a sudden variation in the pre-stripped and fully jacketed data becomes apparent as highlighted by the dashed red ovals seen in figures 4.1 (a to d) and 4.3 (a to d). This anomaly is also shown in greater detail in figure 4.1 (e) and (f) where a distinct change in the data between core exposed and fully jacketed rounds can be seen. Further work, discussed in more detail, was subsequently undertaken to investigate this anomaly. Gas guns were used to investigate the regimes around this point in the forward and reverse configurations, with flash X ray also employed to investigate the impact event itself (please see Sections 4.1.4 and 4.1.5). Essentially, these experiments have suggested a different failure mechanism may be involved across the regions centred on the anomalies in the trends apparent in figure 4.1. Essentially, it is postulated that at this point of inflection that the round has overcome the shear strength of the stripper plate material (see Section 2.4, tables 2.1 and 2.2), resulting in a ‘plug’ being left in front of the penetrating round. It is believed that this plug is having the same effect as a thicker bullet jacket and is helping to protect / cushion the core, thereby allowing it to penetrate even further into the backing material.

It is interesting to note that such a response can be found elsewhere in previous studies (although not highlighted at the time). In particular, Philbey [48], in a study focused on the effectiveness of bullet jackets during the penetration of ceramic armour, presented a series of images extracted from a numerical model showing the penetration of a bullet into a Steel stripper plate. Plugging of the stripper plate material can be seen on the modelled data in front of the penetrating round.

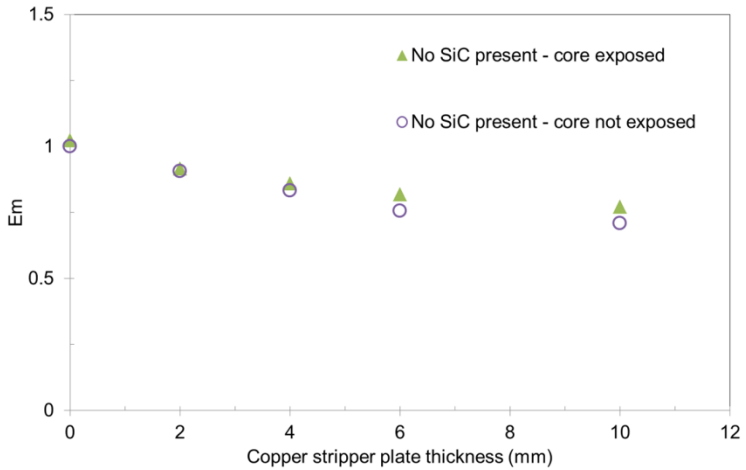

(a) Copper.

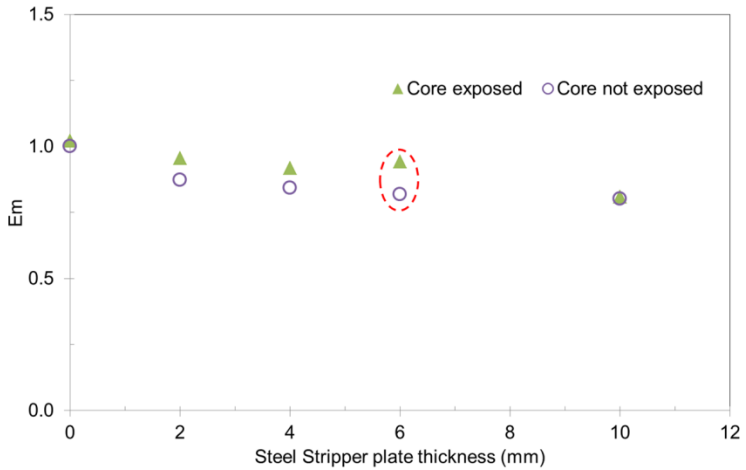

(b) Steel.

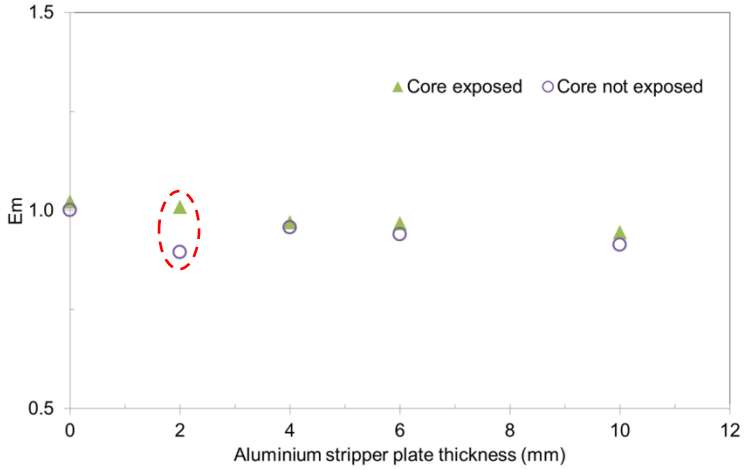

(c) Aluminium.

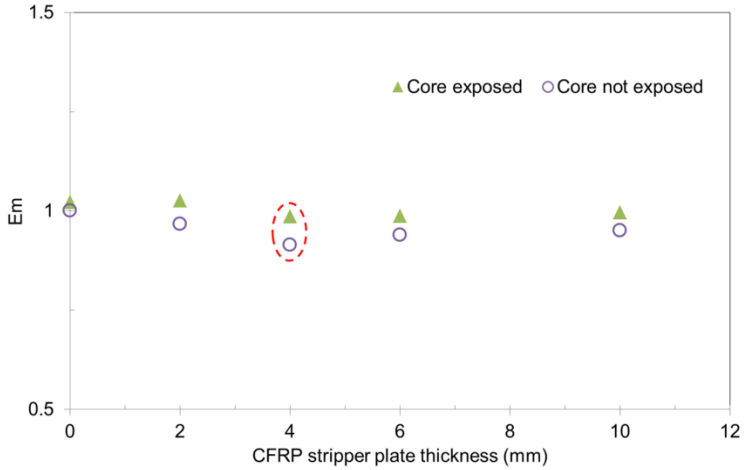

(d) CFRP.

Figure 4.1 - Variation of mass efficiency with stripper plate thickness for forward ballistic experiments. Areas of anomalous data highlighted by a dashed red oval.

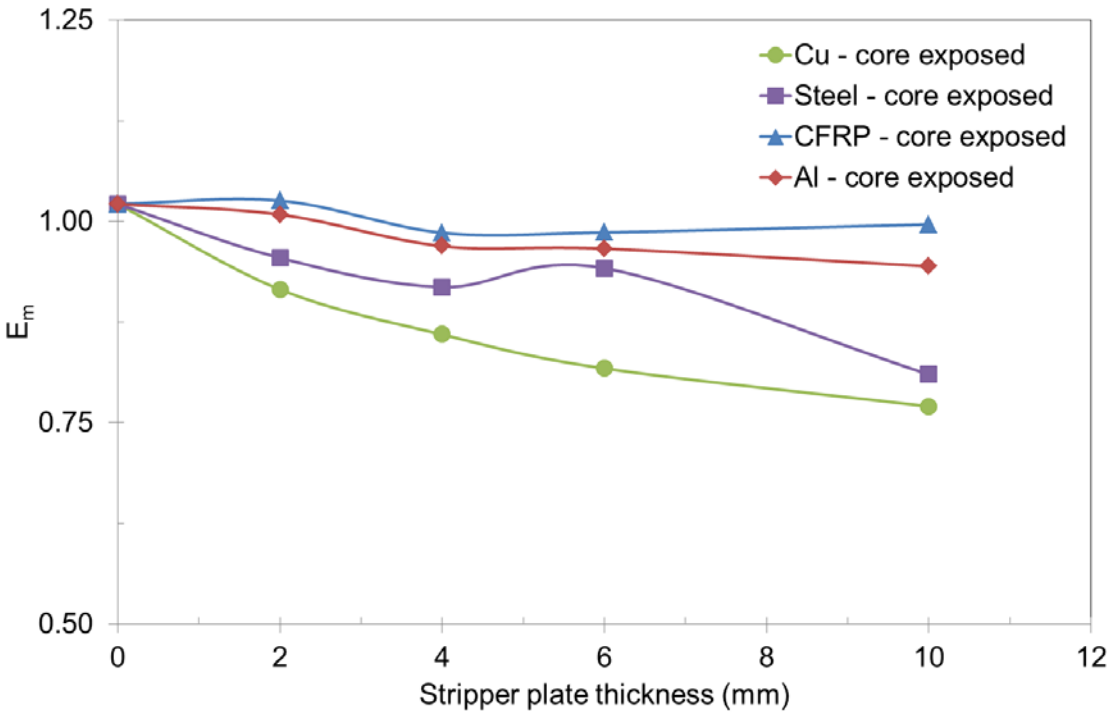

Figure 4.1 (e) - Variation of mass efficiency with stripper plate thickness for forward ballistic experiments. Core exposed only.

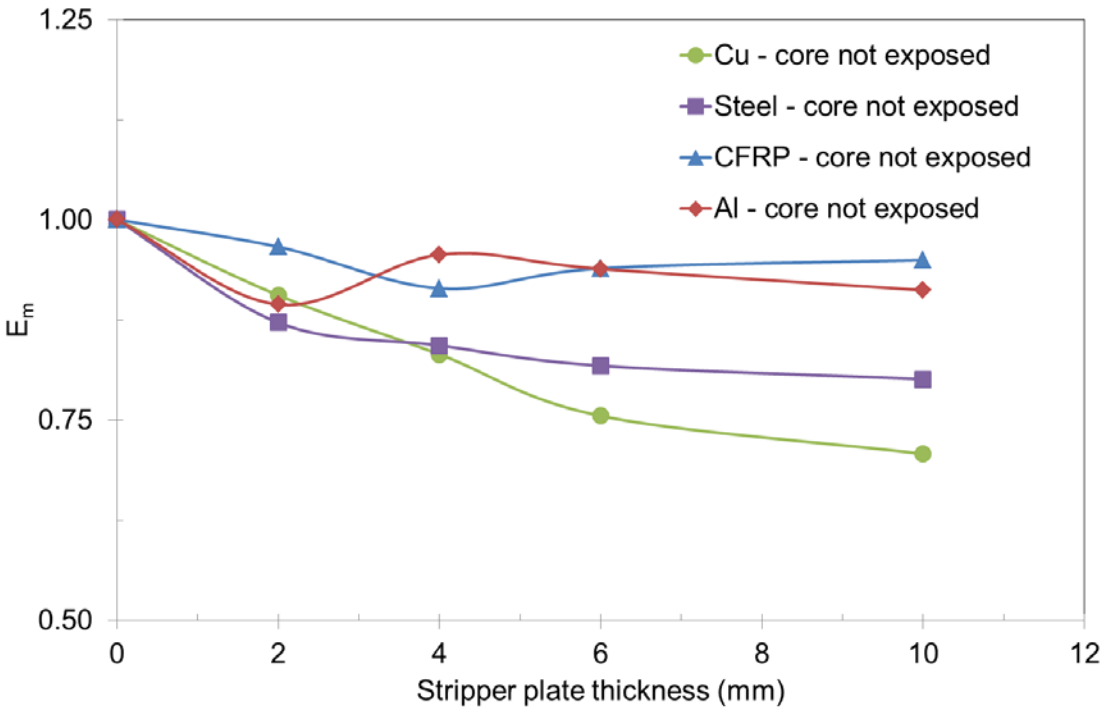

Figure 4.1 (f) - Variation of mass efficiency with stripper plate thickness for forward ballistic experiments. Core not exposed only.

4.1.2 Forward ballistic experiments – Ballistic efficiency

In a similar manner to the investigation of mass efficiency detailed in section 4.1.1, ballistic efficiencies (η) were calculated via a form of the ballistic efficiency equation [79] modified to account for the use of ceramic-faced Al (when used) as a baseline. Calculated ballistic efficiency values, plotted as a function of stripper plate thickness, are presented in figures 4.2(a) to (d) for the stripper plate materials tested (Cu, Steel, Aluminium and CFRP respectively).

$$\eta = \frac{\rho_{Al} p_r + (\rho_c t_c)}{\rho_s t_s}$$

Equation 4.2 – Equation calculating Ballistic efficiency (η).

Where t_c and ρ_c represent the thickness and density of the ceramic – Silicon Carbide (SiC) – respectively (present only where Cu stripper plates were employed), ρ_{Al} is the density of the Al backing and, p_r is the measured depth of penetration for the complete system using both the Al backing and the stripper plate (of thickness t_s and density ρ_s).

Ballistic Efficiency (η) compares the areal density of material penetrated in a standard target (the equation shows the Al backing material penetrated, with the option to include SiC - $\rho_{Al} p_r + (\rho_c t_c)$) with the areal density of an armour introduced in front, in this case a stripper plate – $\rho_s t_s$ to give a measure of ballistic resistance. The areal densities of all of the materials were calculated by multiplying the measured density, ρ (see Section 2.4, tables 2.1 and 2.2) of the material used by their thickness, t. The major difference from the calculation of mass efficiency (Section 4.1.1 and equation 4.1) is that ballistic efficiency does not consider penetration into the baseline material alone. For cases such as that considered here, where the ballistic performance of the baseline material (Al in this case) may potentially dominate that of the applique armour, such an approach – which still considers DOP via the areal density of backing material penetrated – has the potential to provide greater contrast between the performance of differing armours [80].

By definition, smaller values of η represent an improvement in armour performance as a reduction in residual DOP (p_r) will reduce the value of the numerator in equation 4.2. It is clearly shown in figure 4.2 (e) and (f), where materials are plotted together, that a reduction in η – and therefore a corresponding increase in armour efficiency (ballistically, but importantly – as shown in Section 4.1.1, not in terms of mass efficiency) is apparent, as the stripper plate thickness is increased for all materials tested. While cognisant of the fact that the mass efficiency decreased (see figure 4.1) with stripper plate thickness, as touched on previously, the purpose of measuring the ballistic efficiency of the materials tested was, as in the case of the mass efficiency, to identify trends occurring between materials. To this end, the data presented here – while not necessarily directly applicable to a real-world armour system – was considered scientifically useful.

In all cases presented in figure 4.2, a similar trend was apparent with a difference, albeit small, between the fully jacketed and modified rounds. All plots (figure 4.2 a to f) illustrate an initial rapid decrease in η (e.g. enhanced ballistic efficiency, before a point of inflection is reached where the data begins to plateau around the 4 to 6-mm thickness mark. Interestingly, this region corresponds with the data gathered for the mass efficiency where the decrease in mass efficiency (figure 4.1) was observed to plateau around a similar stripper plate thickness. Again, it is postulated that this may well represent the influence of the projectile diameter on penetration / failure mode (e.g. a change in penetration mode appeared to occur at stripper plate thicknesses around the projectile diameter). This could be likely if the stripper plate was having a confining effect on the projectile, whereas a greater amount of material present, due to the materials thickness, is aiding to slow the projectile. Tentative evidence of this can be seen in forward ballistic X ray radiographs taken of a core penetrating a 6-mm thick Cu stripper plate (see Section 4.1.5, figure 4.10), where new material can be seen bulging on the back of the plate, increasing interaction time between core and plate.

Another observation common on all materials tested / which is apparent in figure 4.2, is the convergence of the calculated ballistic efficiency curves for fully- and partially-jacketed rounds at / around the 10 mm stripper plate thickness mark. Taken together, these observations (a change in apparent defeat mode and maximum effective stripper plate thickness where pre-stripping of a round still contributes) appears to suggest that there could be an optimum stripper plate thickness, where increased thickness will have little or no effect on ballistic efficiency.

Overall, Copper (Cu) and Steel show the highest levels of ballistic efficiency of any of the materials considered here at all stripper plate thicknesses (with Cu being nominally more efficient). This is more apparent when viewed on figure 4.2 (e) and (f), where the materials are plotted together. This difference may be attributable to the variation in core material properties of the stripper plate, such as hardness (see Section 2.4, tables 2.1 and 2.2). Importantly, as touched on above, even though the ballistic efficiency of Cu is greater than the rest of the materials tested, the performance of this material is offset by its poor mass efficiency compared to the other stripper plate materials considered (see figure 4.1). Consequently, due to their lower areal densities, the fact that the ballistic efficiency of Al and CFRP at greater thicknesses is comparable to that of Cu and Steel at the lower end may mitigate towards the use of greater thicknesses of the former (lighter) materials. For example, 10 mm of CFRP has comparable mass and ballistic efficiency to Steel and Cu at 4 mm and, taking into account the depth of penetration data (see Section 4.1.3, figure 4.3 (a) to (f)), is comparable at reducing penetration into the backing material. As will be shown later in this thesis in the reverse ballistic data (see Section 4.2, figure 4.11), CRFP is successful at stripping the jacket from a round of thicknesses of 8 mm and above; however, these greater thicknesses may not be practical when thinking about armour design as other factors such as cost and manufacturing routes (as well as logistical issues such as armour bulk) will need to be taken into account. One possible solution might therefore be the use of a CFRP stripping element in thinner thicknesses combined as part of a composite structure alongside other materials. This is an area which this study does not cover but could be a subject for future investigation.

Interestingly, from figure 4.2, Al shows similar trends to CFRP and would make a good alternative to the better performing materials (such as Steel and Cu at the lesser thicknesses); albeit using a greater plate thickness. Measured mass and ballistic efficiency are comparable but penetration resistance is increased (see DOP data in figure 4.3 (a) to (d)). On this front, the fact that Aluminium has already been proven as a ‘real life’ armour solution employed on lightweight infantry vehicles such as the M113 APC [6] makes such an approach (e.g. a spaced Al armour solution, with a thin outer plate acting as a jacket-stripping element) potentially viable.

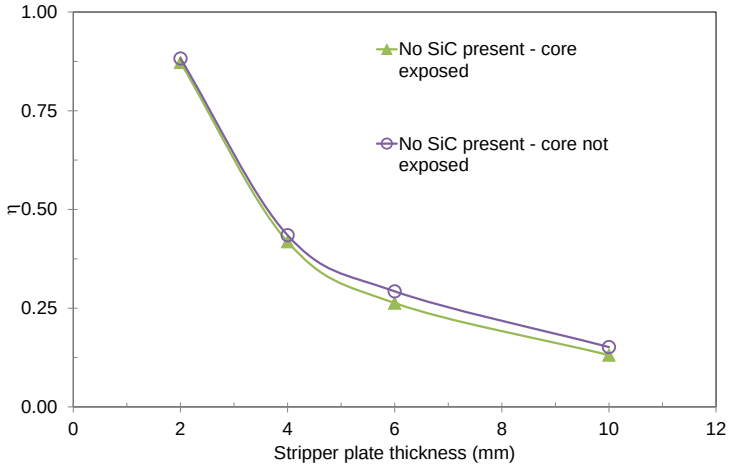

(a) Copper.

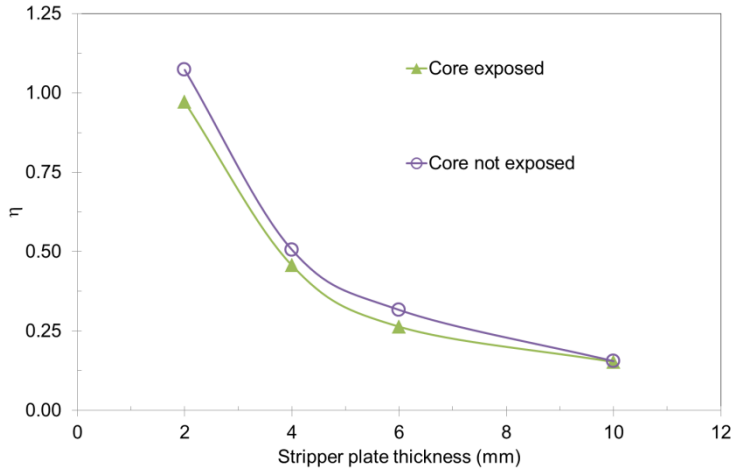

(b) Steel.

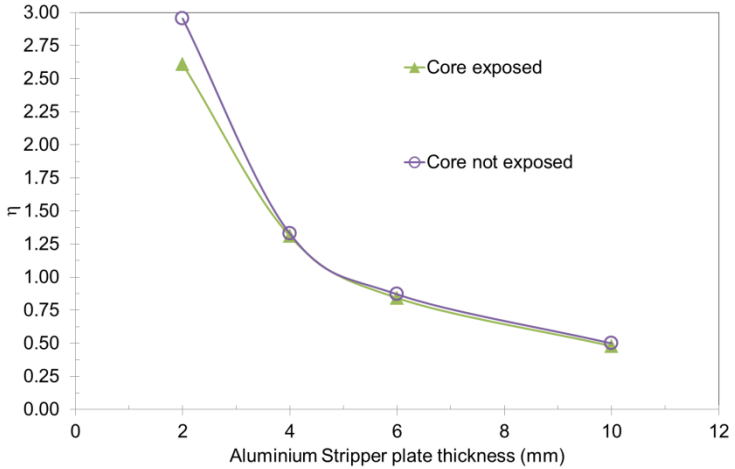

(c) Aluminium.

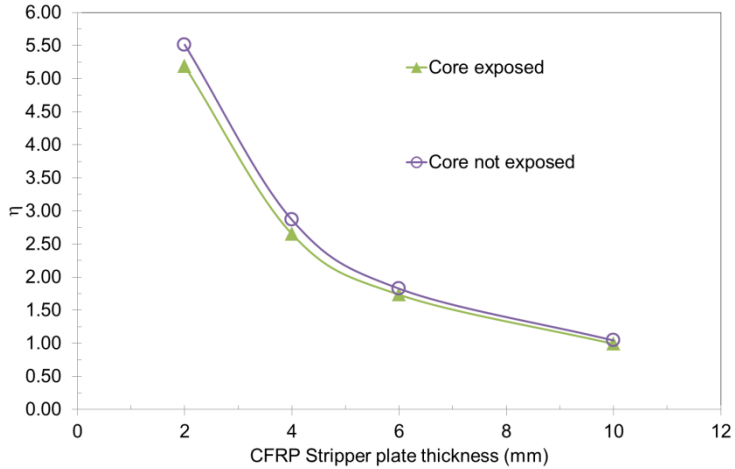

(d) CFRP.

Figure 4.2 - Variation of Ballistic efficiency with stripper plate thickness for forward ballistic experiments.

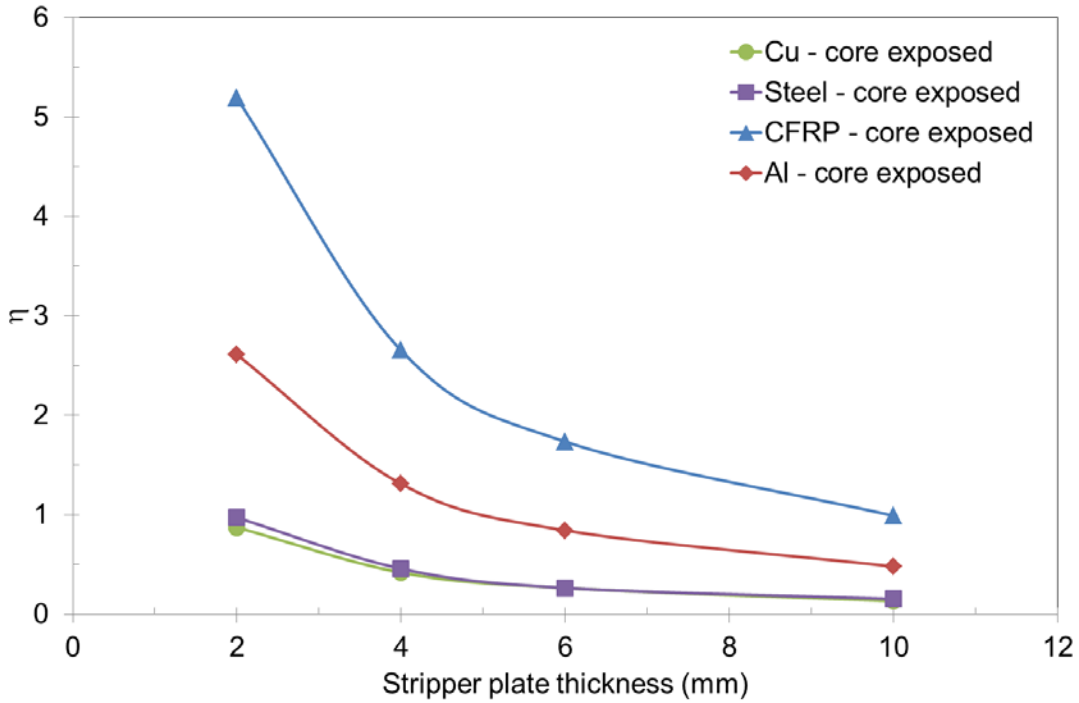

Figure 4.2 (e) - Variation of Ballistic efficiency with stripper plate thickness for forward ballistic experiments, core exposed only.

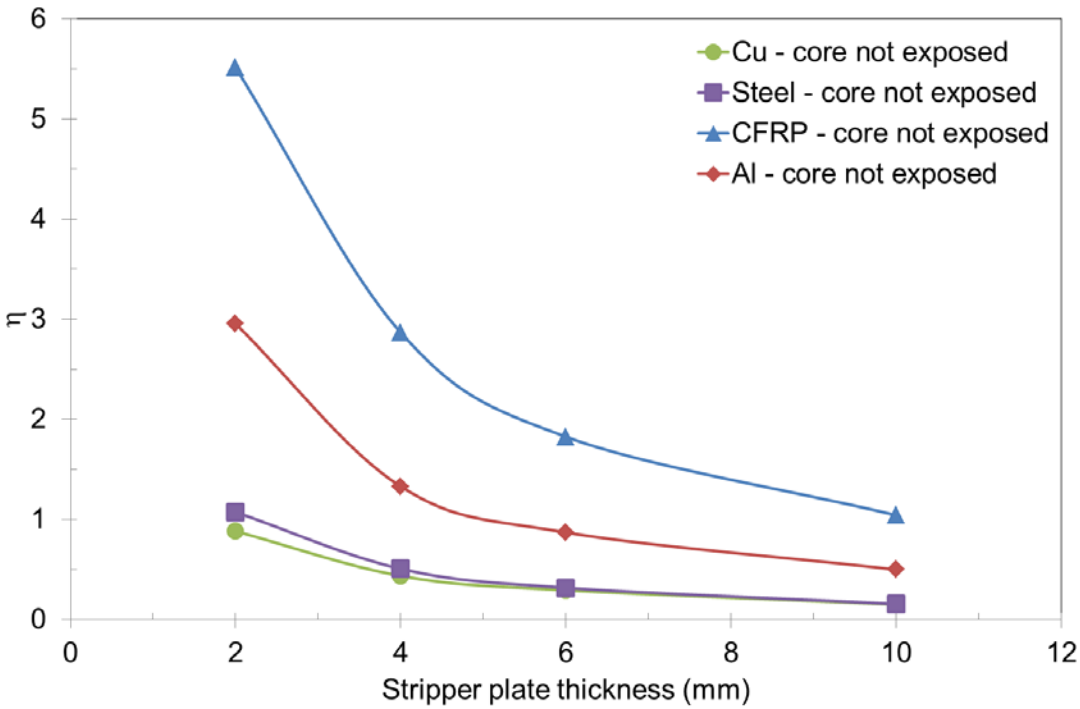

Figure 4.2 (f) - Variation of Ballistic efficiency with stripper plate thickness for forward ballistic experiments, core not exposed only.

4.1.3 Forward ballistic experiments – Depth of Penetration

The depth of penetration test has been used for many years to test the performance of materials in ballistic experimentation [7, 8, 18, 60, 61, 75]. The test works by measuring the depth a projectile has penetrated into a target material (in the case of armour development, both with and without a facing armour). This penetration can be measured by sectioning the material post-impact and measuring the penetration path using a rule, Vernier callipers, or by taking a still X ray image of the target material and then subsequently measuring the penetration path from the images produced. For the purposes of this study, the target materials were sectioned and the penetration path was measured with Vernier callipers.

The introduction of an armour material, or in this case a stripper plate of a given material, will affect the amount of penetration seen in the backing plate. Therefore, by definition, the less the resultant penetration, the greater the affect the armour / stripper plate is having on the round.

Figures 4.3 (a) to (f), shows the resultant depth of penetration into Aluminium backing blocks from the forward ballistic experiments conducted on the four stripper plate materials considered here. Average depth of penetration is given in millimetres and is shown against stripper plate thickness (also in millimetres). Raw data is available in appendix 2.

For all four materials, unsurprisingly, it is immediately apparent that the thicker the stripper plate, the lower the subsequent penetration into the backing blocks. For Cu this appears to be a slightly non-linear trend; whereas for Steel, Al and CFRP, a broadly linear reduction in DOP with increasing plate thickness is observed. Interestingly, apart from the Cu case, there does not appear to be a significant decrease in resultant DOP moving from a stripper plate thickness of 6 and 10 mm. As highlighted previously in Section 4.1.1, where E_m was considered, this is despite the fact that moving from a thickness of 6 to 10 mm will increase added armour (stripper plate) areal density by a factor of 66.7%. To this end, this apparent plateau in DOP – particularly when combined with the inflections previously identified in the E_m and η data (Sections 4.1.1 and 4.1.2 respectively) appears to point, if tentatively, towards the idea of an optimum stripper thickness where the ballistic and mass efficiency would be maximised while still maximising absolute ‘stopping’ ability of the resultant armour construct.

It's also worth noting that the graphs presented in figure 4.3 also in general showed a difference in the penetration between the modified and unmodified rounds, with the pre-stripped rounds (for a given stripper plate configuration) consistently performing better (e.g. exhibiting a reduced DOP). This is consistent not only with the calculated E_m and η values presented in figures 4.1 and 4.2 respectively, but also with other results noted previously elsewhere in the literature and – consequently – was an expected result. As touched on previously, projectile modification encouraged jacket removal. Consequently, the raw data presented in figure 4.3, re-emphasises the importance of the jacket material. Interestingly, the close agreement between some of the modified / non-modified (projectile) data points for the lower thickness Cu plate data – something not seen for the other stripper plate materials considered, where the difference in response was significantly more marked, gives a potential insight into the influence of the jacket. Essentially, it is postulated that the Cu (which has a similar composition to the jacket material) is initially acting to damp the impact – minimising the loading on the core in the pre-stripped projectile cases. If the ability of the jacket to confine the core was the dominant factor a substantial difference in DOP between jacketed and un-jacketed rounds should occur in this low stripper plate thickness region for the Cu case. However, at greater stripper plate thicknesses, this cushioning effect seems to become less important – likely due to the enhanced interaction time between the (thicker) Cu plate and projectile. In such circumstances, the ease of jacket removal would likely be the key effect – leading to the observed differences in Cu DOP results between the modified and un-modified projectiles in figure 4.3.

It can be observed in figure 4.3 that each of the four materials tested shows an anomaly in the results at a particular stripper plate thickness (different for each material), as highlighted by a dashed red oval in figure 4.3 (a) to (d) and more evident in figure 4.3 (e), for core exposed and (f) for fully jacketed rounds. In these instances (at plate thickness of 6, 2, 2 and 4 mm for Cu, Steel, Al and CFRP respectively), the measured depth of penetration was observed to increase – in the case of the Al DOP data, above the average of the baseline shots which involved no stripper plate being present. The fact that such an effect was seen in all cases may suggest that at these points a change in mechanism is allowing the stripper plate to aid in penetration. It is tentatively suggested that at this point the shear strength of the stripper plate material, or indeed the jacket material, had been surpassed. This apparent phenomenon has been investigated further and will be discussed in Section 4.1.4. Interestingly, in all cases, this anomaly was also only witnessed on the unmodified, fully jacketed rounds (see figure 4.3

(f). Not only does this suggest that this was a real – rather than simply anomalous – effect; it also points towards the underlying explanation pertaining to the interaction of the jacket and the stripper plate.

Figure 4.3 (b) shows the resultant DOP on experiments carried out utilising a Steel stripper plate. It is worth noting that this plot shows the greatest difference between modified and unmodified rounds across all of the materials tested. This difference clearly illustrates the fact that the presence – or lack thereof – of the nose of the bullet's jacket is clearly having an effect on the subsequent amount of penetration. As Steel is the hardest of the materials tested (see Section 2.4, tables 2.1 and 2.2) it is believed that other material properties are also having an effect on penetration, not just stripper plate thickness. This corresponds with the DOP data presented in figures 4.3 (c) and (d), for Al and CFRP respectively. These materials are relatively soft in comparison with Steel (284 HV to 125 HV and 66 HV, respectively) and therefore, even at the greater thicknesses do not appear to result in a big increase in performance. It is postulated that this difference in performance (in terms of the effectiveness of the stripper plates) arises as the high hardness of the Steel stripper plate is helping to pre-stress the core and cause the core to fail earlier than in the un-modified rounds. On this front, it is also worth noting that Steel is the only material used with a hardness greater than that of the bullets jacket, namely 284 HV for the Steel compared to 227 HV for the jacket. Building on these results, further experiments were conducted using a Split Hopkinson Pressure Bar, to investigate the amount of shock a WC-Co penetrator sees with and without a jacket present with the aim of investigating this phenomenon of pre-stressing. These are discussed later in Section 4.3. From figure 4.3 (b), it is also interesting to note that the DOP for the modified and un-modified rounds are very close at the 10 mm stripper plate thickness. It was originally thought that due to the interaction time between the core and the 10 mm plate the stripper was also having a confining effect on the round, as well as a cushioning or shock absorbing effect. This supposition is, however, not the case as the effect is not apparent / witnessed with any of the other stripper plate materials considered at this thickness (where the projectile-stripper plate interaction time – as predominantly a function of projectile impact velocity and sample thickness would have been similar). As will be discussed later when the results from the hydraulic press tests are reported in Section 4.4, the amount of pressure required to remove a bullet's jacket is relatively minimal. Consequently, we can assume that very little kinetic energy has been lost in the stripping process. This suggests that the enhanced performance of the Steel (as opposed to the other materials) is

likely a function of the intrinsic stripper plate material properties (such as hardness), with the amount of kinetic energy lost in the round potentially being simply due to the need to penetrate the harder Steel plate (rather than, for example, the softer Al) at this thickness.

Considering another potential stripping material, figure 4.3 (d) shows the CFRP DOP data has remained reasonably flat regardless of stripper plate thickness. As a material, CFRP is known to be very good at dissipating energy (see Section 1.1.5) due to the presence of stiff fibres which carry energy away from the point of impact (coupled to its tougher / more ductile matrix). In this case, it is clear that CFRP has relatively little effect on penetration, with an initial consistent efficiency even at a relatively thin (stripper) plate thickness. However, interestingly, at a higher (10 mm) thickness, a marked reduction in DOP is observed. Reverse ballistic images seen in section 4.2, figure 4.11, serve to back this up by proving that 10 mm of CFRP will indeed strip the jacket from an incident round. Usefully CFRP has a relatively low areal density, even at 10-mm thickness. To this end, it is postulated that use of layers of CFRP in a composite armour solution might be practical.

In conclusion, the graphs shown in figures 4.3 (a) to (d) in general demonstrate that using a thicker stripper plate leads to an increased performance – e.g. in terms of reducing depth of penetration. The results presented here – e.g. the fact that changing stripper plate material changes armour response – also serve to highlight the important role in penetration resistance of plate material properties. For example, hardness (harder being better) acoustic impedance (higher acoustic impedance plates appeared to perform better, emphasising the importance of the pre-loading of a projectile), and Young's modulus or resistance to flexure, which also seems to play a role in material choice. Overall, the higher the modulus or the greater the resistance to flexure the better the material was at stripping and defeating the round. These properties can clearly be seen to be making a difference when comparing the data gathered for the Steel against the data for the Aluminium stripper plates, materials at two ends of the (harness and modulus) scale. It can also be seen that the harder material shows a greater difference in terms of the resultant depth of penetration between the modified and unmodified rounds. This finding, taken together with data gathered from subsequent experiments utilising the Split Hopkinson Pressure Bar (see Section 4.3) arguably give an indication as to how a round fails, the contribution of the jacket and how an armour solution could possibly be manufactured to incorporate these findings.

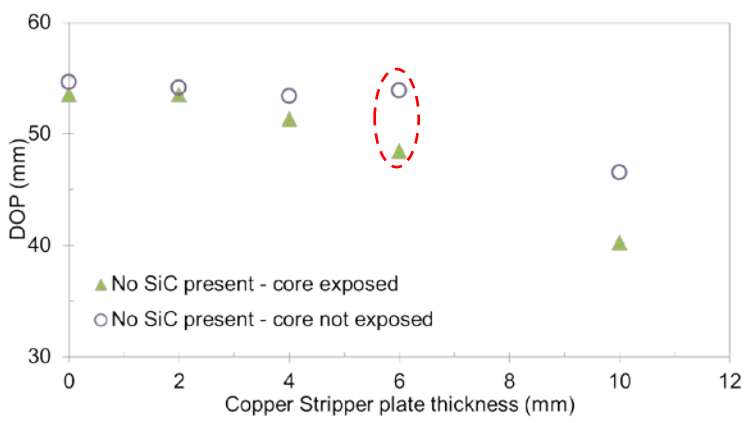

(a) Copper.

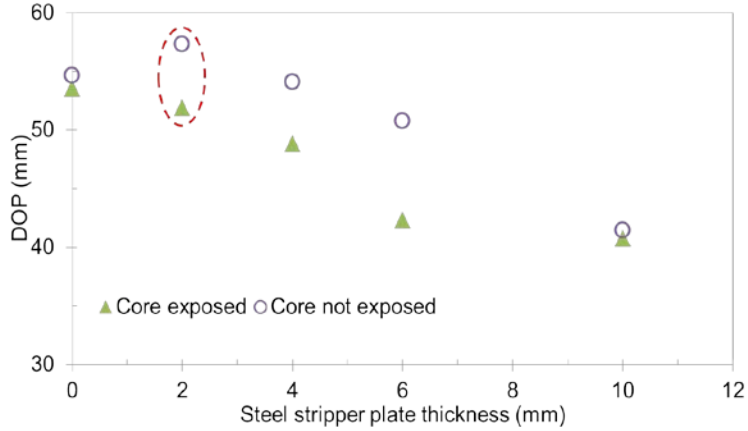

(b) Steel.

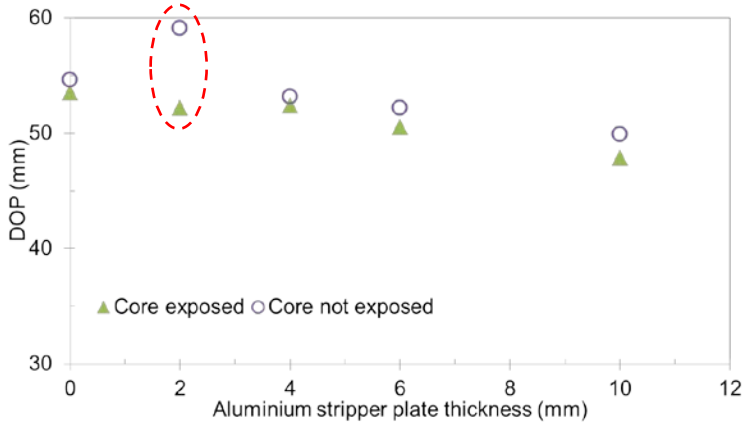

(c) Aluminium.

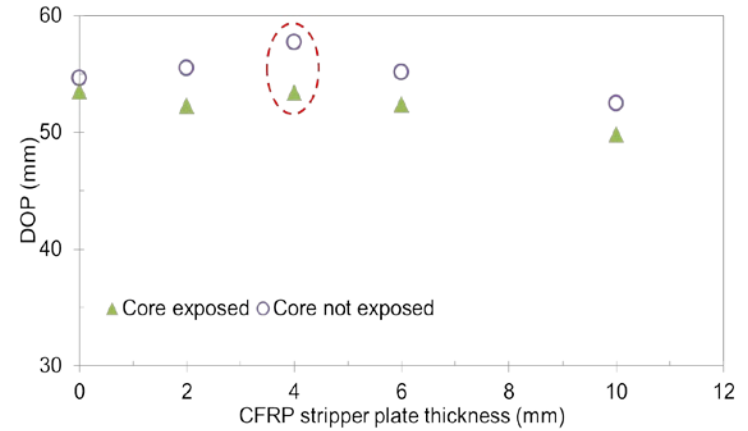

(d) CFRP.

Figure 4.3 - Depth of penetration results for forward ballistic experiments. Anomaly highlighted by a dashed red oval.

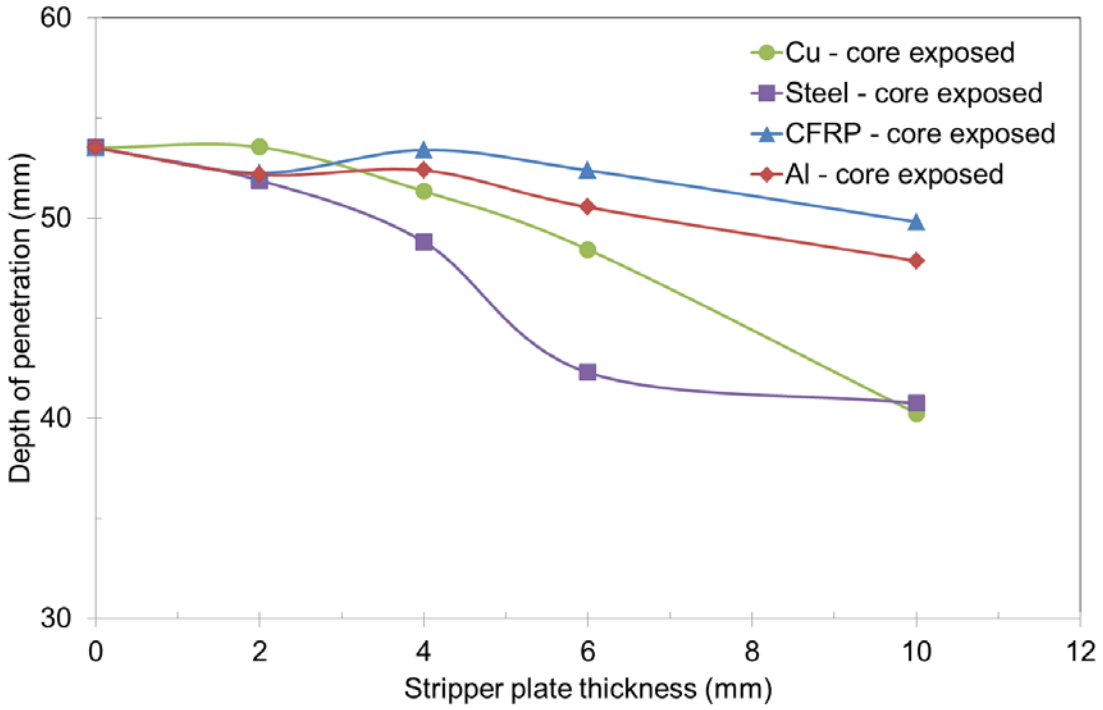

Figure 4.3 (e) - Depth of penetration results for forward ballistic experiments, core exposed only.

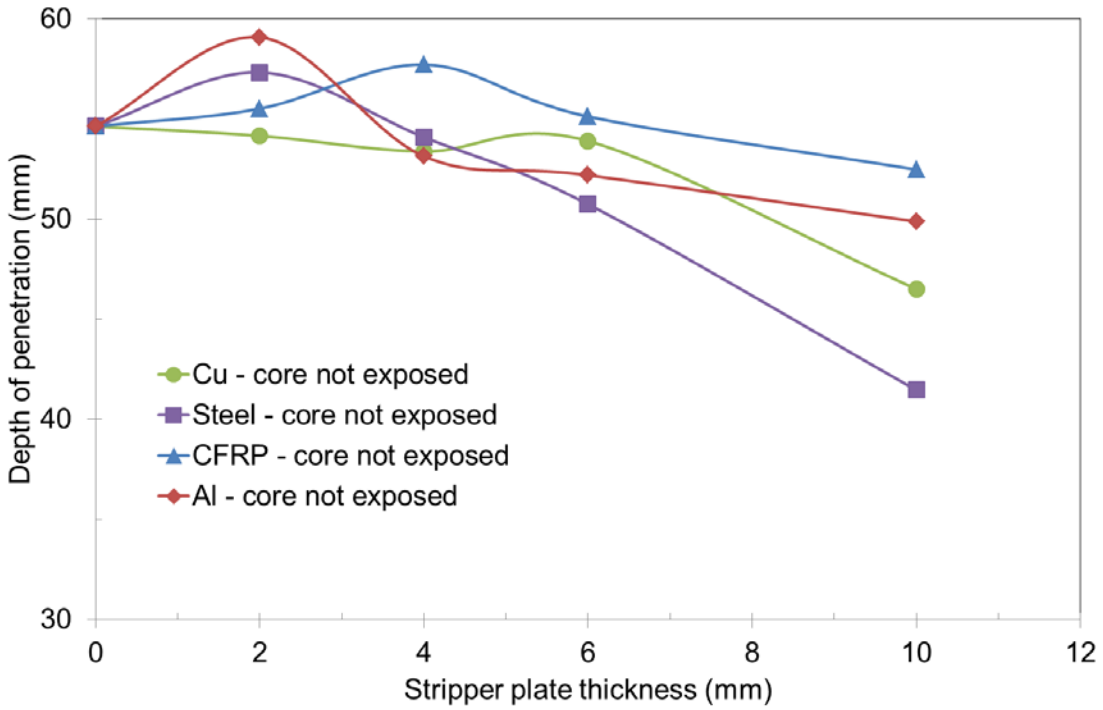

Figure 4.3 (f) - Depth of penetration results for forward ballistic experiments, core not exposed only.

4.1.3.1 Effect of Material Properties on Depth of Penetration

As it was apparent that DOP was giving the clearest data comparison between fully jacketed and modified rounds, a DOP comparison for a 4 mm stripper plate thickness for the differing materials was undertaken with the aim of taking into account the differing stripper plate material properties. A 4-mm thickness plate was considered because at /around this point we can see from the mass and ballistic efficiency data (Sections 4.1.1 and 4.1.2) that for all materials there appears to be a change in underlying armour behaviour / round interaction mechanisms occurring.

Discussions on material properties which aid in the reduction of DOP (see Section 4.7), and from measured material properties taken from table 2.1, Section 2.0, led to Hardness (HV), Yield Strength (GPa), Acoustic impedance (g.mm / μs.cc), and Young's modulus (GPa) being considered. These properties are plotted on the following graphs for comparison against DOP for the differing stripper plates – e.g. figures 4.4 (a) to (d) consider the influence of Hardness, Yield strength, Acoustic impedance and Young's Modulus on DOP, respectively.

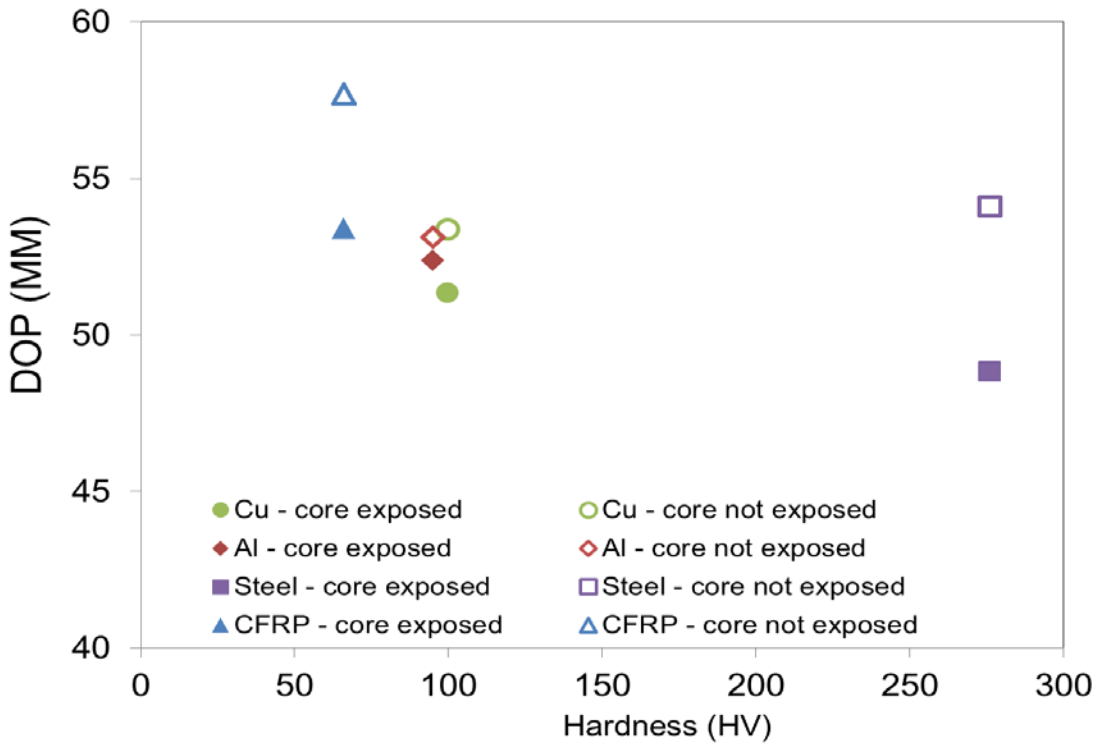

Figure 4.4 – (a) Effect of Hardness (HV) on DOP.

Figure 4.4 (a) displays the effect of hardness on DOP. The graph indicates, if tentatively, that an increase in hardness of the material leads to a slight difference in the DOP between the rounds where the core was exposed and fully jacketed rounds, with a greater difference noted on CFRP and Steel stripper plate samples. Unsurprisingly, DOP is greater where the jacket was present, emphasising the importance of jacket removal in terms of aiding in round defeat. The rounds in which the core was exposed, despite having a random variation, still indicate a general downward trend on the plot, with DOP decreasing as stripper plate hardness increases; whereas the unmodified rounds, again appearing to show a random variation, still generally trend downwards. Both modified and unmodified rounds follow a similar trend with the only difference being the amount of penetration witnessed. This shows, if tentatively, that the bullet jacket is aiding in the cushioning of the impact against the harder materials – enhancing penetration. In the case of the unmodified (core exposed) rounds, the aforementioned decrease in penetration with increased plate hardness is likely a function of the round being pre stressed where no jacket nose is present to cushion the impact. This mechanism is described in greater detail in section 4.7. Figure 4.4 (a) also points to harder stripper materials being potentially better in terms of pre-stripping incident rounds – something which would reduce DOP, e.g. by pre-stressing the core.

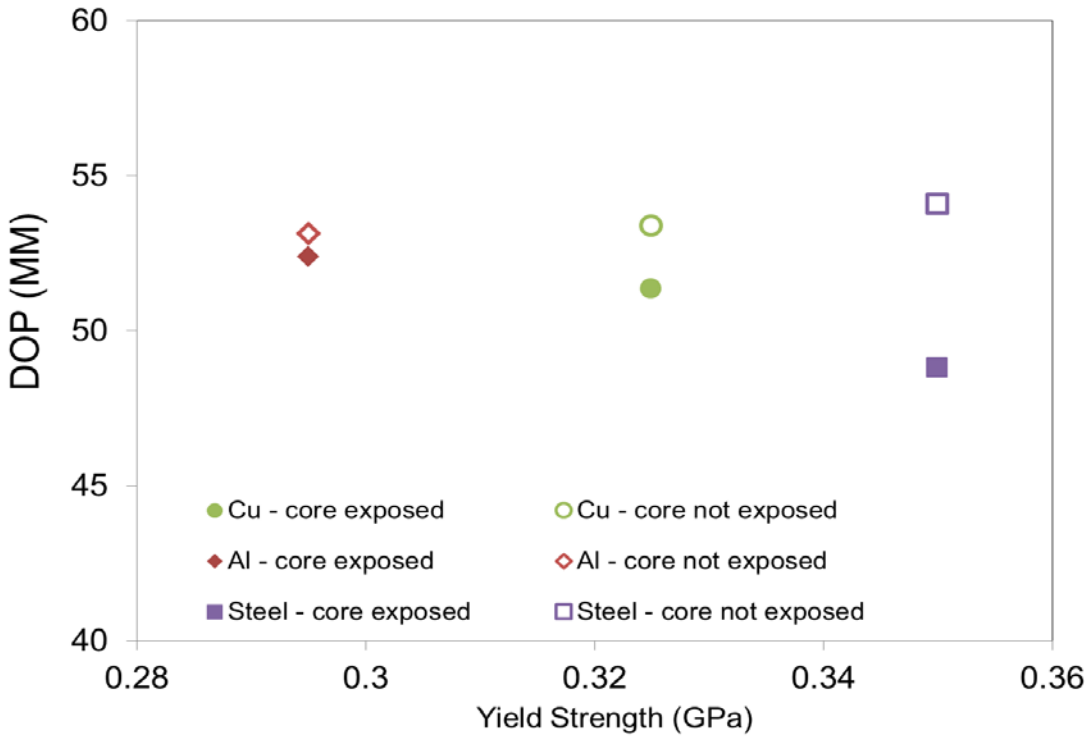

Figure 4.4 – (b) Effect of Yield strength (GPa) on DOP.

Figure 4.4 (b) displays the effect of Yield strength on DOP. Yield strength is the material property defined as the stress at which a material begins to deform plastically. Before this point a material will deform elastically, meaning it will return to its original shape once the applied stress is removed. Once again, as was the case with figure 4.4 (a), the core exposed rounds show a definite decrease in DOP the greater the material property being considered – in this case the yield strength of the material. The yield strength of WC-Co (being between 0.335 and 0.530 GPa [72]) is greater than the yield strength of both Cu and Al, therefore the WC-Co core is overmatching the material. With regards to the Steel, the exposed WC-Co core has a similar, if not greater yield strength (as the start point for the yield strength of WC-Co is less than that of Steel) the stripper plate is therefore over matching, or out perfoming the round. The fully jacketed rounds, however, show a slight increase in penetration the greater the yield strength. As the difference between the core exposed and fully jacketed rounds is apparent it shows, once again having the bullet jacket present has an effect on DOP due to its ability to protect or cushion the impact (e.g. to protect the core from pre-loading). As with hardness, figure 4.4 (b) shows a material with greater yield strength is better at reducing DOP if the bullet jacket is removed. It should be noted that results for CFRP are not featured on this graph as yield strength could not be derived from the material data.

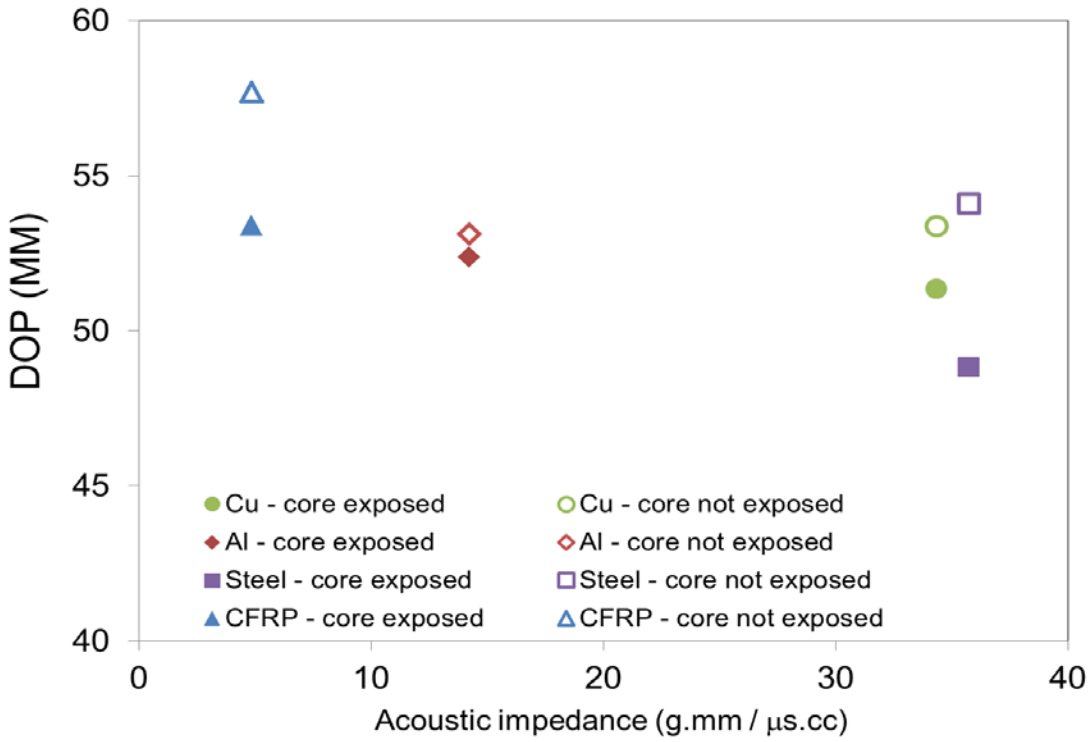

Figure 4.4 – (c) Effect of Acoustic impedance (g.mm / μs.cc) on DOP.

Figure 4.4 (c) shows the effect of acoustic impedance on DOP. Acoustic impedance, as described in Section 2.1, is the ability of a material to couple an incident shock wave. Lower impedance materials (typically, but not always of lower density), would normally reduce subsequent pre-loading of the round. To this end, the lower the value, the better the acoustic impedance of the material with regards to pre-stressing effects. This is reflected in the plot presented in figure 4.4(c). Essentially, the jacket material is not only acting as a physical (pliant) medium to cushion the impact but also, as a function of its acoustic properties relative to those of the projectile and target, acts to mitigate pre-loading of the projectile. If of high enough amplitude, reflected incident shock waves moving back into a round from impact would eventually cause spallation to occur within the round and lead to total defeat; in essence, the inclusion of a bullet jacket helps the incident shockwave couple better with the core allowing for the shock within the core to dissipate reducing the ringing effect seen in Section 4.3, with the SHPB results.

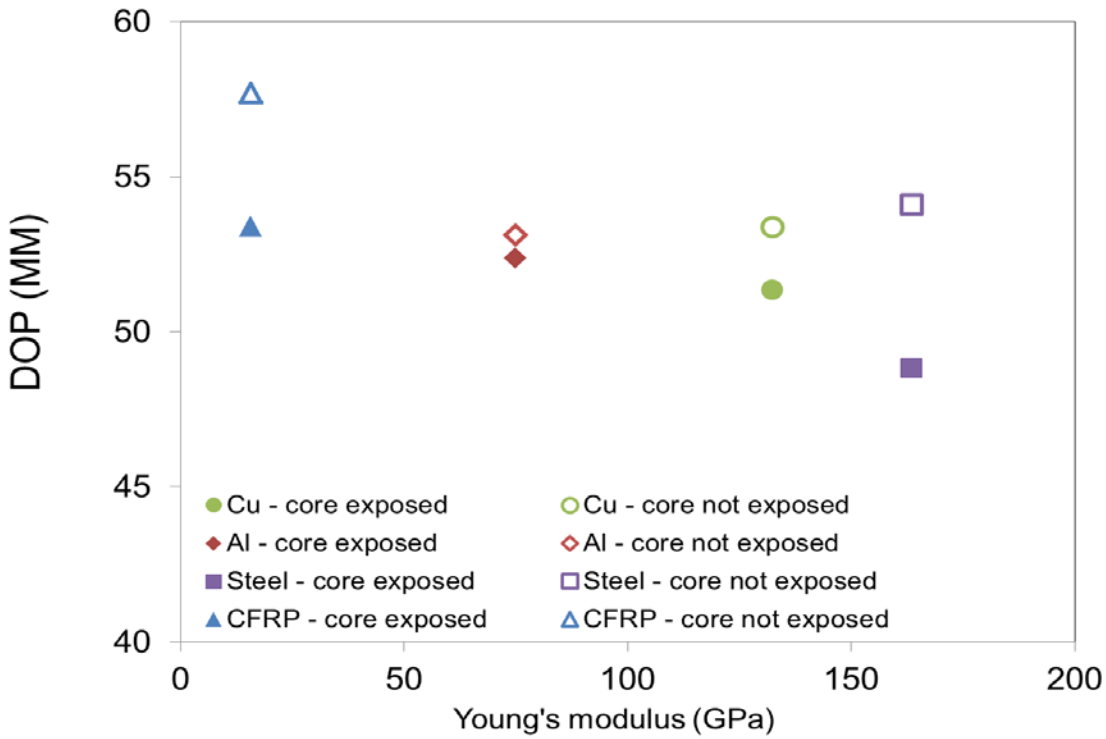

Figure 4.4 – (d) Effect of Young's modulus (GPa) on DOP.

Figure 4.4 (d) shows the effect of Young's modulus on DOP. Young's modulus, as described previously in Section 2.1, is the resistance to flexure of a material. Where ballistic impact is concerned a material with a higher Young's modulus should be better as the material would demonstrate a resistance against flexure which typically results due to the incoming round.

Consistent with the patterns / trends demonstrated with the previously considered material properties, figure 4.4 (d) shows that the rounds where the core was pre-exposed rounds have a reduced DOP, the higher the Young' modulus. The fully jacketed rounds, once again show a general trend downward but as previously seen with other material properties the apparent trend appears less well defined. Once again, a difference in terms of observed DOP between the core exposed and fully jacketed rounds is apparent. Essentially, a material with a higher Young's modulus would push back against the incoming round helping to strip the jacket and therefore leave the core vulnerable to further defeat.

Overall it can be seen by the material properties tested that they all have a clear involvement in the reduction of DOP, especially where the jacket has been removed. This clear difference hints to the role that the bullet jacket has on penetration being one of a cushioning or shock absorbing effect at this particular stripper thickness. It is notable, however, that DOP is linked not to any one material property, but many – likely beyond those considered here. This highlights the multi-faceted nature of core-jacket-target interaction. The figures presented in this section also show that from the stripper plate materials considered, Steel appears to be the best with regards to its ability to remove the jacket / thereby reduced subsequent penetration.

4.1.4 Forward ballistic experiments – 30 mm Gas gun and SAER

Investigation of anomalous data

A 30 mm (smooth) bore gas gun was employed to conduct experiments to help further understand the apparent phenomenon witnessed during the penetration of 2-mm thick Aluminium stripper plates in Section 4.1.3. In this region, the inclusion of the plate was observed to apparently increase the subsequent depth of penetration over the baseline. This phenomenon was also witnessed, albeit to a lesser extent, at plate thickness of 6, 2, and 4 mm for Cu, Steel, and CFRP respectively. (see DOP data, Section 4.1.3).

For these experiments, rounds were fired into a polyurethane replacement resin (PRR) target with a 2 mm Al stripper plate, stood off 25 mm as per the target set up mentioned in Section 3.1.2, figure 3.7, with the aim of capturing the round after penetrating a 2 mm Al cover. Further, it was desired that any plugged material could be identified in the projectiles penetration path. Unfortunately, due to lack of material required and the velocity of the round, these experiments were unsuccessful. The velocity of the round had to replicate the velocity seen on the SAER, <900 m/s, in order to hopefully exceed the shear strength of the material for plugging, not perforation to occur. At these velocities the round completely passed through the target material. Lowering the velocity to 650 m/s allowed the round to be caught in the PRR, but plugging was not witnessed and no Aluminium was found in the penetration path (see figure 4.5).

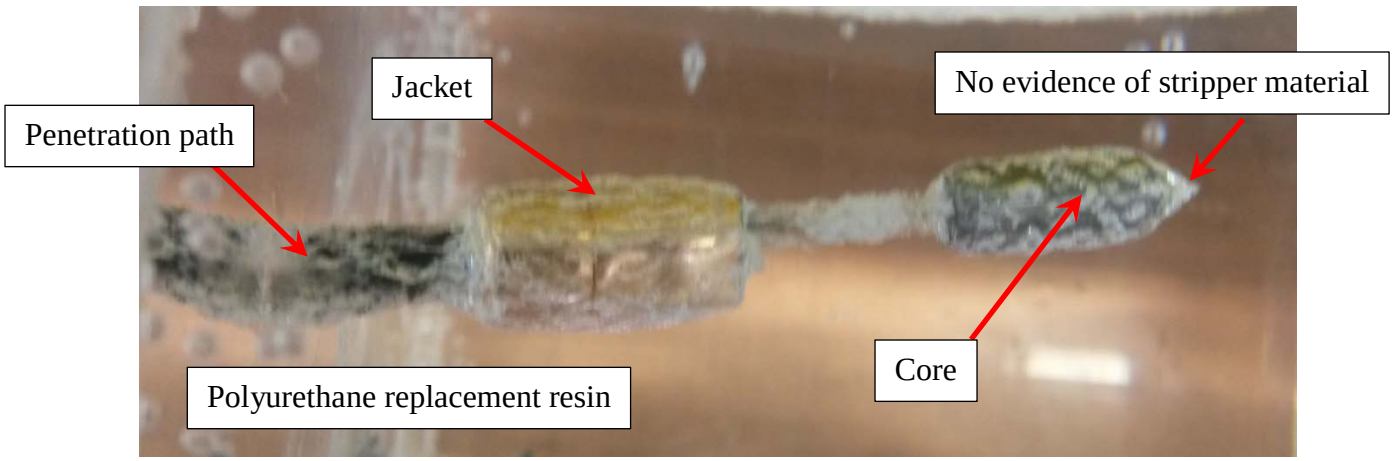

Figure 4.5 – Modified round fired into PRR resin.

To this end, as the lack of sheared / plugged material may well have been linked to the relatively low velocities employed to ensure projectile capture. To investigate this further a final set of experiments were conducted on the SAER. In these tests, both a modified and fully jacketed round were fired through a 2-mm thick 6082 T651 Aluminium plate with no target material behind. The penetration and the subsequent flight of the rounds were then filmed using a high speed Phantom V1212 camera with a frame rate of 70,000 frames-per-second. Still images of the unmodified round passing through the stripper plate can be seen in figure 4.6. It can be clearly seen that there is indeed a plug of Aluminium that remains on the nose of the bullet jacket of an unmodified round. The velocities of the rounds fired were 934 – 940 m/s. From this we can conclude, if tentatively, that the material is indeed having an effect on the penetration of the backing material by protecting the core longer and acting like a secondary jacket / layer of protection.

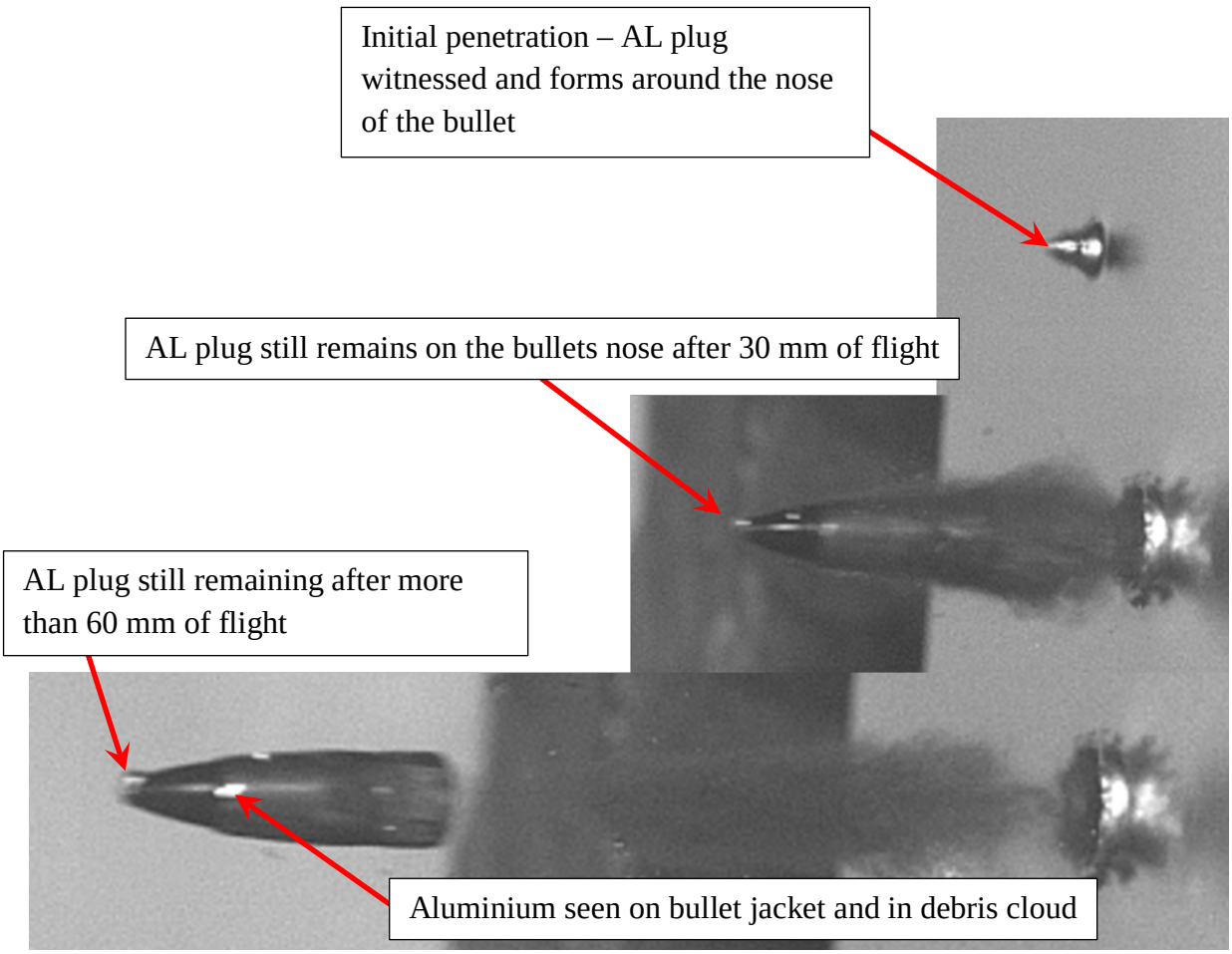

Figure 4.6 – Penetration of a fully jacketed round through 2-mm thick Al6082 T651 plate at 934 m/s.

In contrast, figure 4.7 shows a still image from a firing with a modified round. Some trace indications of Aluminium remain on the tip of the core after penetration but nothing comparable to the amount of Aluminium seen in figure 4.6.

Referring to the DOP data (Section 4.1.3), the largest increase in depth of penetration above the baseline targets witnessed was on the Aluminium data with an unmodified round (see figure 4.3 (c)) The results seen in figures 4.6 and 4.7 are consequently consistent with the experimental results. Essentially, the modified round shows no increase in penetration above the baseline target. If evidence of a greater amount of Aluminium was witnessed present on the tip of the modified penetrating bullet (figure 4.7), one would assume a greater depth of penetration than witnessed in Section 4.1.3, figure 4.3 (a), for this round would result, where it is hinted that the Aluminium would be acting as a bullet jacket.

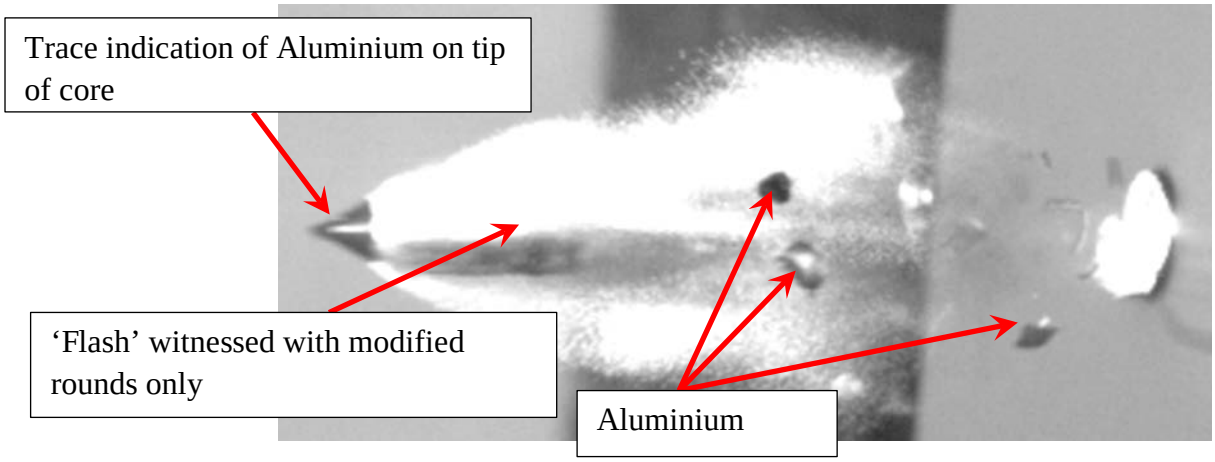

Figure 4.7 – Penetration of a modified round through 2-mm thick Al6082 T651 plate at 940 m/s.

4.1.5 Forward ballistic experiments – 50 mm Gas gun

A 50 mm (smooth) bore gas gun (see Section 3.1.3) was employed to image (using flash X ray – see Section 3.1.3) the penetration process of two thicknesses of Copper stripper plate to achieve a better understanding of the underlying penetration mechanisms.

Experiment number	Stripper plate material	Thickness in mm	Core exposed – YES or NO	Velocity in m/s	X ray power in kV	Number of successful images	Depth of penetration in mm
151105A	Copper	2	YES	876	34	4	49.25
151105B	Copper	6	YES	961	34	4	50.52
151105C	Copper	2	NO	986	34	4	56.34
151105D	Copper	6	NO	961	34	4	52.30

Table 4.1 – Forward ballistic experimental details.

The target was placed 80 mm from the muzzle of the gun and the velocity was estimated for the weight of the projectile used. A time was calculated using equation 4.3, to enable the X rays to fire and capture the penetration event. A total of four images were taken of each penetration event, increasing the chance of capturing full penetration of the plate. Full shot settings including depths of penetration can be found in table 4.5. The images seen below are a zoomed in image of the last X ray of each shot, showing the most information. The subsequent X rays for each shot can be seen in appendix 3.

$$T = \frac{D}{S}$$

Where T is time in µs, D is distance in mm and S is speed in mm/µS.

Equation 4.3 – Equation to calculate time delay from speed and distance.

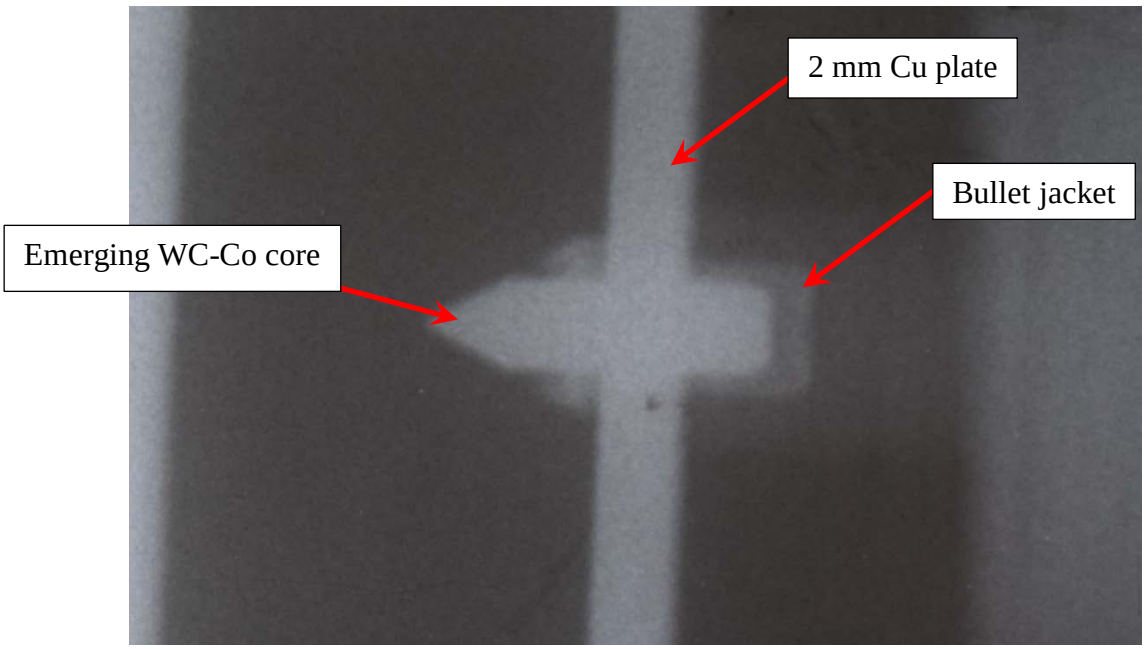

Figure 4.8 - Experiment number 151105A (table 4.5) – X ray D at 65 µs after trigger point. Modified projectile at 876 m/s penetrating a 2 mm Cu stripper plate.

Figure 4.8 shows full penetration of a 2-mm thick Copper (Cu) stripper plate by a modified (nose pre-stripped) round. The remaining jacket material can still be clearly seen to the right of the plate, sat around the back of the round. The material around the front of the penetrating core / to the left of the stripper plate, however, is of a different thickness and is assumed to be Cu being pushed through by the projectile which petals out of its path. It's worth noting that the bullet / penetrator tip appears relatively un-deformed.

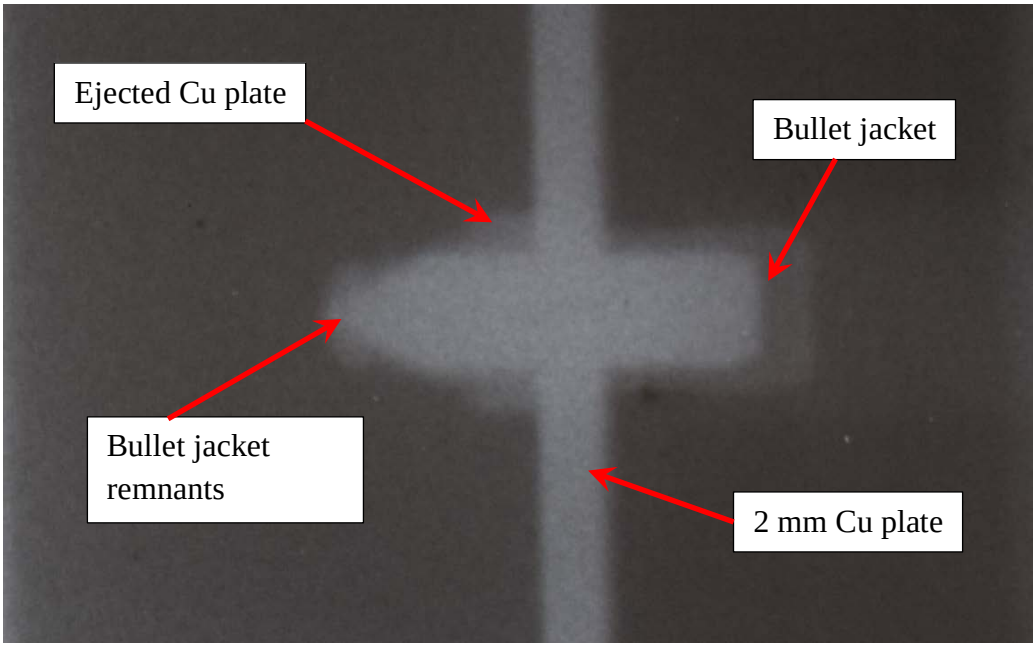

Figure 4.9 - Experiment number 151105C (table 4.5) – X ray D at 61 µs after trigger point. Unmodified projectile at 986 m/s penetrating a 2 mm Cu stripper plate.

Following on from figure 4.8, figure 4.9 shows an unmodified round penetrating a 2-mm thick Cu stripper plate at a similar velocity. Interestingly, while the jacket has been largely stripped to the sides of the core's apex, around the nose of the bullet a feature is clearly apparent on the front of the round. This is likely a remnant of the bullet jacket rather than sheared / plugged material from the jacket stripper (due to the width and apparent density of this material being comparable to the jacket visible to the right of the penetrating round). To this end, this X ray strongly suggests that a 2-mm thickness of Cu is insufficient to fully strip the round. Consequently, in this case, the jacket will continue to aid (to a certain extent) penetration of the backing material along with the core. This result explains the relatively small drop in recorded DOP observed for 2-mm thick Cu stripper plates (see figure 4.3(a), Section 4.1.3) – and for the un-modified round case in particular. Essentially, it is postulated that this inclusion of remaining jacket material ahead of the round in the un-modified case is helping to protect (cushion) the core from induced shock waves set up within the core on impact with the backing material from the backing material upon penetration. Whereas in the pre-stripped case shown in figure 4.8, a slighter greater DOP results in figure 4.3(a). While the difference is small at this 2-mm stripper plate thickness, it never-the-less appears to be a physical effect as the difference between modified and un-modified rounds continues (and enlarges) at higher stripper plate thicknesses.

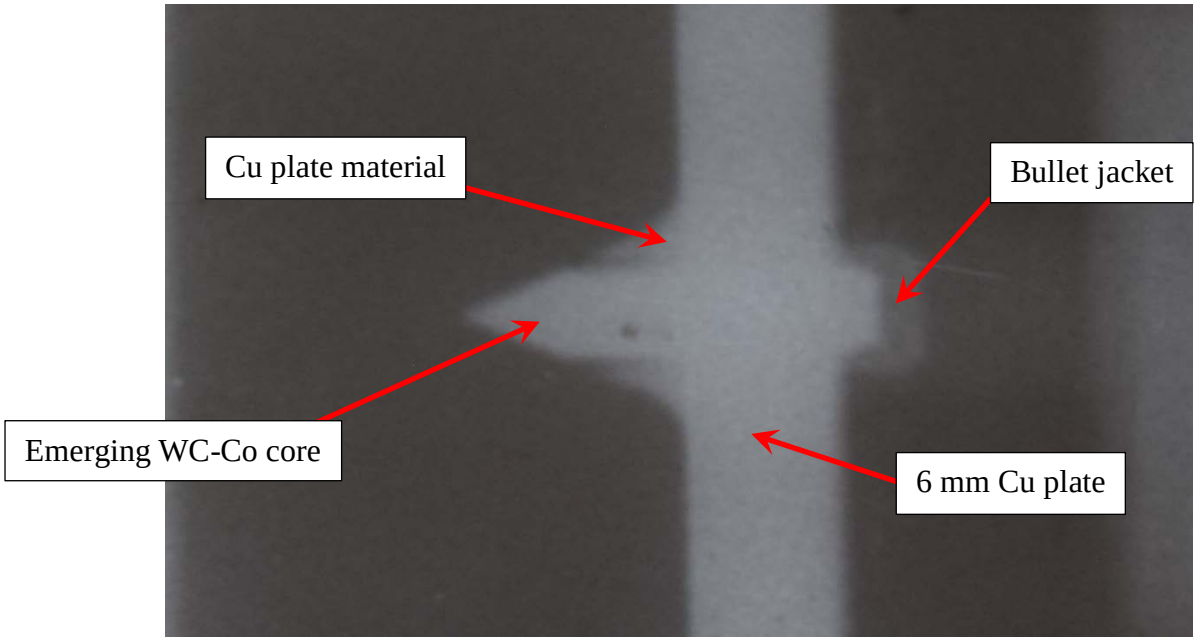

Figure 4.10 - Experiment number 151105B – X ray D at 65 µs after trigger point. Modified round at 961 m/s penetrating a 6 mm Cu stripper plate.

Moving to a greater stripper plate thickness, figure 4.10 shows a modified round penetrating a 6-mm thick Cu stripper plate. In line with figure 4.8, the round can clearly be seen exiting the plate with no jacket present. In this case, it is notable that a greater degree of separation exists between the penetrating core and the material pushed through from the Cu plate (as opposed to figure 4.8, where the petalled stripper plate material was in intimate contact with the core). This is assumed to be a function of the thicker plate and the consummately greater amount of material pushed ahead of the penetrating core. It is also notable that, despite the greater Cu thickness penetrated, the core has still not been blunted.

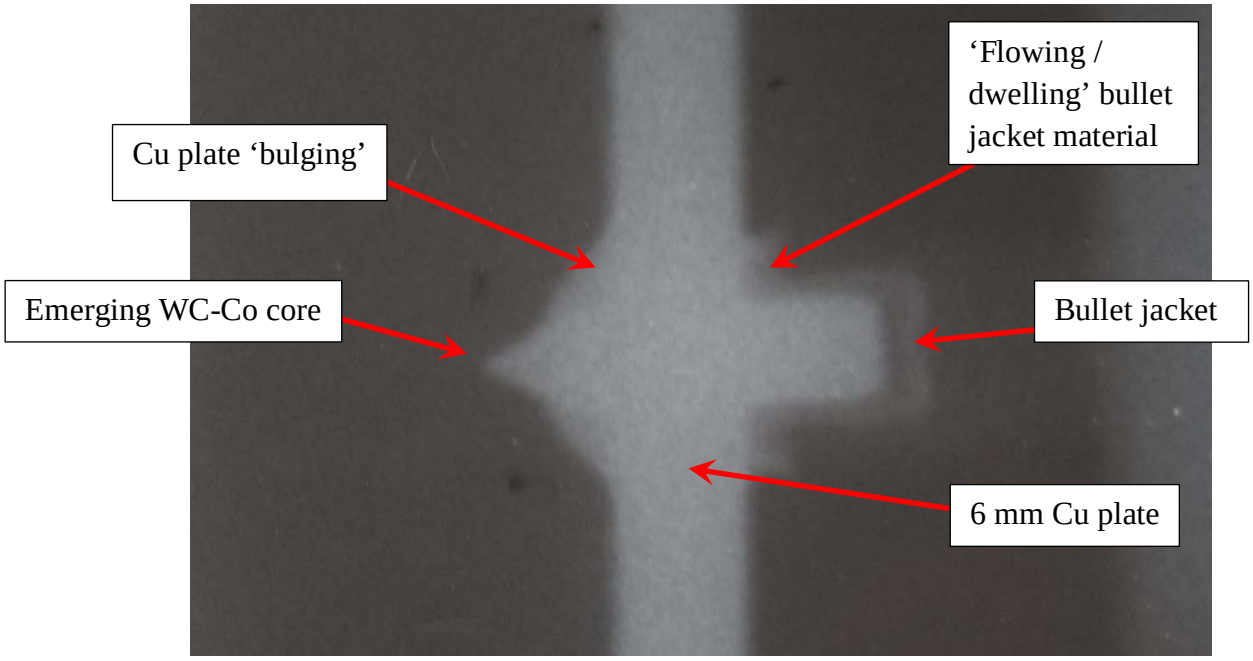

Figure 4.11 - Experiment number 151105D – X ray D at 61 µs after trigger point. An unmodified round at 961 m/s penetrating a 6 mm Cu stripper plate.

Figure 4.11 illustrates one of the flash X rays captured from the final 50 mm gas gun forward ballistics test; in this case, with a 6-mm thick Cu stripper plate, which is being penetrated by an unmodified round. The thicker plate than was the case in figure 4.8 (where an unmodified round is pictured penetrating a 2-mm thick Cu plate) was successful in fully stripping the round. This can be seen by the sharp point of the emerging core on the left of the image. In addition, the back face of the stripper plate can be seen ‘bulging’. This bulging of the plate likely represents the point just before the plate ruptures and the penetrating core pushes the material outwards, as seen in the X rays from the previous three tests. As well as this apparent rupture of the plate as the projectile penetrates, on the right hand side (the impact face) material is apparent flowing on the surface of the stripper plate. It is postulated that this could be jacket material being eroded away by the Copper plate (flowing / dwelling on the surface).

Overall, the X ray images captured over the course of the forward ballistic experiments detailed in table 4.5 illustrate a number of key points.

1) Firstly, thicker 6 mm Cu plates were successful in fully stripping the round, whereas 2-mm thick plates were not.

2) Secondly, the importance of the jacket was highlighted – with stripped rounds being defeated more easily, shown by the resultant DOP data (see table 4.5) into the same backing blocks used for all forward ballistic experiments undertaken on the SAER. This behaviour was consistent with the previously presented DOP data for the Cu stripper plate experiments using the small arms range in Section 4.1.3, figure 4.3 (a).
3) Finally, the captured flash X rays illustrated the importance of not only the stripping process, but also the interaction of the round with the stripping plate (e.g. the use of a modified round fired through a 2-mm plate showed evidence of the stripping plate actually cushioning the subsequent impact via plugging of a disc / piece of jacket material ahead of the round, something not seen with a thicker stripping plate).

The third point highlighted above is of particular significance. From the previous conventional forward ballistic investigation detailed in Section 4.1.3, figure 4.3(a), the DOP for the experiments involving a 6-mm thick Cu stripper plate showed the unmodified round still having an increased penetration into the backing blocks as opposed to the modified rounds. However, as demonstrated in the series of forward ballistic experiments described in this section, in both cases as the jacket is fully stripped, a fully exposed core is – in theory – hitting the backing blocks meaning that the resultant depth of penetration should be the same. However, as shown in figure 4.3(a) this is not the case. Consequently, the difference in performance can only be attributable to the presence of the jacket. It is possible that the Cu stripper plate – with its associated high density (and therefore impedance) – pre-loaded the impacting round. However, from the flash X rays presented in figures 4.10 and 4.11 showing penetration of a 6-mm stripper plate by modified and un-modified rounds respectively, no evidence of resultant core shattering is apparent. Instead, the main difference appears to be the substantially greater amount of material (both jacket and stripper plate) carried through with the round in the un-modified case. Copper is a very soft, malleable material which is significantly more ductile than some of the other stripper plate materials tested even at high strain rates (e.g. Cu is typically used as a shape charge liner material [4, 28, 37, 38]). To this end, while Cu would not be very good at helping to defeat a round through pre-shocking, it would act as a useful tough cushioning material on projectile impact if pulled ahead of the core. Interestingly, however, despite the bulge apparent ahead of the penetrating round in figure 4.11, no evidence of material being extruded ahead of the (now exposed, but originally un-modified) core is apparent (nor is there an apparent plug seen for the 2-mm thickness in figure 4.9). Instead, in this case, it is tentatively postulated that the stripper may have played

a confining role – with the added disruption to the Cu stripping mechanism caused by the presence of the jacket leading to continued confinement of the core as it emerged from the stripping plate.

4.2 Reverse ballistics – 50 mm Gas gun

In order to provide further insight into the jacket stripping mechanism, while removing the influence of factors such as yaw, several reverse ballistic experiment was undertaken using a 50 mm smooth bore gas gun (see section 3.1.3). For these experiments a target material was accelerated into a stationary bullet and the subsequent impact was imaged via flash X ray. In order to optimise use of the experimental facilities, these experiments were conducted alongside an in-house research programme with a third party (Prof. Ian Crouch, RMIT Brunswick, Australia). This necessitated the use of a different AP round. However, the experimental work was conducted by the present author, with interpretation presented here the work of the same. As touched on, the round employed was a M43 7.62 mm Soviet round (see Section 1.2.6, figure 1.23) not a 7.62 mm FFV round, as previously used on the other experiments. This was not a significant issue as the round, for these experiments, was somewhat irrelevant. The idea behind conducting these tests was to see if CFRP would strip a Copper jacket from an armour piercing round, and to identify any associated mechanisms. While the CFRP employed had a different layup to the material used here, its density was comparable and, consequently, in line with work by Hazel *et al*. [25] which suggested that areal density was key in terms of ballistic properties, it was decided that this test would still provide useful – even if not qualitative – data to compare to the conventional forward ballistic test results presented previously in section 4.1.

The X ray image shown in figure 4.12 is the last image of the 4 taken from experiment number 151103A (see table 4.6) and shows the key features observed during this test. For completeness, the rest of the X ray images captured are in appendix 4. Timing for the triggering of the X rays was calculated in the same manner as the timings for the X rays in Section 4.1.5, with full experimental details presented in table 4.6. The results taken from all of the reverse ballistic experiments seen in table 4.6 can also be found in appendix 4, as they all showed similar results, it was decided that experiment number 151103A showed the best images.

Experiment number	Stripper plate material	Thickness in mm	Core exposed – YES or NO	Velocity in m/s	X ray power in kV	Number of successful images
151103A	CFRP	18	NO	733	34	4
151103B	CFRP	20	NO	722	34	4
151104A	CFRP	20	NO	719	34	4

Table 4.2 – Experimental details for reverse ballistic firings.

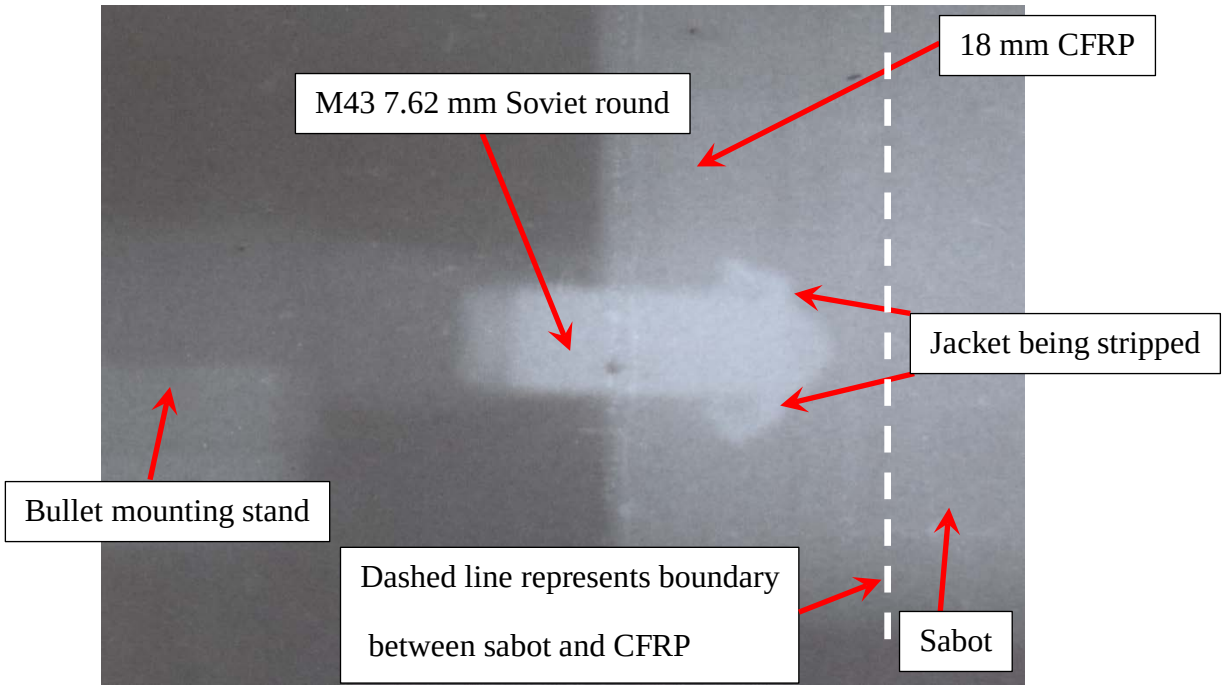

Figure 4.12 - Experiment number 151103A – X ray D at 125 µs after trigger point showing the jacket removal of a Steel cored projectile at 733 m/s.

Figure 4.12 clearly shows the jacket of the penetrating round being removed by the CFRP. The CFRP target was 18-mm thick. From the X rays, it was calculated that the round was being stripped at a depth of approximately 8 mm from the front face of the CFRP 'target' material. Taking this information, it seems reasonable to assume that the CFRP forward ballistic targets considered in the conventional ballistics experiments were successfully

stripping the round at the 10 mm stripper plate thickness. By comparing this with the depth of penetration data (see Section 4.1.3, figure 4.3 (d)) it can be concluded that the CFRP will strip a round but have little effect on arresting the bullets penetration into a target. Essentially, it appears that in terms of jacket removal other material properties, such as hardness (66 HV compared to Steel – 284 HV, Copper – 100 HV and Al – 125 HV) are important. However, the fact that higher thicknesses of the relatively low density CFRP have been shown to successfully strip a jacket does suggest that if combined with a hard material (to pre-stress the core), the inclusion of CFRP as a key element of a composite jacket stripping solution might be a practical proposition.

4.3 Split Hopkinson Bar Experiments (SHPB)

In addition to the ballistic testing, a Split Hopkinson Pressure Bar (SHPB), detailed in Section 3.1.5, was employed to further understand the passage of shock through a WC-Co core and jacket material. This equipment was not used to investigate stresses directly – but instead to look at the influence of differing material configurations on an initial input wave. Consequently, while strain gauge data is only presented in voltage-time form, this was considered sufficient for such qualitative analysis (e.g. as strain is directly proportional to voltage).

As an example of the resultant output, Figure 4.13 shows two transmitted stress traces taken from the transmission bar; one for a shot that just had a plain core as the target between the bars, and the second for the case of a core with a Copper plate (representative of a ‘jacket’) in front. In both cases the input velocity was within 1 m/s using the same chrome Steel striker bar (as mentioned in Section 3.1.5) and the resultant trace from the input bar was consequently the same (please see appendix 3 for all SHPB gauge traces). Full shot settings can be found in table 4.7.

Shot number	Target configuration	Velocity (m/s)	Shot pressure (Bar)	Notes
160226A	Core	26	2	Used in figure 4.13
160226B	Core + Cu	26	2	
160226C	Core + Cu	25	2	
160226D	Core + Cu	25	2	
160226E	Core	25	2	
160226F	Core + Cu	26	2	Used in figure 4.13
160226G	Cu	25	2	

Table 4.3 – SHPB shot settings. Note, in all cases Cu plates were nominally 0.75-mm thick.

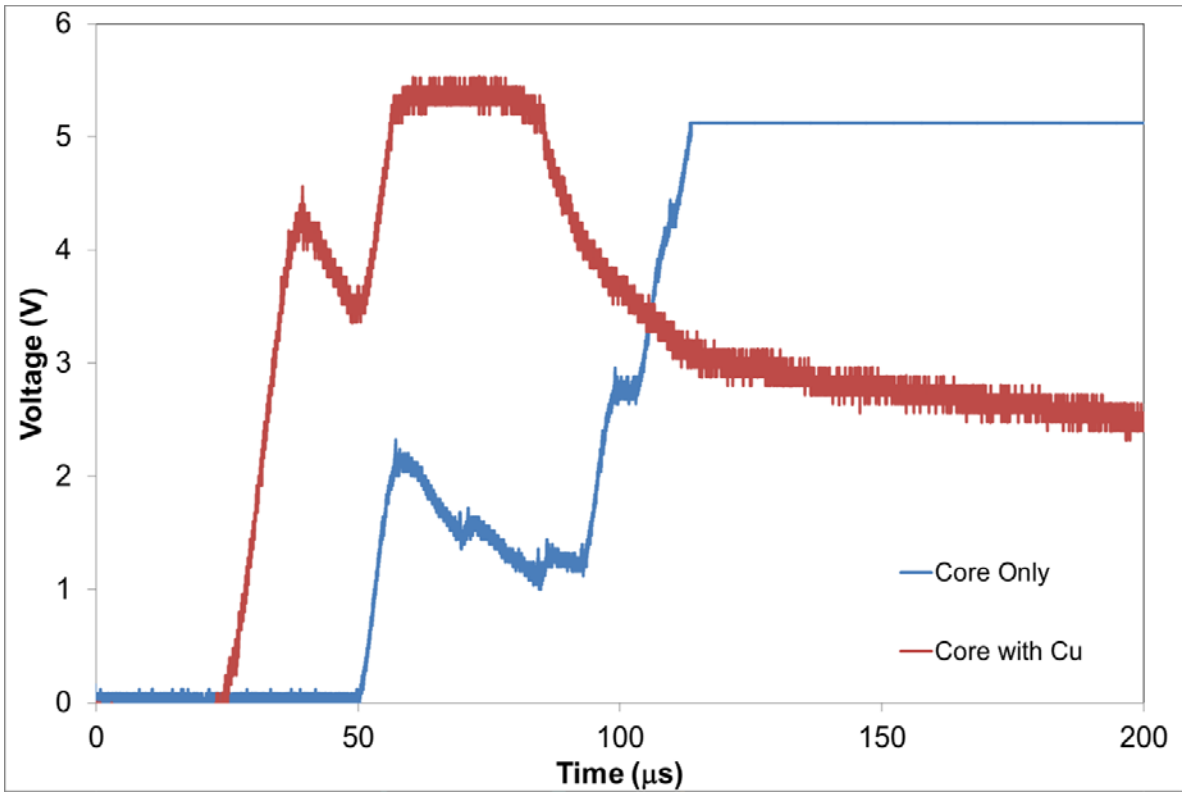

Figure 4.13 – SHPB trace comparisons for shots 160226A and 160226F at 25 and 26 m/s, respectively.

Figure 4.13 shows the resultant voltages from the transmitted bar for shot numbers 160226A and 160226F. Shot 160226A (the blue trace) illustrates the resultant (transmitted) voltage from a shot with just the core present. An initial rise to just over 2 volts is apparent, with this decaying before a further increase to just under 3 volts. While a subsequent ring-up occurs to a small plateau around 4 volts before a final rise to a point where the gauge trace clips the top of the oscilloscope settings. This staged rise, or ringing up, suggests multiple reflections off different surfaces / interfaces and could also be the first indications of spallation occurring within the round leading to ultimate defeat. Given the gauge was located 250 mm from the target as well as 775 mm from the end of the chrome Steel bars, it is possible that this could represent a series of reflections from one of these interfaces. However, given a chrome Steel sound speed of 5.96 mm / μs [81] and a distance of 1550 mm for the shock to travel (775 mm from the gauge to the other end of the bar and back again) would lead to a time period of nominally 260 μs calculated from a rearrangement of equation 4.3 in Section 4.1.5. A greater time than the initial (approx.) 200 μs observed here. In addition, it is notable that these oscillations appear to decrease in frequency. This suggests that they are inherent to the target itself which would be compressing – maybe due to reflections from induced micro-cracks or similar. Such a failure mode with loading and un-loading would suggest the beginning of spallation (e.g. dynamic tensile failure – resulting from reflection of compressive waves at a free / lower impedance surface, leading to net tensile stresses [82]). Interestingly, while anything beyond incipient spall would not be occurring here, this supposition is consistent with the recovered modified rounds from the Steel stripper plate experiments, where complete failure of the round has occurred (see Section 4.6, figure 4.19) through spallation. In addition to these large period features, a very high frequency oscillation is also apparent superimposed on the main trace (in both cases). This could represent a well-known phenomenon called Pochhammer Chree which arises due to the fact that the elastic waves in the SHPB's are not one-dimensional in nature [41]. The waves could also be partly attributed to digitisation of the data when transferring it from the oscilloscope.

The second (red) trace in figure 4.13 represents the transmitted pulse for shot 160226F, which involved a target comprising a WC-Co core and a 0.75-mm thick Copper plate in front to (nominally) simulate a bullet jacket. Pochhammer Chree / digitisation oscillations are again visible. However, interestingly, it is immediately apparent that the simple inclusion of this Cu plate (in intimate contact with the end of the WC-Co core) leads to a significantly higher amplitude transmitted pulse than was the case with the core-only shot. There is also evidence

of a secondary rise up to the same voltage as witnessed on the input gauge on the input bar, 5.3 Volts. This is likely a result of the presence of the additional Cu-WC-Co interface. Essentially, the addition of a Copper 'jacket' eases transmission of energy (the stress pulse) through the bars. This implies that where a bullet jacket is present, this will help couple energy away from the core (which would otherwise be reflected back into it). This mechanism helps reduce the peak stress encountered by a significant margin.

Overall, the SHPB traces presented in appendix 3 and those presented in figure 4.13, strongly suggest that the inclusion of a 'jacket' material in front of the round helps to attenuate the extent of pre-loading / 'shocking' of the round. In addition, the reduced large-scale oscillations / ringing (tentatively attributed to micro-cracking within the sample for the WC-Co core-only case in figure 4.13) strongly suggest that this attenuation caused by a Cu buffer is reducing the peak stress sufficiently to reduce susceptibility of the core to failure modes which would normally lead to spallation (see Section 1.1.2). In this manner, while limited in extent, these SHPB experiments illustrate the importance of bullet tip removal. Essentially, this helps in terms of maximising the magnitude of the reflected waves in the projectile resulting from initial penetration of a target material; this pre-stresses the round, leading to an enhanced chance of failure / defeat (e.g. via dwell or spallation), subsequently lessening penetration.

4.4 Hydraulic press tests

In addition to the ballistic tests and SPHB experiments, hydraulic press tests were performed on jacketed and modified rounds to quantify the difference in the peak pressure needed for a WC-Co core to penetrate a stripper plate material as well as the bullet jacket. Experiments were conducted on each type of round at two different stripper plate thicknesses and the results were recorded. The data presented in table 4.8 is very consistent between the two stripper plate thicknesses. The increase in pressure to push the core through the added jacket material is similar for the 2 mm plates and the 4 mm plates, between 0.43 and 0.57 kg/mm^2, respectively. The difference in the peak pressure required to push a round through the plate is due to the plates overall thickness, 2 mm against 4 mm. This helps to show that very little pressure is required to remove a bullet jacket. Therefore, it can be assumed that any differences in penetration seen on the DOP data (see Section 4.1.3, figure 4.3 (a) to (d)) are

attributable to the interaction of the bullet with the stripper plate and the subsequent interaction of the 'stripped' round with the target, rather than energy lost in stripping the jacket itself.

Stripper plate material	Thickness (mm)	Projectile type	Peak pressure required for full penetration (kg/mm^2)
Copper	2	Core only	0.40
Copper	2	Core only	0.41
Copper	2	Core and jacket	0.43
Copper	2	Core and jacket	0.43
Copper	4	Core only	0.55
Copper	4	Core only	0.55
Copper	4	Core and jacket	0.57
Copper	4	Core and jacket	0.56

Table 4.4 – Data from hydraulic pressing experiments.

4.5 Numerical simulation

As discussed in the introduction, computational modelling represents a potentially economical approach to the development of armour systems. However, as highlighted, the accuracy of simulations are inherently linked to material and associated failure properties. To this end, given the resultant variability due to the large number of material and experimental parameters involved in most situations, use of computer models on their own is arguably insufficient. Instead they need to be underpinned by experimental studies – hence the work

contained in this thesis. However, given their importance, it was decided to investigate whether a basic hydrocode model could simulate some of the core features identified in this thesis. As nominally outside the main sphere of this study, the author worked closely with an in-house expert with regards to creation of the models and rather than concentrating on this element (which is described briefly below), the results are instead the main focus of this section.

In order to provide a useful and accessible baseline, the experiments considered here were two shots undertaken by the author in conjunction with a previous local project [83] in the build-up to this project. These comprised two reverse ballistic experiments in which a stationary (AP) Steel-cored M43 round (see figure 1.24) was impacted by a Boron Carbide (B_4C) fronted sabot both with and without a Cu cover. Details are shown in table 4.9, following the experimental approach that is covered in section 4.2.

Experiment number	**Copper present – YES or NO**	**Velocity in m/s**	**X ray power in kV**	**Number of successful images**
140515A	NO	721	34	4
140515B	YES	735	34	4

Table 4.5 – Experimental settings for reverse ballistic firings to correspond with numerical models.

4.5.1 Numerical model setup

The computational model developed in conjunction with the in-house numerical modelling expert comprised a Stainless Steel core of the same nominal dimensions of the M43 round and an impactor comprising a 10-mm thick and 50-mm diameter (modelled as a 25-mm radius, axially symmetric component) B_4C ceramic plate both with and without a 1-mm thick Cu cover. The model was axially symmetric and constructed with a Lagrangian mesh (see

Section 1.3) of density 0.1 mm^2, with impact events occurring at 730 m/s. Key material properties were taken from the in-built Ansys® Autodyn material models and are summarised in table 4.10. In addition, several gauge points were included in the modelled (stationary) projectile, at a distance of 0.5, 1.0, 1.5 and 2.0 mm back from the core tip and are labelled accordingly in figures 4.16, 4.17 and figures 4.19 and 4.20.

Element of model	Material	Equation of state	Strength model	Failure model	Erosion model type
Core	Stainless Steel	Shock	Piecewise Johnson Cook	None	Geometric strain (default value)
Ceramic disk	B_4C	Shock	Johnson-Holmquist	Johnson-Holmquist	Geometric strain (default value)
Copper cover	Cu	Shock	Piecewise Johnson Cook	None	Geometric strain (default value)

Table 4.6 – Key material properties taken from Ansys ® Autodyn.

4.5.2 Flash X ray data

The flash X rays which resulted from the experimental programme previously undertaken are presented for reference in figure 4.14 and figure 4.15 below. They illustrate flow of the (stationary) projectile following the impact event in both cases – however it was noted at the time that the remaining core material had a substantially reduced length in the case of the B_4C-only impactor (13 mm to 9 mm Cu / no Cu respectively) [27]. Full flash X ray radiographs from these experiments can be seen in appendix 4.

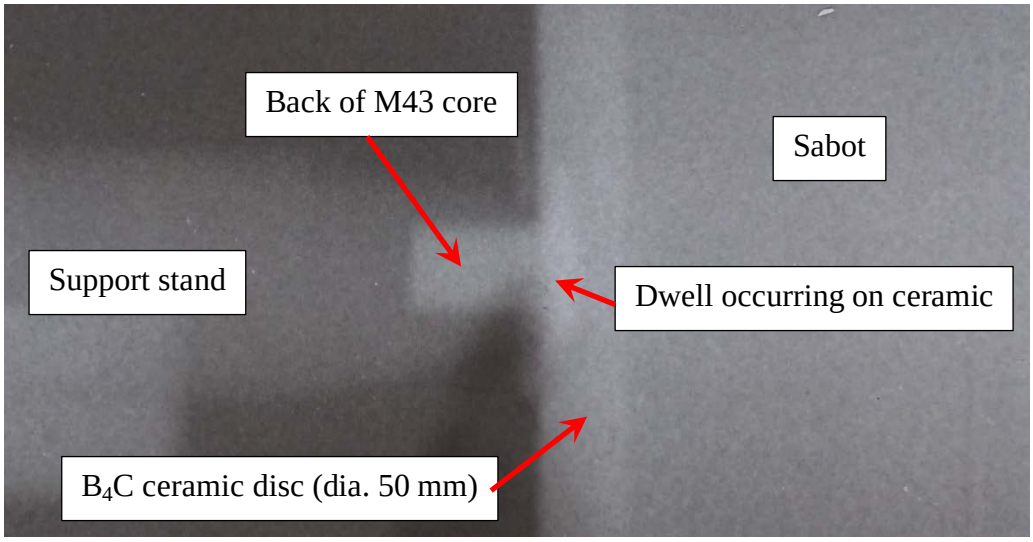

Figure 4.14 – Reverse ballistic impact at 721 m/s of a B_4C impactor into a stationary M43 Steel bullet core (No Copper present).

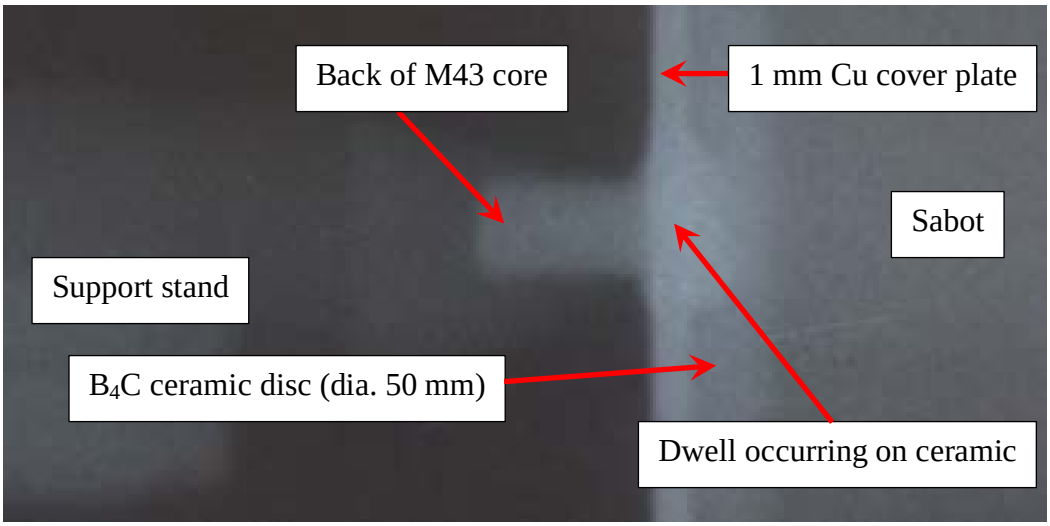

Figure 4.15 - Reverse ballistic impact at 735 m/s of a B_4C impactor into a stationary M43 Steel bullet core (Copper cover present).

From the X ray images featured above it can be clearly seen that figure 4.14 shows a greater amount of deformation and dwell (see Section 1.1.3) of the impacted Steel core. In figure 4.15, where a 1 mm Copper cover has been included to simulate a bullet jacket on the surface of the ceramic, a lesser amount of dwell is observed. Both of these impacts occurred at very similar velocities (721 m/s with no Copper and 735 m/s with Copper) and at the same time after the initial impact event (10 μs), meaning that the differences in behaviour can reasonably be attributed to the presence, or lack thereof, of the Cu cover [83].

4.5.3 Model results

Output from the numerical models took two forms. The first was visual, with images captured as the model ran designed to illustrate the nature of projectile flow to see whether it matched that illustrated in the flash X rays presented in Section 4.5.2 above. The second set of data was in-plane (x-axis) stress from the aforementioned gauge / node point 1, 0.5 mm behind the tip of the stationary core. The aim of monitoring stress at this point was to investigate the influence of the Cu disc on peak stress within the core (in line with the arguments made previously in Section 4.1.3, 4.1.5 and Section 4.3, that the Cu jacket on a penetrating round cushions impacts). To this end, captured images highlighting material flow are shown in figure 4.16, no Cu present, and figure 4.17, inclusion of a Cu cover plate.

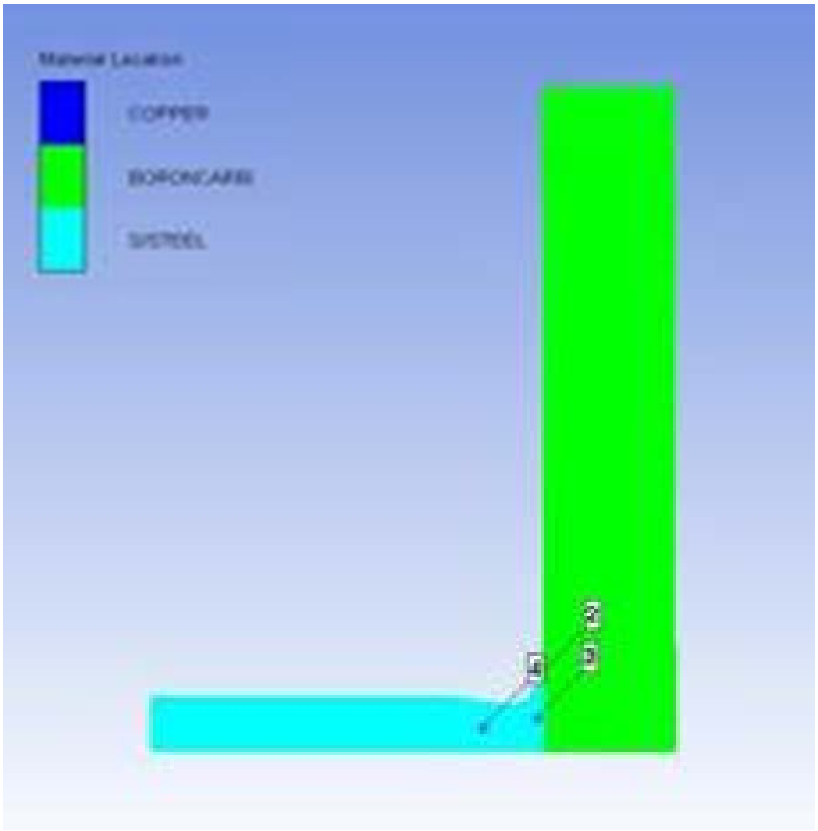

Figure 4.16 – Computational model showing impact of a stationary Steel core by a 50-mm diameter B_4C impactor (the right of the image) at 730 m/s, approx.10 μs after initial impact. Points 2, 3 and 4 represent the corresponding gauge points. Point 1 has been deleted by the impact at this stage.

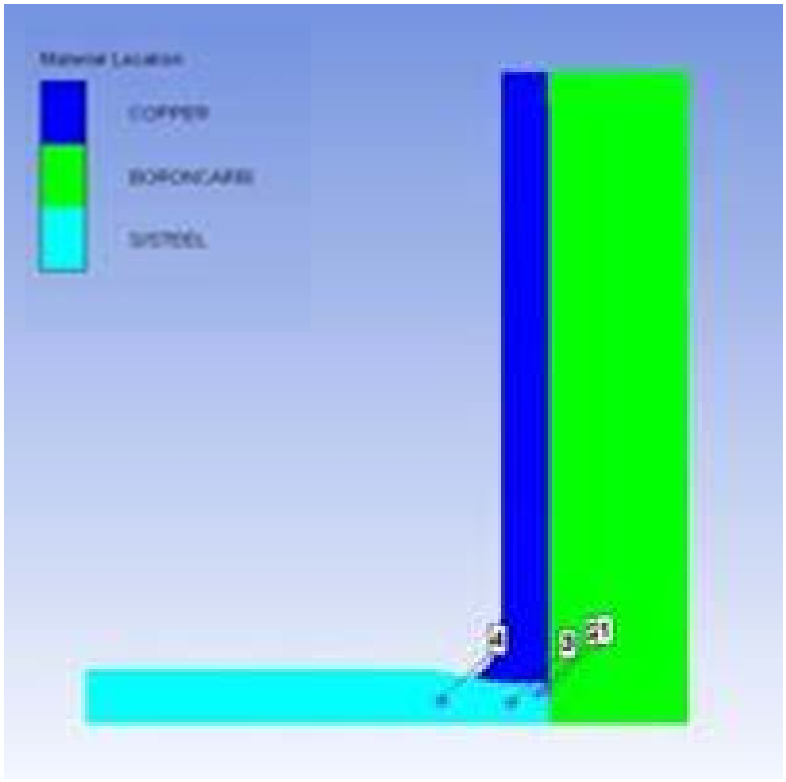

Figure 4.17 – Computational model showing impact of a stationary Steel core by a 50-mm diameter B_4C impactor with the inclusion of a 1 mm Copper cover plate (the right of the image) at 730 m/s, approx.10 μs after initial impact. Points 1, 2, 3 and 4 represent the corresponding gauge points.

The images extracted from the numerical models presented in figures 4.16 and 4.17 are nominally consistent with the flash X rays captured from the corresponding experiments (see figures 4.14 and 4.15 respectively in Section 4.5.2). Essentially, the models and experiments are comparable; in each case the projectile is observed to dwell on the surface of the ceramic, with the experiments involving the inclusion of a Cu cover plate (or surrogate 'jacket') showing considerably less. This difference in response is more evident on figure 4.16, taken from the computational modelling.

However, as discussed previously, both in the experiments considered in this section and in the core work conducted as part of this project, the presence of a Cu or similar material cover (e.g. a jacket in this research) was found to substantially alter penetration. To this end, the stress profiles recorded on gauge point 1, in the tip of the stationary core from the computer models considered here, are presented in figure 4.18 below. It was postulated that although the gauge points showed similar stress profiles, point 1 showed the smoothest profile for viewing purposes.

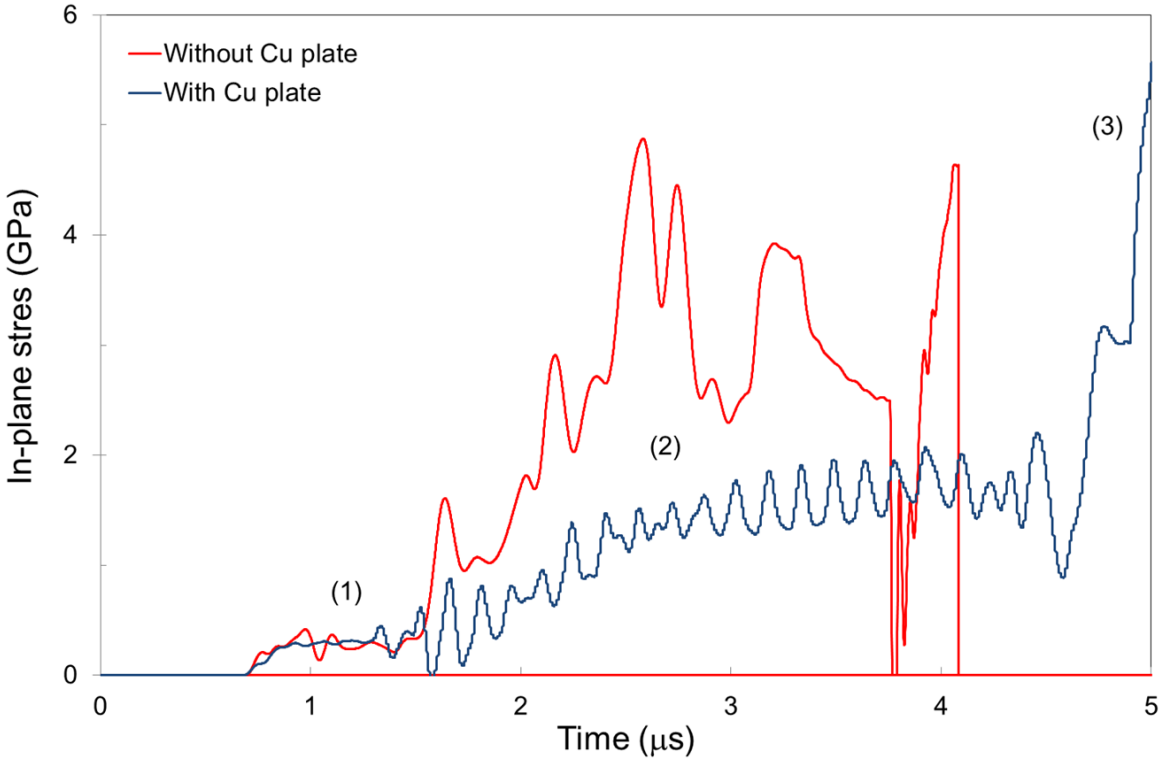

Figure 4.18 – Comparison of modelled gauge traces taken from gauge point 1, 0.5 mm behind the tip of the Steel core at the point of impact.

This graph is extremely interesting; in both the Cu and without Cu cover modelled experiments an initial peak in stress followed by a relatively constant plateau is apparent (area 1 on the graph). This initial peak stress is of the order of the same magnitude for both situations. However, the amplitude and duration of this nominally constant loading period is substantially different for the two differing experiments. This is supported by figures 4.19 and 4.20. The figures represent still frames from the models as they were conducted, ranging from the point of impact and then every ½ μs up to 2 μs duration, covering the initial impact. It can be seen from figure 4.19, where there is no Copper present on the target that within the first stages of penetration the core material is already starting to behave hydrodynamically and flow / dwell is occurring on the surface of the ceramic. This is more evident at 1.5 μs, where coincidently, referring to figure 4.18 the stress is seen to greatly increase. The opposite can be seen in figure 4.20, covering the initial stages of penetration where a Copper plate is present. At the 1.5 μs mark the core is just breaking through the Copper plate and the initial stages of dwell are starting to occur. This can also be seen on figure 4.18 where the pressure is seen to start to increase. These frames also help show the importance of the jacket during

penetration by not only helping to cushion the impact, but also to delay it – potentially meaning the difference between full or partial penetration before the round is defeated.

As they move into area 2 on the graph, it can be seen that the stress in the case of the experiment without the inclusion of a Cu cover, increases to a higher amplitude, almost 5 GPa, in a little over 2.5 μs. The experiment involving the Cu cover plate at this time period is still at relatively low amplitude, compared to the other. Both experimental situations show reverberations over the loading period, this could be due to reflections from interfaces seen within the computational models or indeed they could be a factor of the introduced stress waves ringing up within the Copper plate as the duration of the peaks corresponds with the time taken for the shock velocity to reflect back and forth within the Copper. In the latter part of the graph, area 3, moving toward 4 to 5 μs, it can be seen that the stress in the case of the experiment with no Cu present has already started to decay and reflections are increased in amplitude. By this time it can be postulated that the round is already failing and the dwell witnessed on the surface of the ceramic in the flash X rays and the modelled data is occurring. The experiment with the Cu cover plate is still yet to reach its overall peak stress, and doesn't appear to until well after 5 μs. This delay would encourage a fully jacketed bullet to be able to withstand the peak stresses placed upon it by an armour system for several μs longer, enabling a deeper penetration into the armour system, as witnessed between the fully jacketed and modified rounds from the DOP data (Section 4.1.3). This could mean the difference between defeat and complete penetration.

Overall, it is apparent from the discussion above that the computational model constructed here successfully captures the core elements of the projectile behaviour. While there are inevitably discrepancies between the flash X ray images and the basic models – likely a function of both the differing sample times and factors such as material properties and mesh densities – the qualitative agreement between the models and experiments suggests that a hydrocode could successfully be used to simulate phenomena such as the stripping arrangement presented previously in figure 3.2, Section 3.1.

Importantly, the simulations also highlighted a key mechanism which is associated with the concept of jacket removal. Presence of a Cu spacer between a (stationary) projectile and a hard ceramic impactor was shown to substantially decrease the induced stress in the projectile (see figure 4.18). This is directly analogous to the concept of the jacket cushioning an impactor. As discussed in section 4.3, spall is more likely to occur when an increased

loading occurs on impact; this will eventually lead to enhanced magnitude tensile reflections / releases and – therefore – a greater chance of dynamic tensile failure (spall).

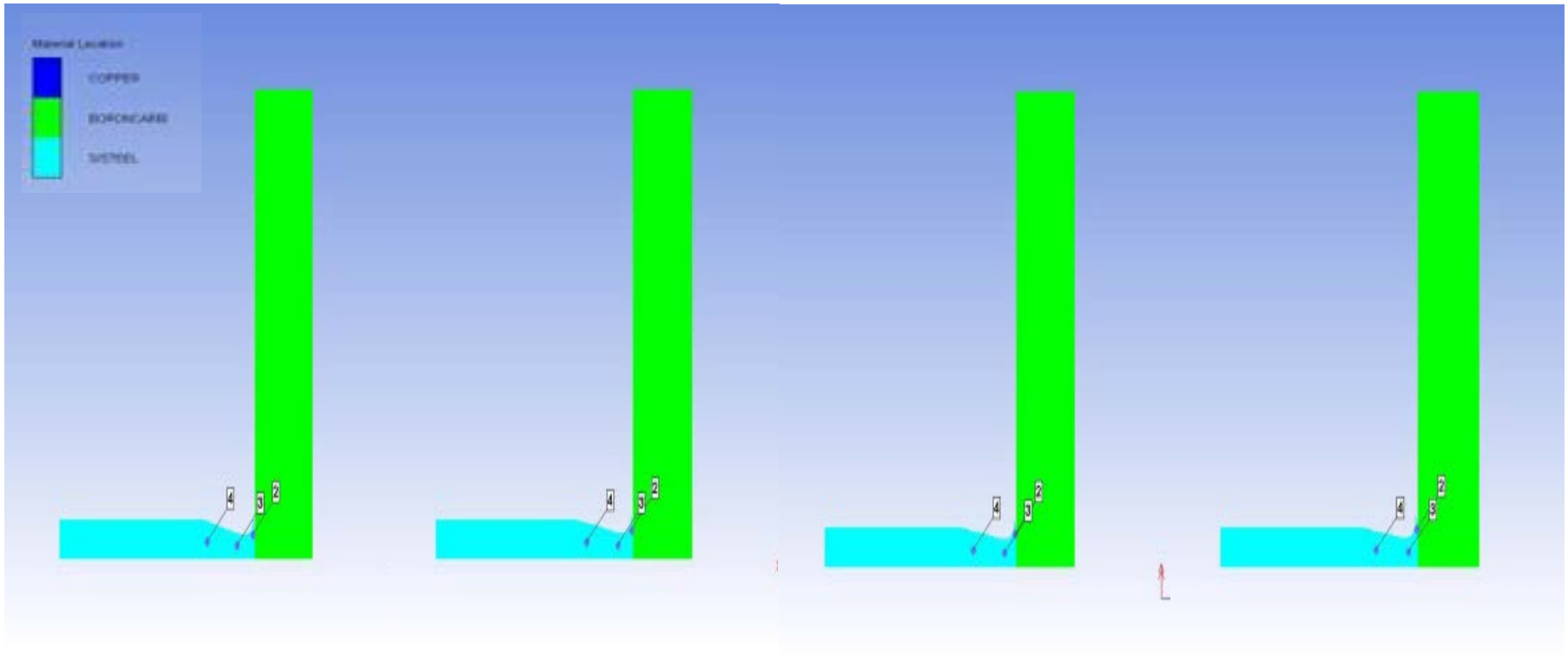

Figure 4.19 – Computational model showing impact of a stationary Steel core by a 50-mm diameter B_4C impactor. Running from ½ μs, 1 μs, 1.5 μs and 2 μs from left to right. 1, 2, 3, 4 denote gauge point positions.

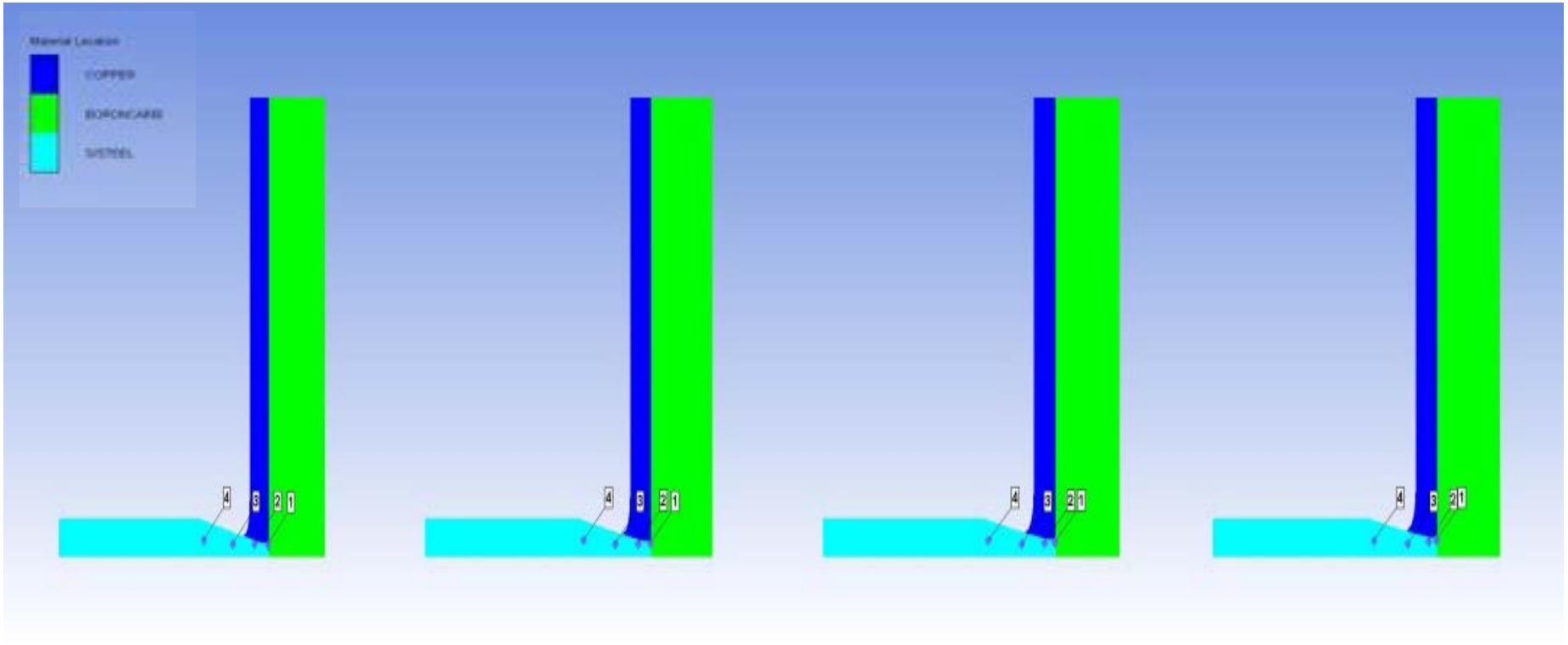

Figure 4.20 – Computational model showing impact of a stationary Steel core by a 50-mm diameter B_4C impactor with the inclusion of a 1 mm Copper plate (jacket). Running from ½ μs, 1 μs, 1.5 μs and 2 μs from left to right. 1, 2, 3, 4 denote gauge point positions.

4.6 Summary and discussion

The overarching aim of the experiments discussed previously has been to try and provide a better understanding of the behaviour of a penetrating bullet with and without a jacket present, and, consequently, the role a bullet jacket has on penetration. As a result of this research, in parallel, insight into potential mechanisms to enhance defeat of an incoming threat has also been gleaned. The ballistic and mass efficiency data (see Section 4.1.1 and 4.1.2) has given insight into the type of material that would be useful when designing an armour solution and has also been useful with regards to identifying trends and mechanisms that can be exploited when choosing materials for these applications. While mass efficient solutions were not directly identified, evidence of an optimum stripper plate thickness has been shown – with tentative indications that removing the jacket is beneficial. In particular, the potential advantages of a stripping plate (e.g. a spaced armour appliqué) were highlighted by increases in ballistic efficiency which appeared to asymptote for all materials considered around a plate thickness of 4-6 mm (figure 4.3 – consistent with the projectile / core calibre).

The DOP data (presented in Section 4.1.3) was the basis for the mass and ballistic efficiency values calculated separately and was the main form of diagnostic employed. A clear difference between the penetrability of modified (tip of the jacket pre-stripped to encourage jacket stripping / expose the core) and unmodified rounds was apparent across all stripping plate materials tested. Harder materials such as Steel were found to be more efficient with regards to both the overall defeat of the round as well as reduction in subsequent (post stripping plate) penetration. This was evident in the reclaimed cores from the Steel stripper plate shots. The image on the left of figure 4.21 shows an intact core taken from a shot which employed a 10-mm thick stripper plate and a fully jacketed round at 907 m/s. Whereas the core shown on the right, which was from the same experimental setup and stripper plate material / thickness, but at a slighter lower velocity of 892 m/s has been broken through spall (see Section 1.1.2). In this case, the difference was purely that the core on the right came from a modified (tip pre-stripped) projectile. Consequently, jacket removal would have been much easier.

Figure 4.21 – An intact core from a full jacketed round at 907 m/s (left) against a fully defeated core from a modified round at 892 m/s (right). In both cases 10 mm Steel stripper plates were employed. Note both the shattered nature of the core on the right, as well as the blunted nose in comparison to that on the left.

It can also be noted that the core from the picture on the right has some damage to the point of the nose compared to the core pictured on the left. The area at the back of both cores is covered in remnants of Aluminium from the target / backing blocks.

Building on the conventional ballistic experiments, use of flash X ray (forward ballistic experiments described in Section 4.1.5) allowed direct interrogation of the stripping process. Use of thinner stripping plates gave an interesting insight into the underlying effects of jacket stripping, showing clear evidence of material (Cu) from the stripping plate being sheared ahead of the penetrating core. Presence of such material appeared to have a small influence of this on subsequent penetration – reducing this a little – however, the effect was minimal. This importance of interaction of the projectile with the stripper plate was highlighted for thicker (6 rather than 2 mm) stripper plate, material. This was again observed to be dynamically flowing with a penetrating core – but instead, appeared to be confining the core (as opposed to extruding ahead to prevent pre-loading). This potential interaction of several different mechanisms has, to the author's knowledge, not been identified elsewhere previously and is potentially useful in terms of optimising a stripping arrangement.

In order to support the ballistic tests, a series of (basic) experiments were conducted on the SHPB with the aim of understanding the influence of the presence of jacket material on stress

transmission. Without the 'jacket' (a Cu spacer) present, the amplitude of induced waves transmitted was observed to be significantly higher than was the case when a Cu spacer (a jacket) was introduced. This backed the theory developed from the 2 mm Al stripper plate tests – that in some cases sheared material acted to cushion impacts, minimising loading and – thereby – reducing the chances of subsequent spall (see Section 4.1.4) and increased penetration. On the latter front, evidence of ringing (albeit elastic rather than shock waves) was significantly more apparent where cu spacers were not present on the SHPB firings – strongly suggesting that pre-loading (or lack thereof when the jacket is present) did indeed lead to the spallation noted in figure 4.21 in recovered cores. Essentially, having the jacket present stops the spalling occurring and therefore the round survives for longer, increasing the penetration. Even though the Steel stripper plates were the only plates to cause total defeat of the round (through shattering or cracking), indications of incipient spall were still present, indicated by damage to the nose and cone of the modified rounds as seen in figure 4.21, right hand picture. This damage was not observed on the fully jacketed rounds where the jacket would not have been removed to the same extent. However, this initial failure process was apparent in the form of the notable difference in penetration between the fully jacketed and modified rounds across all stripper plate materials considered, illustrating the importance of jacket removal in projectile defeat. By using the generic relations shown in equations 4.4 and 4.5 [4] (where the square root of the product of elastic modulus and density is more generally known as the materials acoustic impedance, *Z*), a ratio can be calculated to demonstrate the amount of reflected shock a WC-Co core would see with and without a jacket present.

$$\frac{\sigma_R}{\sigma_I} = \left(\frac{\sqrt{E_B\rho_B} - \sqrt{E_A\rho_A}}{\sqrt{E_B\rho_B} + \sqrt{E_A\rho_A}}\right)$$

Equation 4.4 – Calculation of the ratio of reflected to incident stress at an interface between two materials (A and B).

$$\frac{\sigma_T}{\sigma_I} = 2\left(\frac{\sqrt{E_B\rho_B}}{\sqrt{E_B\rho_B} + \sqrt{E_A\rho_A}}\right)$$

Equation 4.5 – Calculation of the ratio of transmitted to incident stress at an interface between two materials (A and B).

Material	Density (ρ)	Young's modulus (E)	Sound speed (C_L)	Acoustic impedance (Z)
WC-Co [84]	14.74	600.1	6.83	94.05
Aluminium	2.71	70	6.36	13.77
Copper	8.93	130.2	4.76	34.06

Table 4.11 – Values required for equations 4.4 and 4.5.

The approach taken to calculate the stress finally reflected after impact into the WC-Co core is shown schematically in figure 4.22. Essentially, in the non-jacketed case, the incident shock is reflected directly into the WC-Co core. Applying equation 4.4 (and using Young's modulus (E) and density (ρ) values from table 4.11), this results in 74% of the original input stress being reflected back into the core. For the more complex scenario of the jacketed round impacting the Al plate, the calculation followed a two-stage process. First, in line with the upper diagram in figure 4.22, equation 4.4 was used to calculate the reflected stress back into the Cu jacket. Next, as shown in the lower diagram, this reflected stress (labelled σ_{R2}) was taken as the input or initial stress moving into the WC-Co core. At this interface, equation 4.5 was then used to calculate the resultant transmitted stress (σ_{T2}) into the core. This was found to be just 62% of the initial input stress, σ_{I1}, some 16% (12% absolute) less than the stress which resulted in the WC-Co core in the un-jacketed case. Consequently, this clearly shows that the inclusion of a bullet jacket reduces the amount of stress seen in the core – and hence will inevitably enhance the survivability of the round, thereby enhancing the potential of the round to penetrate a target.

Another example to show the benefit of the bullet jacket is the period of time taken for the shock to transfer into the core from the target material and start reflecting. Basically, with the jacket in place the period is increased, therefore increasing the time required for the bullet to penetrate before spall / defeat stops the round. A nominal thickness bullet jacket (0.75 mm), using equation 4.3, will add nearly 1 μs to the period of time needed for the reflected shock waves to transmit into the core. Albeit a small amount, however when the round is travelling nearly 1000 m/s this equates to nearly 1 mm distance, which could be the difference between full penetration of a target material or the defeat of the round.

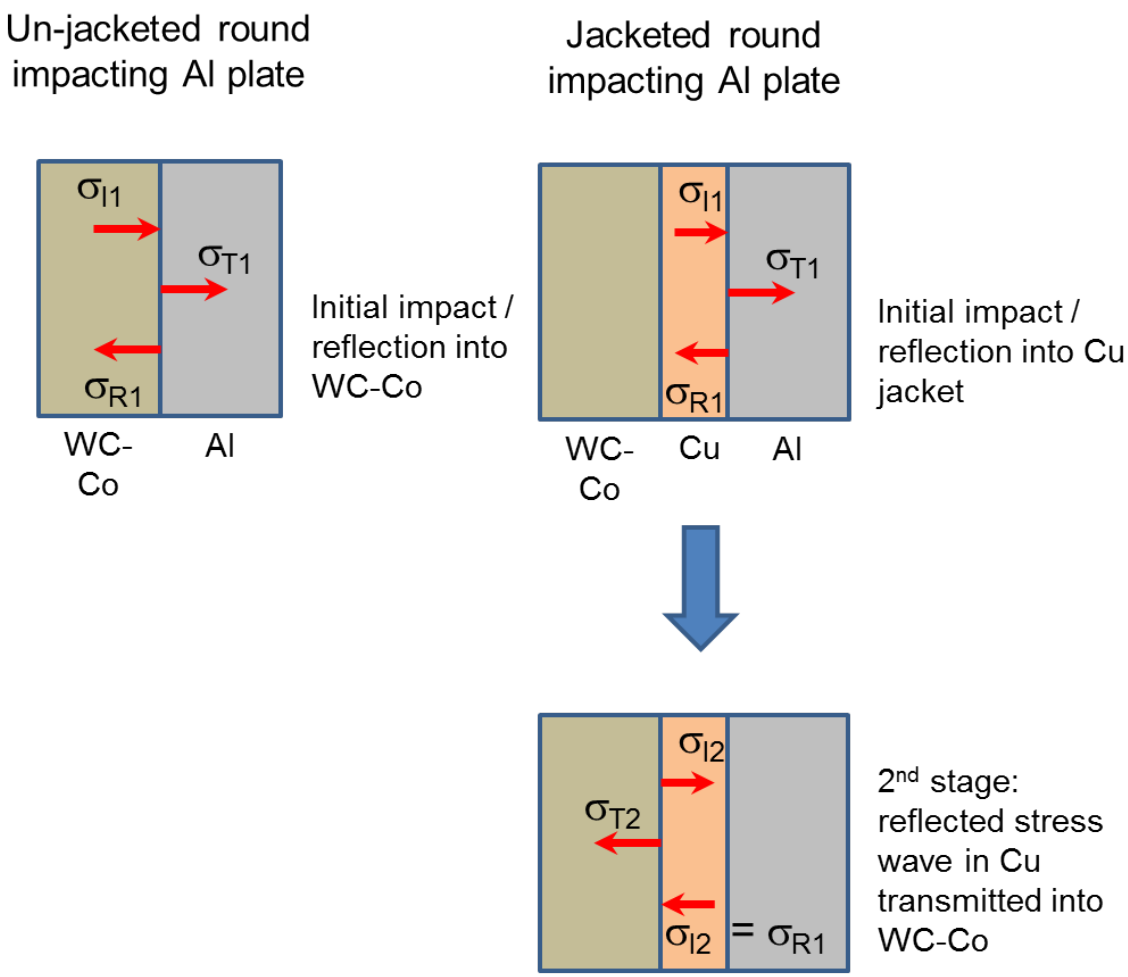

Figure 4.22 – Explanation of how calculations were undertaken using equations 4.4 and 4.5.

Supporting this theory further, the computational modelling (Section 4.7) also showed the importance of, in this case, a 'buffer' plate, or normally a jacket, in front of a penetrating projectile. The modelled figures (4.16, 4.17) show similar images to the experimental data seen in the flash X ray images, figures (4.14, 4.15) showing greater amounts of projectile defeat, in the form of dwell, where a Cu buffer / jacket is not present. The graph featured in figure 4.18 serves yet again to back up the theory of the importance of a bullet jacket by displaying the amplitude of the shock within the nose of the core. This being considerably less than what is seen in a core with no buffer / jacket present (see Section 4.5).

Overall, accept for its very high density, Steel would make an appropriate stripping plate armour material as not only is it able to effectively strip the round, its high impedance also means it is able to pre-load cores, leading to spallation. While Cu was found to be very

effective as a stripping plate material, its high areal density means that it would not be practical. It was also interesting to note that Cu – likely due to its ductility – seems (dependant on stripper plate thickness) to add resistance to penetration both via jacket removal and – at higher plate thicknesses – by core confinement. Interestingly, Al – which in grades such as Al5083 and Al7010 is currently extensively used as an armour material, was also found to be relatively effective at jacket removal. Equally, CFRP – albeit at greater thicknesses – showed some promise. To this end, it seems likely that if a jacket stripping system were to be operationally employed, that it would need to comprise a composite of heavier, harder, backing materials, faced by relatively thick layers of low areal density material such as Al or CFRP.

5.0 Conclusions

This project evolved from the work by Hazell *et al*. [56] and on the 2012 MSc thesis by Philbey [48], with the aim of further investigating the theory that a bullet jacket aids in the subsequent penetration of a target material. Materials were characterised and selected due to their properties to aid a study into a suitable material that would enable stripping of a round and identify trends and mechanisms that can be used to fully investigate the role of the bullet jacket. The core experiments were conducted using 7.62 x 51 mm armour piercing FFV rounds (fully jacketed and modified to reveal the tip of the core) on an indoor small arms experimental range with a 7.62 mm proof barrel and experimental gun to ascertain depth of penetration data as well as ballistic and mass efficiency. Additional work using both forward and reverse ballistic techniques was also undertaken on a single stage and 50 mm smooth bore gas gun to collect data via the means of flash X ray to further evaluate results. A split Hopkinson Pressure Bar was also employed to evaluate the results gained from recovered cores after firings, depth of penetration data and X ray radiographs. Ansys® Autodyn computational simulations were used to further support the results gained elsewhere.

Overall, this project has been successful – with experimental results successfully highlighting the role of the bullet jacket during penetration and indicating that a stripper plate material could potentially successfully be used to dynamically strip a bullets jacket to help enhance armour performance. This study has also given insight into the mechanisms involved in the defeat of a round of this type and (while not the central thrust of this project), what material properties are advantageous in aiding the defeat of the round. From the results of data gathered, a number of conclusions can be drawn, as outlined below.

- It is clear from the investigation detailed in this thesis that the jacket definitely plays a key role in the penetration of a target material. Results showing a notable difference in penetration between the modified and unmodified rounds, with the latter penetrating deeper into a target, have clearly highlighted this. Essentially, jacket removal enhances ballistic efficiency.

- All stripper plate materials used, above 2-mm thickness, were noted to be capable of dynamically removing the jacket of an incoming round, leaving the core vulnerable to further defeat.

- Two different protective mechanisms attributable to the jacket (or, more generally, the presence of surrounding ductile material) were identified:

    - **Cushioning**: Bullets fired with the modified jacket revealing the core against Steel stripper plates showed evidence of complete failure due to shattering (spallation). This pointed to the jacket acting as a shock absorber, e.g. enabling reflected waves from initial penetration to be attenuated by the front of the bullet jacket. Helping to demonstrate this, the use of equations 4.4 and 4.5 have quantified the amount of reflected stress that can be seen in the core with and without the jacket being present, with the stress in the unjacketed case being some 16% higher than in the jacketed round. On this front, basic Split Hopkinson bar experiments indicated that the presence of the jacket acts as an attenuator, confirming the point discussed above. Ansys® Autodyn computational modelling served to further support the findings of the SHPB experiments, showing a penetrating core with no jacket present, witnessed larger amplitudes of shock earlier in the penetration process. The simulations also showed the amplitude of shock in the jacketed core to be attenuated for longer, meaning greater protection for the penetrating round.

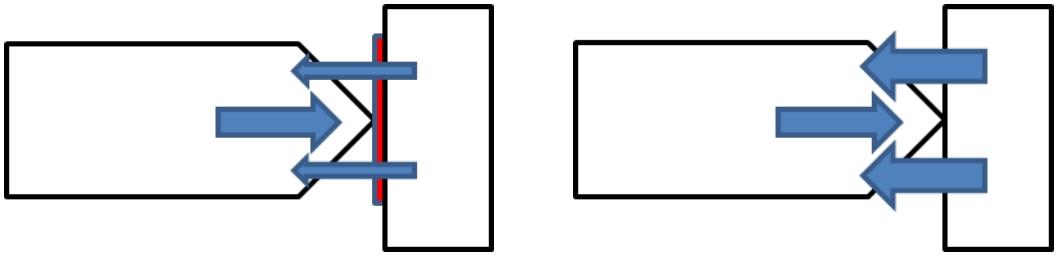

Figure 5.1 – Diagram to show the role of buffer plate / jacket. Left diagram denotes impact with attenuator and smaller return shock waves (represented by blue arrows, the larger the arrow, the greater the pressure), from target material. Right diagram denotes impact with no attenuator present. Larger return shock waves can be seen from the target material.

- **Confinement**: tentative evidence that confinement might play an important role emerged from experiments with thicker Cu stripping plates, where interaction of the jacket and stripper plate with un-modified rounds appeared to lead to continued confinement and reduced penetrative ability compared to modified rounds (where jacket stripping was assured).

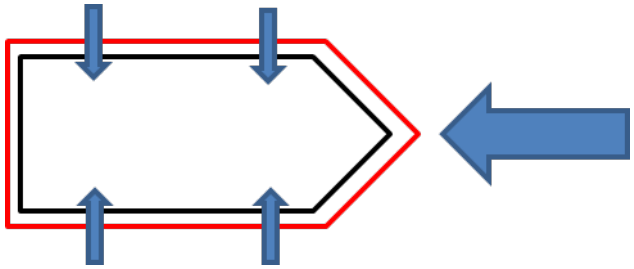

Figure 5.2 – Diagram to show the confining effect of the bullet jacket.

- The defeat of a round of this type (a hardened AP round) is largely due to spallation of the round. This is the mechanism which causes the shattering witnessed on the recovered rounds from the Steel stripper plate experiments (see figure 4.21). Interestingly, the ability of a jacket material to supress such wave (shock) reverberation was highlighted, albeit tangentially, by the SHPB experiments and by the Ansys® Autodyn computational modelling.

- Mass and ballistic efficiency results highlighted the fact that an optimum stripper plate thickness appears to exit. Too thick and mass efficiency will drop off too greatly, whereas too thin and insufficient jacket removal will result. In terms of jacket stripping efficiency, core material properties appear to include hardness, acoustic impedance and Young's modulus and yield strength (see Section 4.1.3.1) In particular, harder (typically high acoustic impedance) materials such as Steel tended to be very efficient at jacket removal / subsequent reduction in DOP / increase in ballistic efficiency (η). This strongly suggested that the stripping plate was pre-loading the round in these cases, leading to fracture and subsequent reduced DOP.

- Even though full defeat of the core was not witnessed on cores recovered from the non-Steel materials (Copper, Aluminium and CFRP), the removal of the jacket was still causing the round to penetrate less into a target. This again suggested that pre-loading was occurring – but not to the extent where full spallation would occur (instead, sub-surface fracture / micro cracking was considered likely). This again, may be the result of a combination of material properties.

5.1 Recommendations for further work

From the results gained in this study, it is believed that further investigations should be considered in the following areas (see below), to continue to enhance the knowledge of the behaviour of a bullet jacket during penetration.

- The use of a different armour piercing round – such as the M43. Whether a softer (compared to WC-Co) cored projectile would gain the same results?

- What effect would using an AP round with a different jacket material, such as the M43 which also has a lead filler, have on experimental results?

- Varying the hardness of the stripper plates employed – tool Steel instead of mild Steel, harder grade of Aluminium instead of AL6082. Would results be similar or better?

- The use of multi layered composite structures, a combination of the materials already studied and other materials (such as UHMWPE) in various lay ups. Can results be improved?

- From previous conclusions it seems that only the tip of the bullet jacket aids in penetration of a target material. If this is indeed the case can an inclusion to the tip of a SLAP (saboted light armour piercing) round or even a long rod penetrator (APFSDS) be advantageous?

- What effect could the standoff distance of the stripper plate have on penetration of a target material and in fact is one even needed?

- Could the convergence of the lines on the ballistic and mass efficiency graphs be altered by using a projectile of a different diameter (calibre)?

6.0 References

[1] Laible R., Barron E., Ballistic materials and penetration mechanics (1980) Chapter 2 – A history of Armour, pages 9 -22.

[2] Picture of ancient armour [Internet]. 2015. Available at www.ancientegyptianfacts.com (Accessed: November 2015).

[3] Picture of medieval armour [Internet]. 2015. Available at www.medieval.stormthecastle.com (Accessed: November 2015).

[4] Hazel P.J. Ceramic Armour (2006). Argos Press, Canberra, Australia.

[5] Appleby-Thomas G. J., Hazell P. J., A study on the strength of an armour grade Aluminium under high strain rate loading (2010), J of App. Phys. 107; Article 123508.

[6] Picture of M113 APC [Internet]. 2015. Available at www.military-today.com (Accessed: November 2015).

[7] Manes A., Serpellini F., Pagani M., Saponara M., Giglio M., Perforation and penetration of Aluminium targets by armour piercing bullets (2014). Int. J. of Imp. Eng 69; 39-54.

[8] Radin J., Goldsmith W., Normal projectile penetration and perforation of layered targets (1988). Int. J. of Imp. Eng 7; 229-259.

[9] Bourne N.K., A 50 mm bore gas gun for dynamic loading of materials and structures (2003). Meas. Sci. Technol 14; 273-278.

[10] Doig A., Military Metallurgy, Maney Publishing (1998), Chapter 8, Page 62-65.

[11] Ogorkiewicz R.M., Technology of tanks, Janes information group (1991), Coulsdon, ISBN 0-7106-0595-1.

[12] Picture of King Tiger tank [Internet]. 2015. Available at www.mark-1-tank.co.uk (Accessed: December 2015).

[13] Kilic N., Bulent E., Ballistic resistance of high hardness armour Steels against 7.62 mm armour piercing ammunition (2013). Mater. and Design 44; 35-48.

[14] Borvic T., Dey S., Clausen A.H., Perforation resistance of five different high strength Steel plates subjected to small arms projectiles (2009). Int. J. of Imp. Eng 36; 948-964.

[15] Florence A.L., Interaction of projectiles and composite armour, part 2 (1969). Stanford research institute, Report number AD 698 543.

[16] Medvedovski E., Ballisitc performance of armour ceramics: Influence of design and structure. Part 1 (2010). Ceramics international 36 ; 2103-2115.

[17] Hazell P.J., Roberson C., Resistance of silicon Carbide to penetration by a Tungsten Carbide cored projectile(2003). Ceramic Transactions 151; 165–174.

[18] Appleby-Thomas G. J., Hazell P. J. and Cleave R., Penetration mechanisms in glass laminate/resin structures (2012). Mater. and Design 34; 541-551.

[19] Talladay T. G. and Templeton D. W., Glass Armor – An Overiew (2014). Int. J. of Appl. Glass Sci. 5(4); 331-333.

[20] Krell A., Klimke J. and Hutzler T., Advanced spinel and sub-μm Al_2O_3 for transparent armour applications (2009). J. of the European Ceram. Soc. 29; 275-281.

[21] Appleby-Thomas G.J., Hazell P.J. and Cleave R., Penetration mechanisms in glass laminate / resin structures (2012). Materials and design 34; 541-551.

[22] Hazell P.J., Edwards M.R., Longstaff H., Ersking J., Penetration of a glass faced transparent elastomeric resin by a lead-antimony-cored bullet (2009). Int J Impact Eng. 36; 147-153.

[23] http://www.boeing.com/commercial/aeromagazine/articles/qtr_4_06/article_04_2.html [Internet]. Accessed September 2016.

[24] Cantwell W.J. and Morton J., Impact perforation of carbon fibre reinforced plastic (1990). Composites Sci & Tech. 38; 119-141.

[25] Hazell P.J., Kister G., Stennett C., Bourque P., Cooper G., Normal and oblique penetration of woven CFRP laminates by a high velocity Steel sphere (2007). Composites Sci & Tech. Part A 39; 866-874.

[26] Wood D. C., Hazell P. J., Appleby-Thomas G. J., Barnes N. R., Shock behaviour of a phenolic resin (2011). Int J. of Mat. Sci. 46; 5991-5999.

[27] Crouch I.G., Appleby-Thomas G.J., Hazell P.J., A study of the penetration behaviour of mild Steel cored ammunition against Boron Carbide ceramic armours (2014). Int J Impact Eng. 80; 203-211.

[28] Hazell P.J., Armour; Materials, Theory and design (2015). CRC Press.

[29] Iremonger M. J., Polyethylene composites for protection against high velocity small arms bullets (1999). 18th International symposium on ballistics.

[30] Held M., 'Explosive reactive armour patent'. European patent number DE2008156, 21 February (1970).

[31] Modern day tank with ERA cassettes [Internet]. 2015. Available at www.survincity.com (Accessed: December 2015).

[32] Held M., Mayseless M., Rotataev E., Explosive reactive armour (1998). 17th International symposium on ballistics. 23-27 March 1998.

[33] Rosenberg Z., Dekel E., A parametric study of the bulging process in passive cassettes with 2-D numerical solutions (1998). Int J of Imp Eng. 24; 297-305.

[34] Swatton D. J. R., Pack D. C., Brown J., Endersby P. C. and Ratcliffe P. R., The effect of obliquity and conductivity on the current distributions within electric armour (2001). 19th International symposium on ballistics. Switzerlan 7-11 May.

[35] Sterzelmeier K., Brommer V., Sinniger L., Active armour protection conception and design of steerable launcher systems fed by modular pulsed power supply units (2001). IEEE Transactions on magnetics 37; 238-241.

[36] SoldierMod.com – Soldier Modernisation, Volume 11, May 2013 [Internet]. Available at http://www.soldiermod.com/volume-11/us-rad.html (Accessed: January 2017).

[37] Goad K.J.W. and Halsey D.H.J., Battlefield weapon systems and technologies, volume 3 - Ammunition (including grenades and mines) (1982). Brassey's publishers ltd.

[38] Courtney-Green P.R., Battlefield weapon systems and technologies, volume 4 – Ammunition for the land battle (1990). Brassey's publishers ltd.

[39] Powel J. G. *et al*. Fragment hazard investigation program: Natural communication detonation of 155 mm projectile (1981). NSWC TR 81-54, Dalgren, Virginia.

[40] Field Manual, Hand grenades and pyrotechnic signals (2000). Headquarters of the U.S army, Washington D.C.

[41] Meyers M. A., Dynamic Behaviour of Materials. 1994. John Wiley and Sons publications.

[42] Appleby-Thomas G. J., Hypervelocity Lecture, Explosive Ordnance Engineering MSc, Cranfield University.

[43] Appleby-Thomas G. J., Introduction to Ammunition and Armour, AS3 Lecture, Cranfield University.

[44] Cooper P. W., Explosives Engineering. 1996. Wiley-VHC inc, publishers.

[45] Picture of EFP formation [Internet]. 2016. Available at www.wikipedia.org (Accessed: January 2016).

[46] Picture of small arms round make up [Internet]. 2016. Available at www.madehow.com (Accessed: January 2016).

[47] Picture of varying small arms rounds [Internet]. 2016. Available at www.quora.com (Accessed: January 2016).

[48] Philbey D. Reverse ballistic study of bullet jackets during the penetration of ceramic armour (2012). Explosive ordnance engineering MSc thesis. Cranfield University, Defence academy of the Uk.

[49] Hazell P. J., Roberson C. J. and Moutinho M., The design of mosaic armour: The influence of tile size on ballistic performance (2008). Mater. and Des. 29; 1497-1503.

[50] Martineau R. L., Prime M. B. and Duffey T., Penetration of HSLA-100 Steel with Tungsten Carbide spheres at striking velocities between 0.8 and 2,5 km/s (2004). Int J Impact Eng. 30; 505-520.

[51] Hazell P. J., Appleby-Thomas G. J., Herlaar K., Painter J., Inelastic deformation and failure of Tungsten Carbide under ballistic loading conditions (2010). Mater Sci Eng. 527; Iss 29-30; 7638-7645.

[52] Herlaar K., Diederen A. M., Appleby-Thomas G. J., Hazell P. J., Ballistic impact experiments of Tungsten Carbide projectiles onto Tungsten Carbide targets (2008). 24th International Symposium on Ballistics, New Orleans, Sept 22-26; 744-751.

[53] GrujisisM., Pandurangan B.,Koudela K., Cheeseman B. A computational analysis of the ballistic performance of light weight hybrid composite armours (2006). App. Surf. Sci. 253; 1010-1016.

[54] Anderson, C. E., An overview of the theory of hydrocodes, Int. Jour. of Imp. Eng. (1987). 5; 33–59.

[55] ANSYS® Autodyn Training manual [Internet], 2009. Available at www.ansys.com/support/training. Accessed : September 2016.

[56] Zhang W., Yue H., Gongshun G., Baojin P. the experimental and numerical studies of laminated glass subject to hypervelocity impact (2005). 4th European conference on space debris. 18th – 20th April 2005. Darmstadt, Germany.

[57] Cronin D., Bui K., Kaufmann C., M^{c}intosh G., Berstad T. Implementation and validation of the Johnson-Holmquist ceramic material model used in LS-Dyna (2003). 4th European LS-Dyna users conference. 22nd-23rd May. Ulm, Germany.

[58] Forrestal M. J., Borvik T., Warren T. L., Perforation of 7075-T651 Aluminium armour plates with 7.62 mm APM2 bullets (2010). Exp Mech. 50(8); 1245-1251.

[59] Borvik T., Forrestal M. J., Warren T. L., Perforation of 5083-H116 Aluminium armour plates with ogive nosed rods and 7.62 mm APM2 bullets (2009). Exp Mech. 50(7); 969-978

[60] Hazell P. J., Appleby-Thomas G. J., More on penetration of ceramic based targets by non-deforming projectiles (2012). Advances in applied ceramics, Vol 111 (3); 171-173.

[61] Hazell P. J., Appleby-Thomas G. J., Philbey D., Tollman W., The effect of gilding jacket material on the penetration mechanics of a 7.62 mm armour piercing projectile (2013). J. of Imp. Eng. 54; 11-18.

[62] Gooch W. A., Burkins M. S., Kingman P., Hauver G., Netherwood P., Benck R., Dynamic X ray imaging of 7.62 mm APM2 projectiles penetrating Boron Carbide (1999). 18th international symposium of ballistics. San Antonio, Texas; 15-19 November 1999. P. 901-908.

[63] Holmquist T. J., Anderson Jr C. E., Behner T., Orphal D. L., The mechanics of dwell and post dwell penetration (2010). Advances in applied ceramics. 109 (8); 467-179.

[64] Lundberg P., Renstrom R., Holmberg L., An experimental investigation of interface defeat at extended interaction time (2001). 19th international symposium on ballistics, Interlaken, Switzerland; 7-11th May 2001. P. 1463-1469.

[65] Holmquist T. J., Anderson Jr C. E., Behner T., Design, analysis and testing of an unconfined ceramic target to induce dwell (2005). 22nd international symposium on ballistics, Vancouver BC, Canada; 14-18th November 2005. P. 860-867.

[66] Shear strength estimation [Internet]. 2016. Available at http://www.portlandbolt.com/technical/faqs/calculating-strength/ (Accessed: April 2016).

[67] Edwards M.R., Mathewson A. The ballistic properties of tool Steel as an improvised armour plate (1997). Int. Jour. Imp. Eng 19; 297-309.

[68] 7.62 mm FFV round information [Internet]. 2016. Available at http://www.inetres.com/gp/military/infantry/rifle/762mm_ammo.html (Accessed: April 2016).

[69] Referenced material hardness values [Internet]. 2016. Available at http://www.matweb.com/ (Accessed: March 2016).

[70] Marsh S.P., LASL Shock hugoniot data, University of California press, 1980.

[71] Millett J.C.F., Bourne N.K., Rosenberg Z. The effect of orientation on the shock response of a carbon fibre – epoxy composite. (2007) Comp Sci and Tech 67; 3253-3260.

[72] Callister Jr. W. D., Materials science and engineering – An introduction, 2003.

[73] Millett J.C.F., Bourne N.K., Rosenberg Z. Observations of the Hugoniot curves for glasses as measured by embedded stress gauges (1998). Jour of App. Phys. 84; 739.

[74] Millett J.C.F., Bourne N.K., Rosenberg Z. Shear stress measurements in Copper, iron, and mild Steel under shock loading conditions (1997). Jour of App. Phys. 81; 2579.

[75] Rosenberg Z. and Yeshurun Y., The relationship between Ballistic efficiency and compressive strength of ceramic tiles (1988). Int J Impact Eng; 7, 357-362.

[76] Anderson, Jr. C. Gooch, W. Numerical simulations of dynamic X-Ray imaging experiments of 7.62mm APM2 projectiles penetrating B4C. (2001) 19th international Symposium of ballistics. Interlaken, Switzerland.

[77] Scandiflash instruction manual – Model 300. Scandiflash AB, Palmbladsgatan 1A, S-754 50 Uppsala, Sweden.

[78] Gray III G. T. Classic Split Hopkinson Pressure Bar testing. (1972) Los Alamos national laboratory.

[79] Carlucci D. E., Jacobson S. S., Ballistics – Theory and design of guns and ammunition (2008), CRC Press, London, UK.

[80] Hameed A., Appleby-Thomas G. J., Wood D.C., Hazell P.J., and Jaansalu K.M. On the Ballistic Response of Comminuted Cermaics. (2014) 18th APS-SCCM and 24th AIRAPT, Seattle, U.S.A.

[81] Sapate S.G., Chakravarthi G.,Rathod A., Singh A. Microstructure and Abrasive wear properties of Chrome Alloy Steel (2012). Int Jour Manu. Mat. Sci. Vol. 02, No. 02.

[82] Hazell P.J.,Appleby-Thomas G.J.,Wielewski E.,Escobedo J.P. The shock and spall response of three industrially important hexagonal close packed metals: magnesium, titanium and zirconium (2014). Phil. Trans. R. Soc. A; 372.

[83] Verma G. Investigation of the importance of the contribution of the bullet jacket during the penetration process: Exploitation of jacket removal for protective purposes (2014). Gun Systems design MSc thesis. Cranfield University, Defence academy of the Uk.

[84] Appleby-Thomas G. J., Hazell P. J., Stennet C., Cooper G., Helaar K. and Diederen A.M. Shock propagation in a cemented Tungsten Carbide (2008). Int J Applied Physics; 105. 064916.

7.0 Appendices

Appendix 1 – Tensile test graphs

Appendix 2 – Depth of penetration (DOP) data

Appendix 3 – Split Hokinson bar traces

Appendix 4 – X ray images (Forward ballistics)

Appendix 5 – Reverse ballistic X ray images

Appendix 6 – Health and Safety and Ethics

Appendix 1 – Tensile test graphs (Copper)

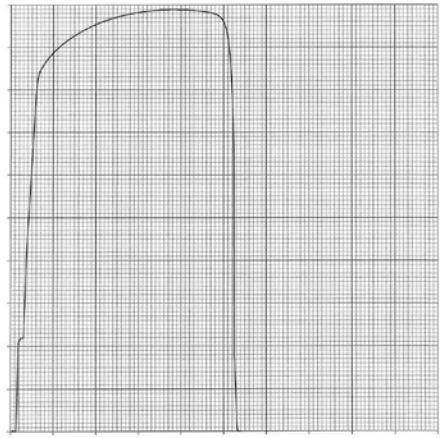

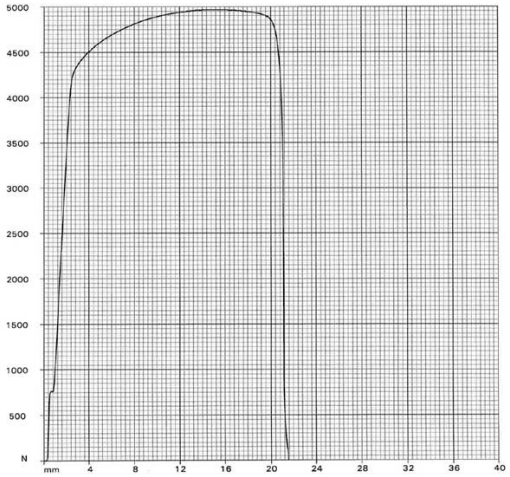

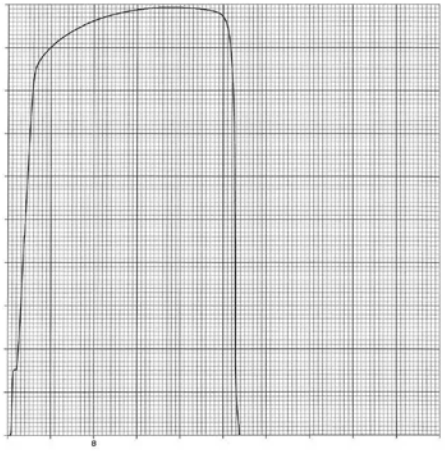

Tensile test graphs (Steel)

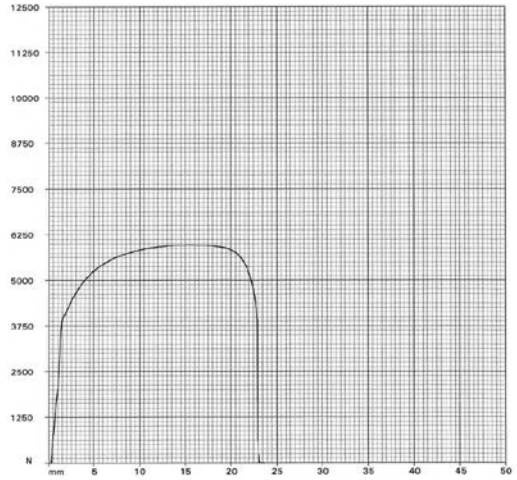

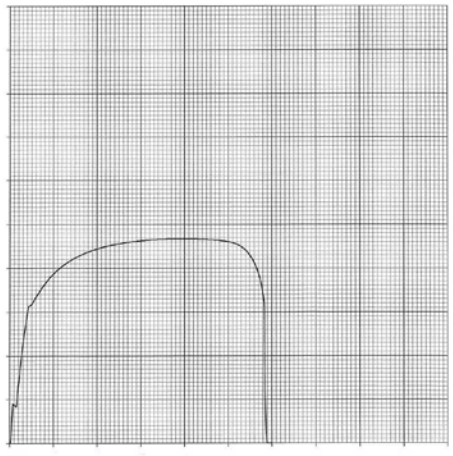

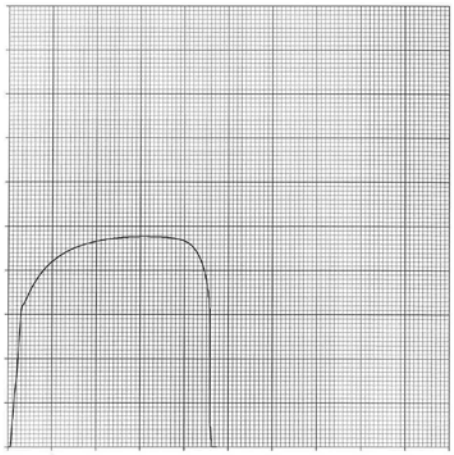

Tensile test graphs (Aluminium)

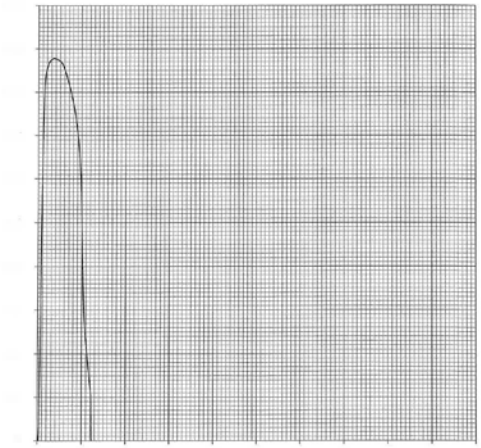

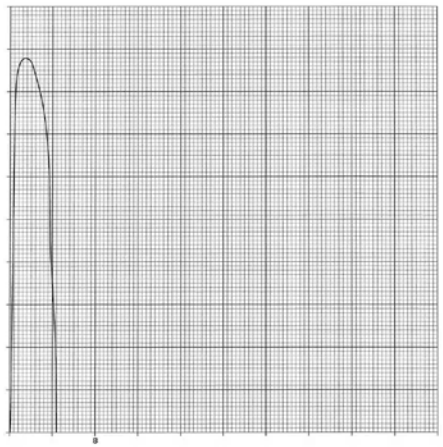

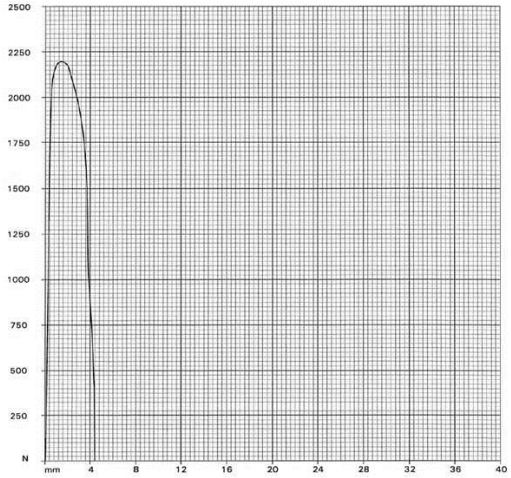

Tensile test graphs (CFRP)

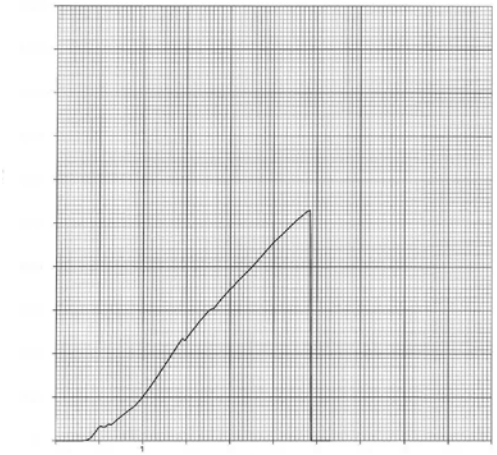

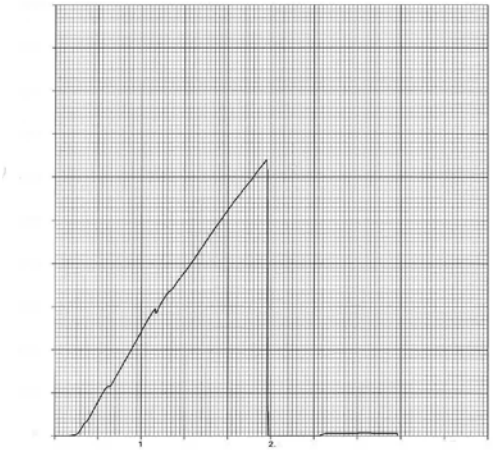

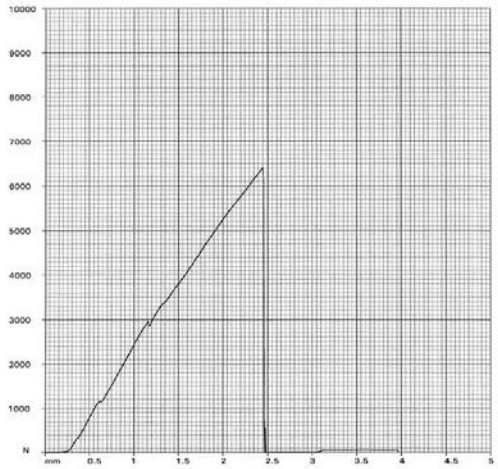

Appendix 2 - DOP data for Copper stripper plate.

Shot Designation	Stripper plate material	Thickness in mm	Core exposed – Y or N	5 mm SiC present – Y or N	Velocity in m/s	DOP in mm into backing	Comments
A	-	0	NO	NO	921	53.39	Baseline
B	-	0	NO	NO	928	55.88	Baseline
C	-	0	YES	NO	900	52.16	Baseline
D	-	0	YES	NO	912	54.86	Baseline
E	-	0	NO	YES	924	7.51	Baseline
F	-	0	NO	YES	915	17.70	Baseline
G	-	0	YES	YES	915	8.83	Baseline
H	-	0	YES	YES	909	9.39	Baseline
I	Copper	2	NO	YES	923	15.38	
J	Copper	2	NO	YES	918	9.93	
K	Copper	2	YES	YES	909	9.34	
L	Copper	2	YES	YES	913	14.07	
M	Copper	2	NO	NO	924	54.22	
N	Copper	2	NO	NO	938	54.10	
O	Copper	2	YES	NO	906		No impact
P	Copper	2	YES	NO	916	53.54	
Q	Copper	4	NO	YES	919	7.28	
R	Copper	4	NO	YES	933	9.43	
S	Copper	4	YES	YES	905	4.28	
T	Copper	4	YES	YES	910	11.39	
U	Copper	4	NO	NO	939	54.11	
V	Copper	4	NO	NO	939	52.64	
W	Copper	4	YES	NO	920	53.13	
X	Copper	4	YES	NO	911	49.54	
Y	Copper	6	NO	YES	934	4.48	
Z	Copper	6	NO	YES	939	4.14	

DOP data for Copper stripper plate – continued.

A1	Copper	6	YES	YES	921	3.08	
B1	Copper	6	YES	YES	935	7.45	
C1	Copper	6	NO	NO	943		No Impact
D1	Copper	6	NO	NO	940	53.9	
E1	Copper	6	YES	NO	915	48.82	
F1	Copper	6	YES	NO	909	48.03	
G1	Copper	10	NO	YES	934	1.91	
H1	Copper	10	NO	YES	908	2.91	
I1	Copper	10	YES	YES	910	3.91	
J1	Copper	10	YES	YES	920	4.91	
K1	Copper	10	NO	NO	939	45.02	
L1	Copper	10	NO	NO	944	47.99	
M1	Copper	10	YES	NO	914	41.21	
N1	Copper	10	YES	NO	911	39.3	
O1	Copper	10	NO	YES	920	1.16	
P1	Copper	10	NO	YES	920	1.16	
Q1	Copper	10	NO	NO	939	38.3	
R1	Copper	10	YES	NO	903	47.44	

DOP data for Aluminium stripper plate.

Shot Designation	Stripper plate material	Thickness in mm	Core exposed – Y or N	5 mm SiC present – Y or N	Velocity in m/s	DOP in mm into backing	Comments
A	Aluminium	2	NO	NO	940	58.71	
A1	Aluminium	2	NO	NO	912	54.17	
B	Aluminium	2	NO	NO	941	59.45	
C	Aluminium	2	YES	NO	891	52.20	
C1	Aluminium	2	YES	NO	938	56.46	
D	Aluminium	2	YES	NO	897	52.14	
E	Aluminium	4	NO	NO	939	54.47	
F	Aluminium	4	NO	NO	933	51.8	
G	Aluminium	4	YES	NO	900	53.39	
H	Aluminium	4	YES	NO	901	51.37	
I	Aluminium	6	NO	NO	928	51.44	
J	Aluminium	6	NO	NO	936	52.94	
K	Aluminium	6	YES	NO	898	50.64	
L	Aluminium	6	YES	NO	903	50.45	
M	Aluminium	10	NO	NO	937	49.74	
N	Aluminium	10	NO	NO	935	50.02	
O	Aluminium	10	YES	NO	909	48.12	
P	Aluminium	10	YES	NO	895	47.60	

DOP data for Steel stripper plate.

Shot Designation	Stripper plate material	Thickness in mm	Core exposed – Y or N	5 mm SiC present – Y or N	Velocity in m/s	DOP in mm into backing	Comments
A	Steel	2	NO	NO	939	58.3	
B	Steel	2	NO	NO	935	56.35	
C	Steel	2	YES	NO	891	51.59	
D	Steel	2	YES	NO	900	52.18	
E	Steel	4	NO	NO	941	54.14	
F	Steel	4	NO	NO	939	54.04	
G	Steel	4	YES	NO	899	48.01	
H	Steel	4	YES	NO	898	49.61	
I	Steel	6	NO	NO	937	50.83	
J	Steel	6	NO	NO	937	50.65	
K	Steel	6	YES	NO	891	46.54	
L	Steel	6	YES	NO	907	38.03	
M	Steel	10	NO	NO	936	41.25	
N	Steel	10	NO	NO	930	41.67	
O	Steel	10	YES	NO	911	41.53	
P	Steel	10	YES	NO	903	39.96	

DOP data for CFRP stripper plate.

Shot Designation	Stripper plate material	Thickness in mm	Core exposed – Y or N	5 mm SiC present – Y or N	Velocity in m/s	DOP in mm into backing	Comments
A	CFRP	2	NO	NO	933	55.72	
B	CFRP	2	NO	NO	939	55.31	
C	CFRP	2	YES	NO	897	51.87	
D	CFRP	2	YES	NO	890	52.64	
E	CFRP	4	NO	NO	938	57.94	
F	CFRP	4	NO	NO	941	57.49	
G	CFRP	4	YES	NO	912	53.31	
H	CFRP	4	YES	NO	905	53.49	
I	CFRP	6	NO	NO	931	55.61	
J	CFRP	6	NO	NO	939	54.64	
K	CFRP	6	YES	NO	911	53.10	
L	CFRP	6	YES	NO	910	51.66	
M	CFRP	10	NO	NO	939	53.23	
N	CFRP	10	NO	NO	938	51.71	
O	CFRP	10	YES	NO	904	49.72	
P	CFRP	10	YES	NO	913	49.90	

Appendix 3 – Split Hopkinson Pressure Bar traces.

Experiment number 160226A

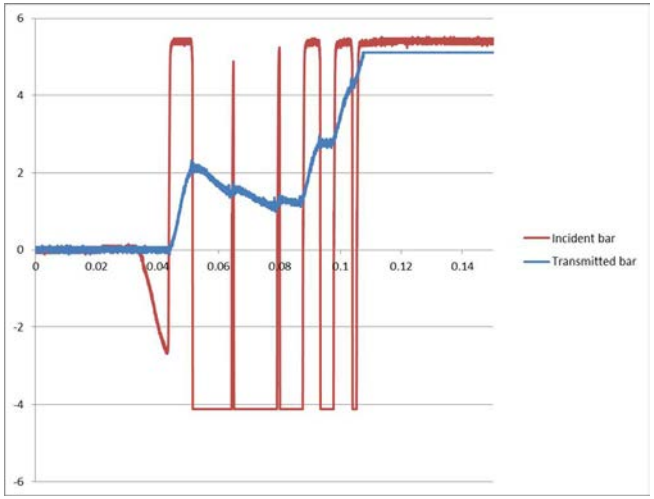

Experiment number 160226B

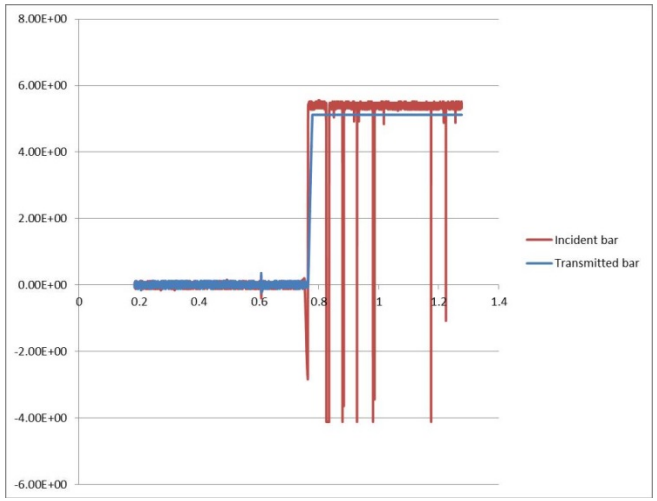

Experiment number 160226C

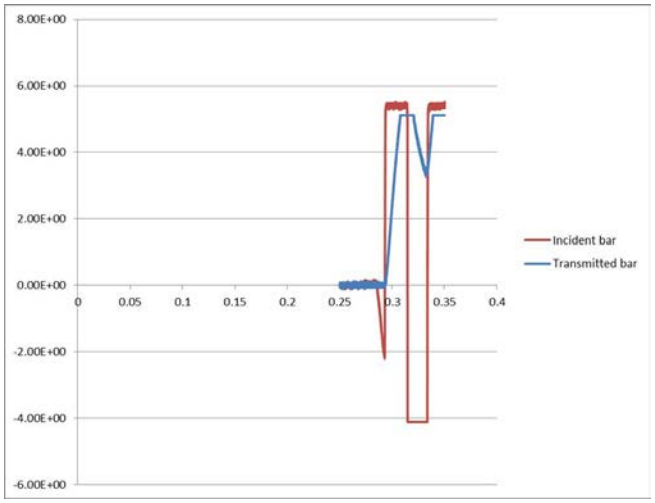

Experiment number 160226D

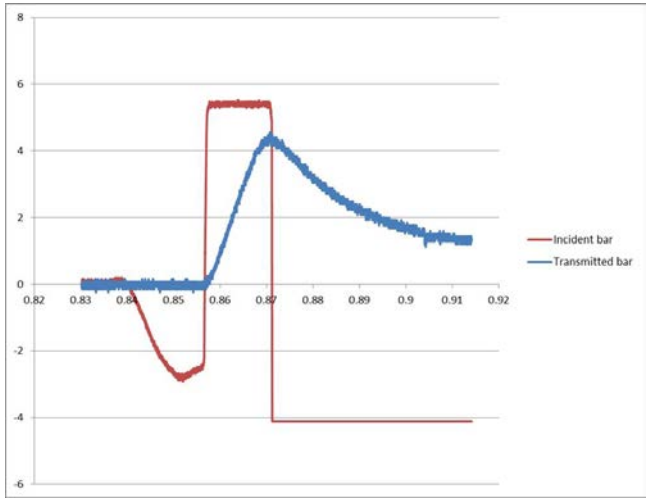

Experiment number 160226E

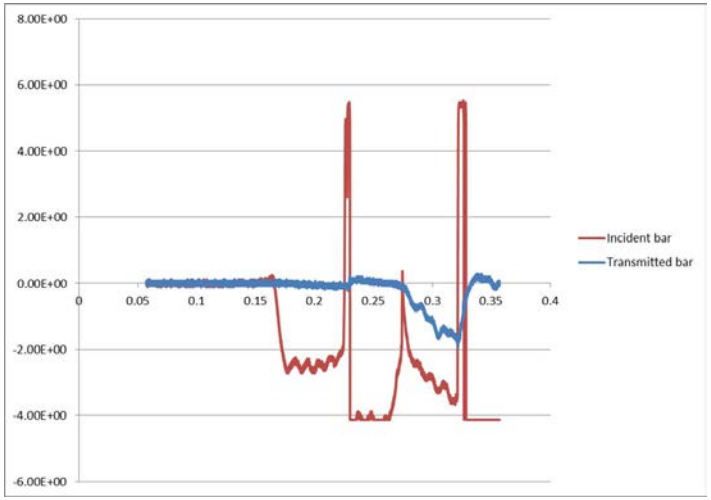

Experiment number 160226F

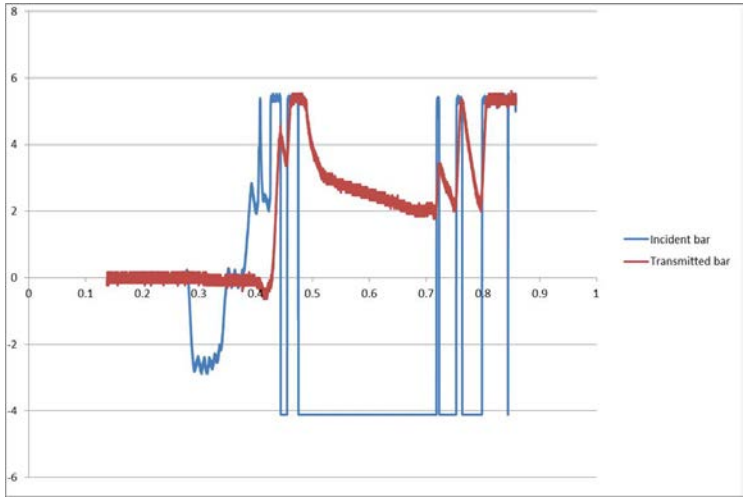

Experiment number 160226G

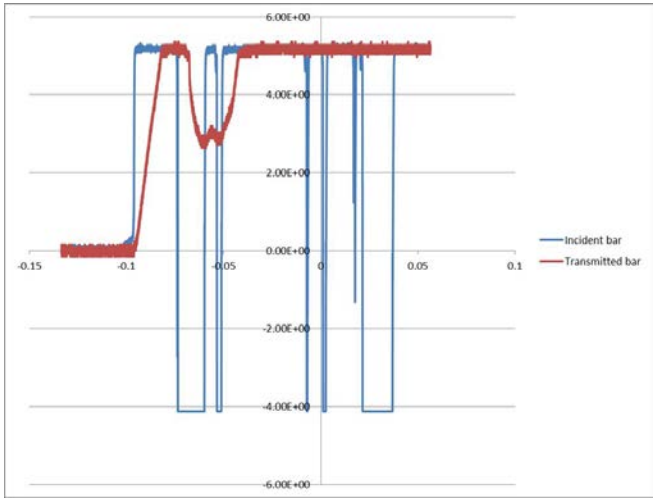

Appendix 4 – Forward ballistic X ray images.

Experiment number 151105A

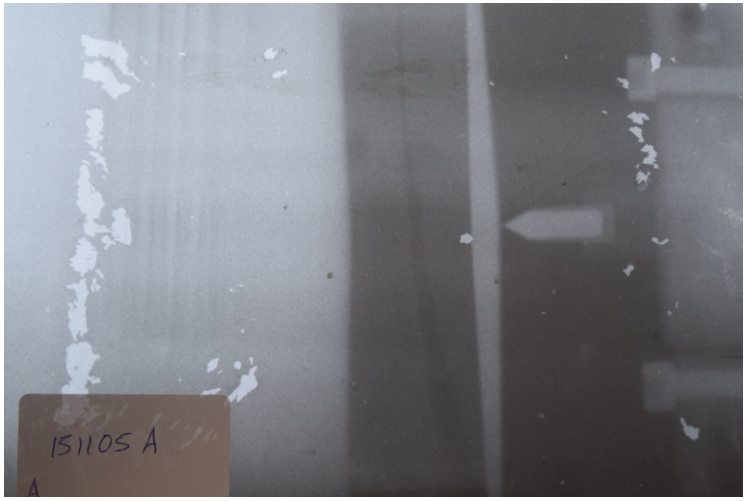

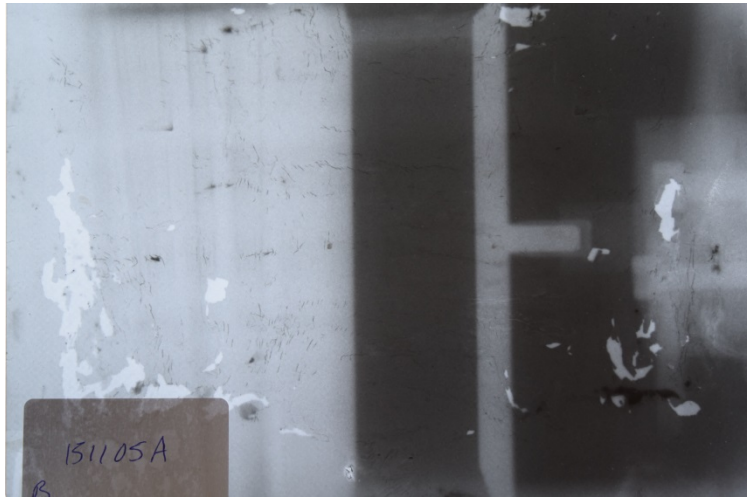

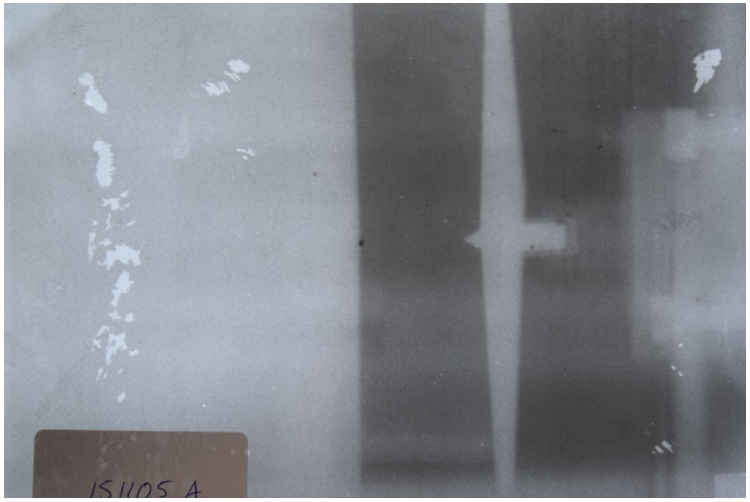

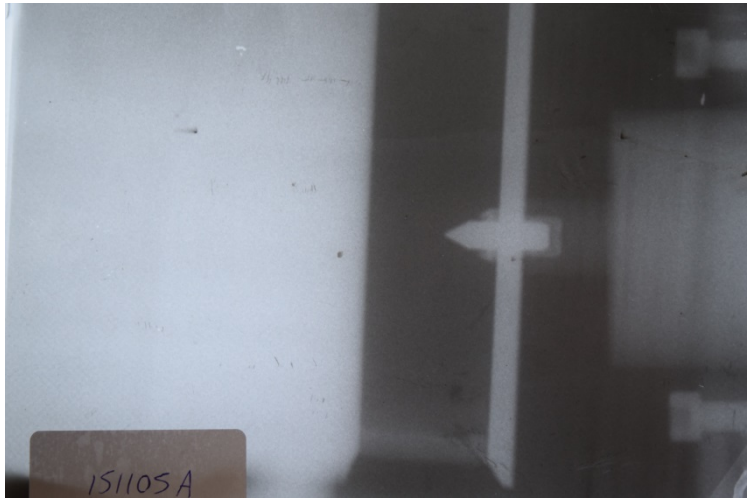

Experiment number 151105B

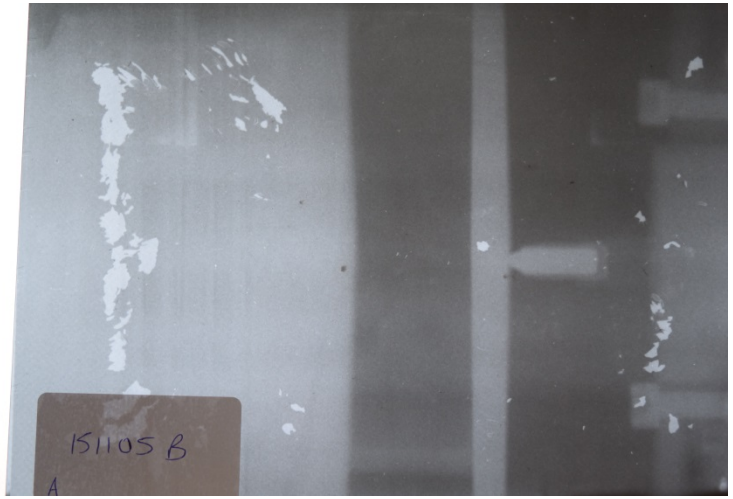

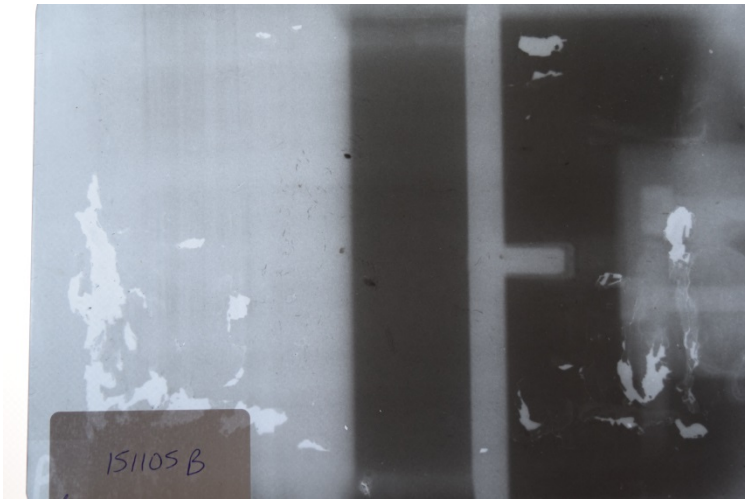

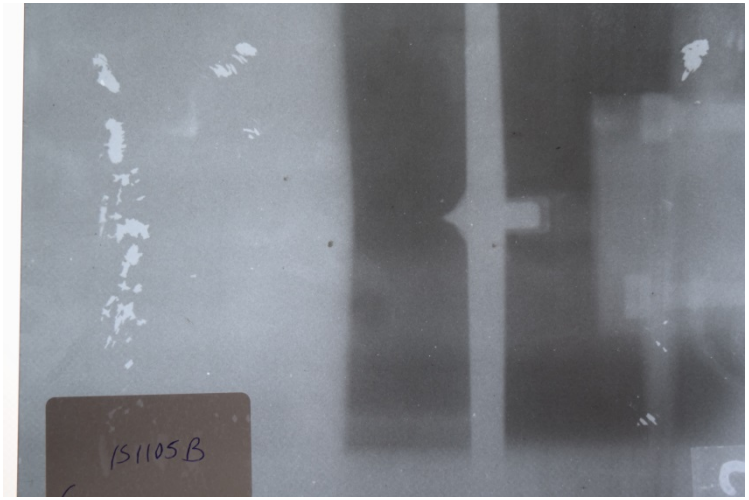

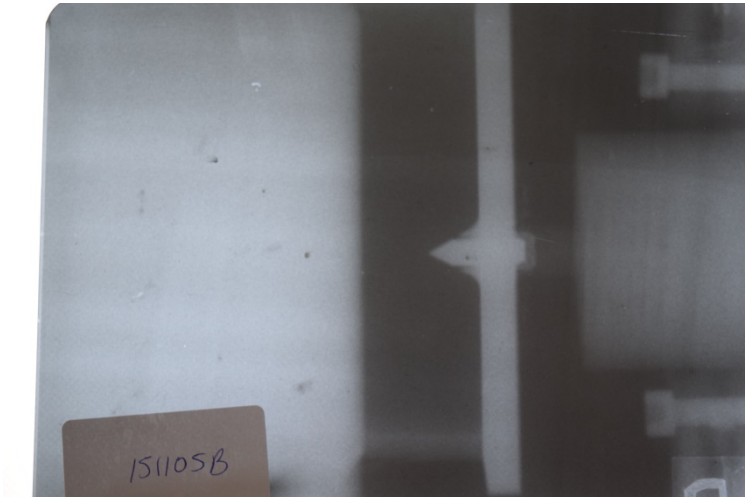

Experiment number 151105C

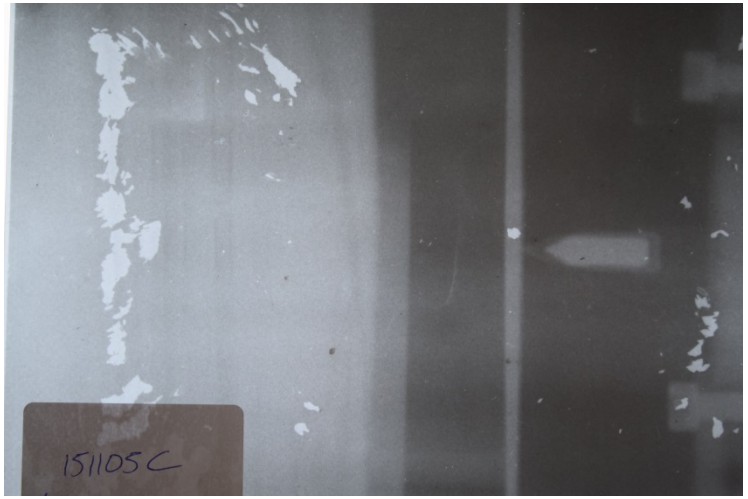

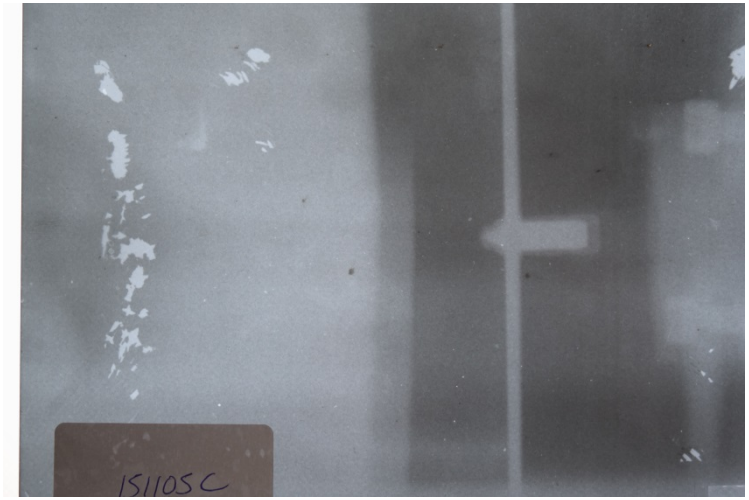

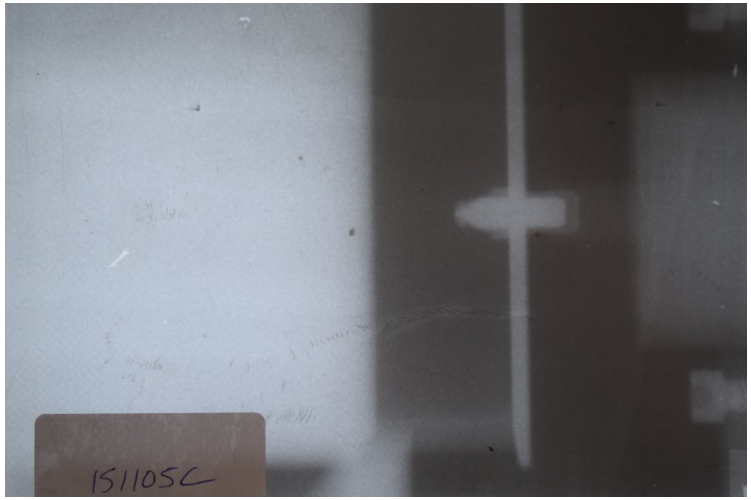

Experiment number 151105D

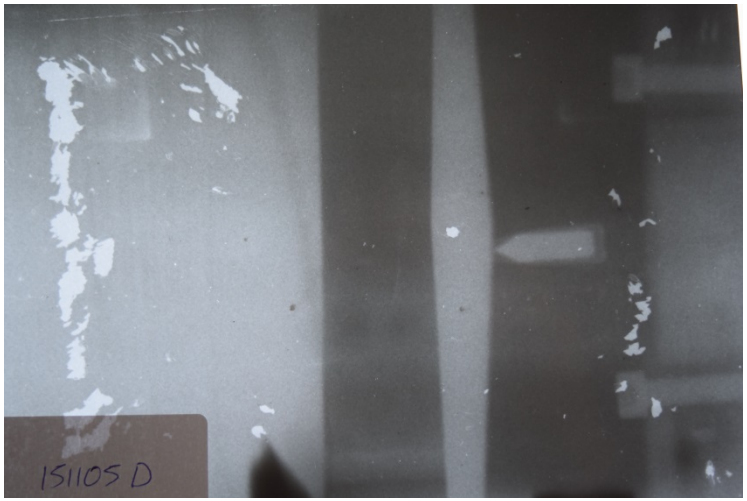

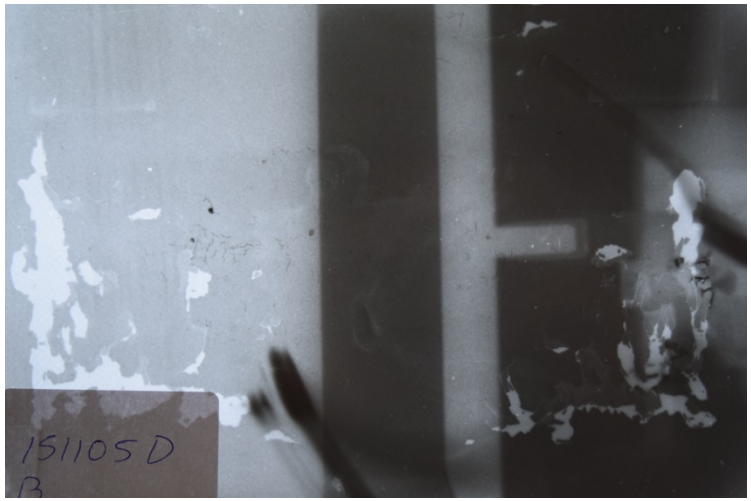

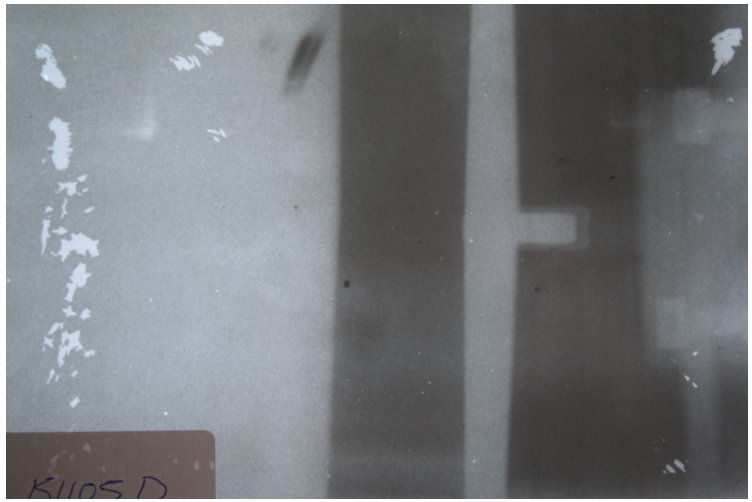

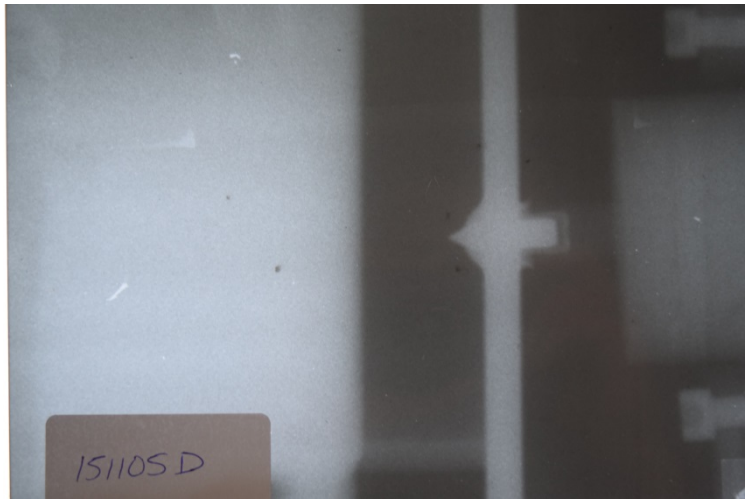

Appendix 5 – Reverse ballistic X ray images.

Experiment number 151103A

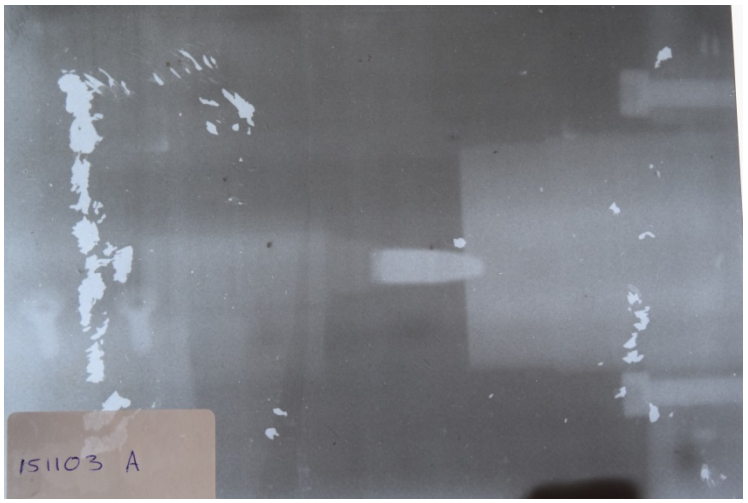

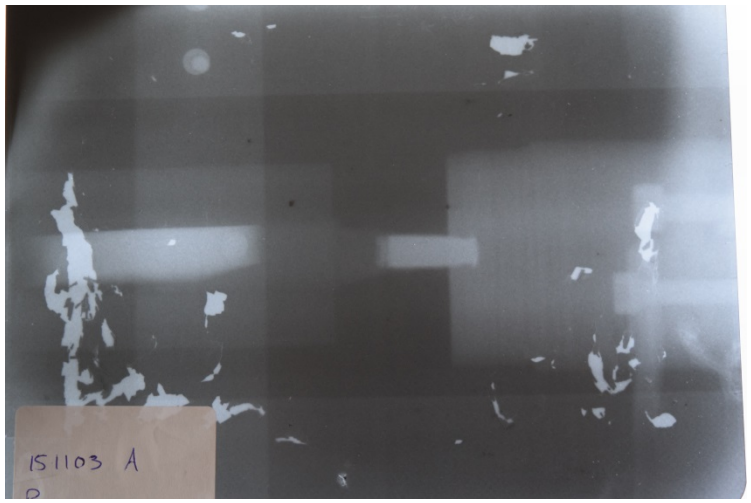

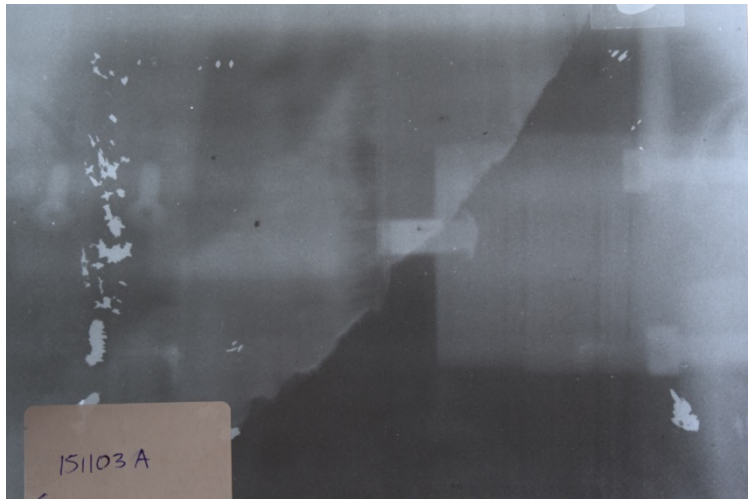

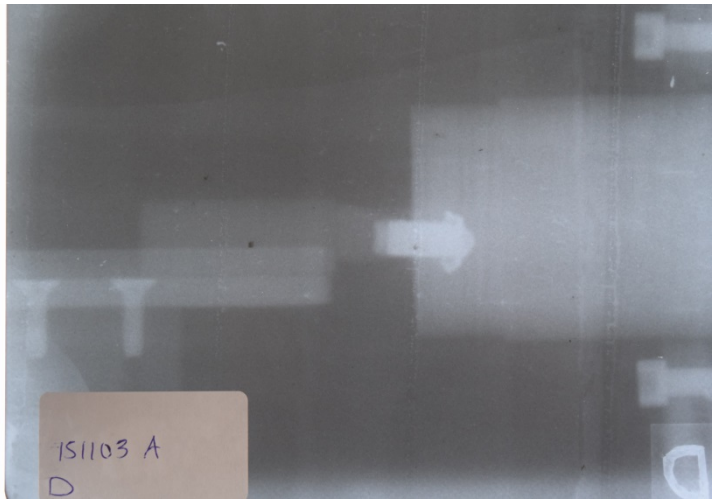

Experiment number 151103B

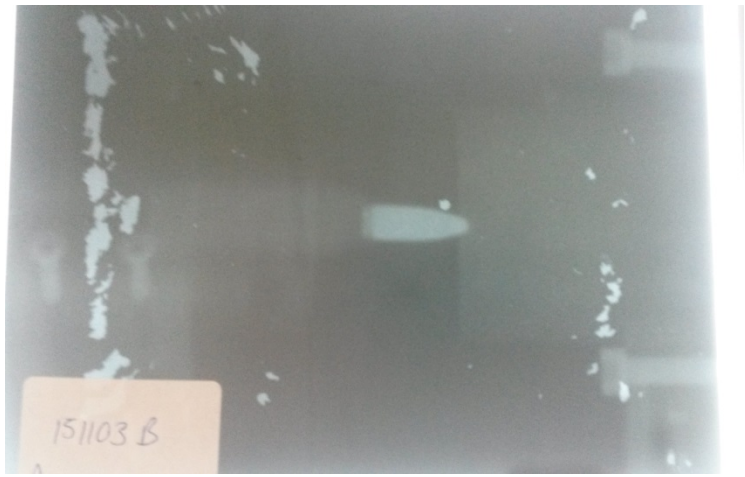

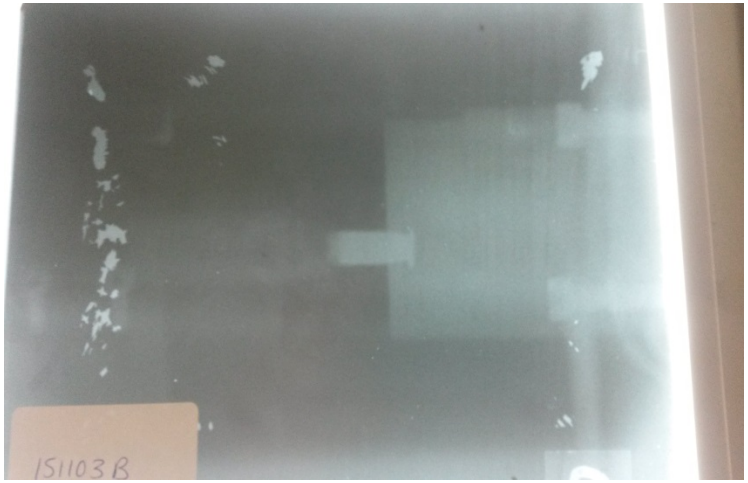

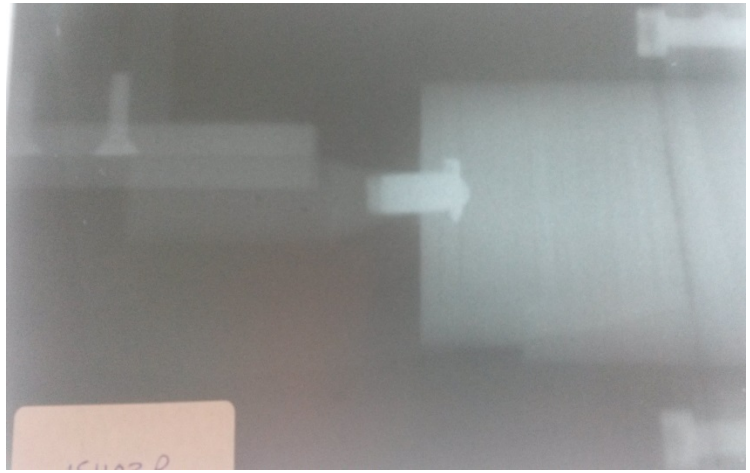

Experiment number 151104A

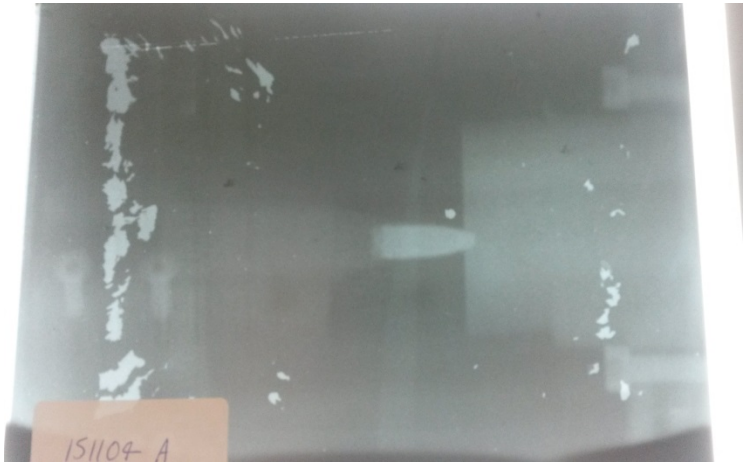

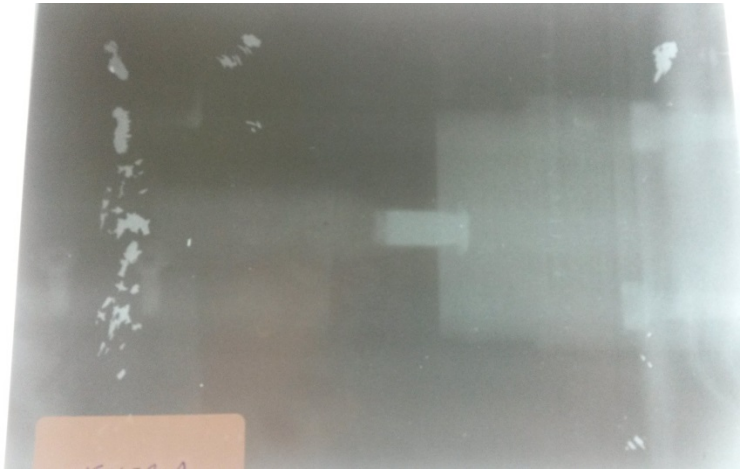

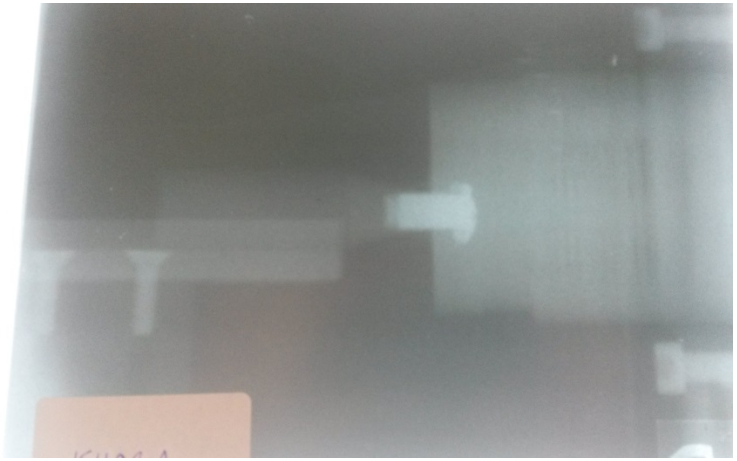

Experiment number 150515A

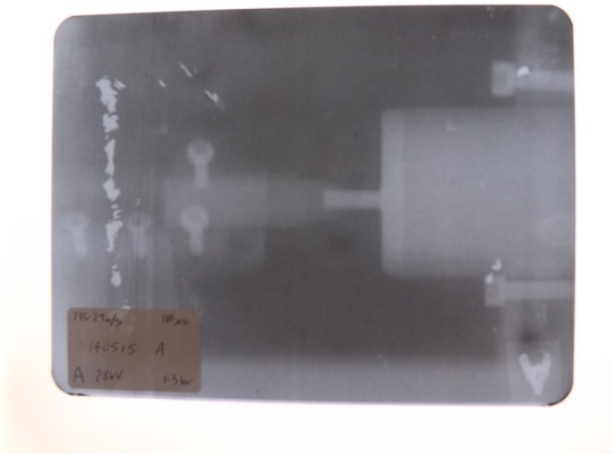

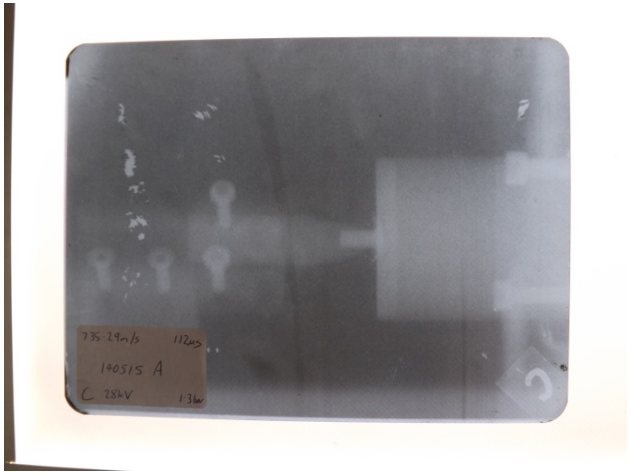

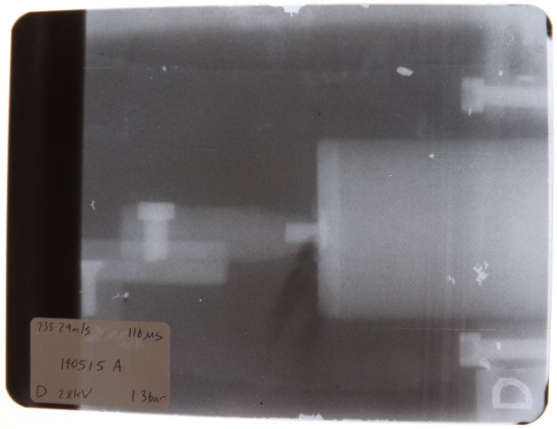

Experiment number 150515B

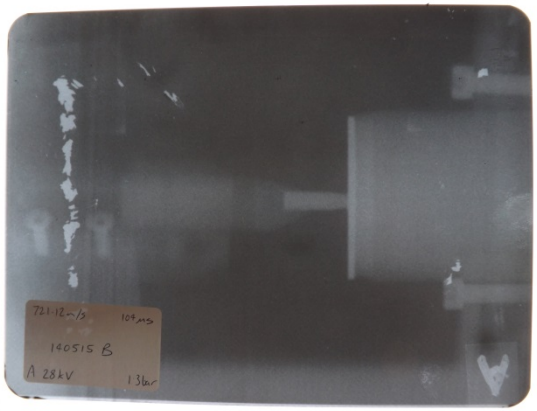

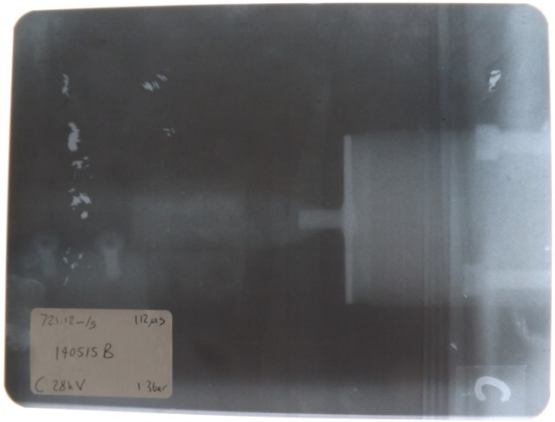

Appendix 6 – Health and Safety and ethics.

All practical work to produce this thesis was co-ordinated within the health and safety policies and guidelines of Cranfield University. Below can be seen the 'in date' operating procedures and risk assessments needed to successfully conduct the experiments for this MSc. and a risk assessment for the project itself.

Risk assessments and Safe operating procedures

This MSc project consists of conducting ballistic firings at targets using existing equipment and facilities. These facilities are covered by their own operating procedures and risk assessments.

Below is a list of standard risk assessments and safe operating procedures that are in place within Building 18 (the dynamic response group) and on the small arms experimental range (SAER – Impact and armour group). These cover the use of the equipment involved in this MSc and the safe use thereof. All SOPs and RAs have been read and fully understood before commencing work on that process / equipment.

RA-12-1014-DW-Feb16 and SOP-12-1014-DW-Feb16 →The Set up of the Blue gun in B18

RA-12-1015-DW-Feb16 and SOP-12-1015-DW-Feb16 →The firing and cleaning of the Blue gun

RA-12-1023-AR-Feb16 →General lab working in B18

RA-12-1054-AR-Jan15 and SOP-12-1054-AR-Jan15 →Operation of the vertical bandsaw in B18

RA-12-1056-AR-Jan15 and SOP-12-1056-AR-Jan15 →Operation of the hydraulic press in B18

RA-12-1003-AR-July15 →Safe use of lifting equipment in B18

RA-12-1066-AR-July15 →Safe use of the overhead gantries in B18

RA-12-1012-AR-Dec15 and SOP-12-1012-AR-Dec15 →Using the 30mm gun in B18

RA-12-1010-AR-Nov15 and SOP-12-1010-AR-Nov15 →The safe use of the flash X ray system in B18

RA-10-1002-IH-July15 →General RA for the Small arms range (SAER)

RA-10-1009-MT-Feb15 →Conducting ballistic firings on the SAER

Risk Assessment Form
CU-HAS-FORM-3.01(A) 2.0

Cranfield UNIVERSITY

Risk Assessment Number:[1]	RA-12-0001-AR-Oct14	Task/Activity assessed:[2]	RA for MSc by research project for A Roberts – The dynamic removal of a bullets jacket		
Name/job role of people consulted during assessment:[3]	Dr D Wood	Date of Assessment:	October 2014	Review Date:[4]	October 2016

Acknowledgements, Sign off and Authorisation

	Acknowledgement	Name	Signature	Date
Risk Assessor:[5]	By signing this risk assessment I acknowledge my responsibility as the Risk Assessor for conducting this risk assessment in accordance with CU-HAS-PROC-3.01, Risk Assessment Procedure	Mr Andrew Roberts		05-01 2016
Checked by:[6] (where required)	By signing this risk assessment acknowledge my responsibility as the checker for this risk assessment in accordance with CU-HAS-PROC-3.01, Risk Assessment Procedure.	Dr David Wood		5/1/16
Authorising Person:[7]	By signing the risk assessment I acknowledge my responsibility as the department management for reviewing and approving this risk assessment and communicating controls and any additional controls to staff/students (as appropriate)	Dr Gareth Appleby-Thomas		7/1/16

	Possible hazards effecting project	What could happen as a result of these hazards?	Controls or solutions to hazards	Existing Risk Rating (Consequence x Likelihood = Total) C[12]	L[13]	TOTAL[14]
1	Long term sickness	Unable to do work for the project, unable to finish in specified time.	Suspend registration or get an extension to project hand in deadline. Seek help of supervisor and support staff in Doctrine centre.	4	3	12
2	Long term sickness of supervisor	Ability to carry on working but with no guidance or structure. Could delay hand in date, extension would have to be sought	Seek another supervisor in the field or approach support staff.	3	3	9
3	Family problems or problems at home	Ability to continue but at a diminished rate	Seek advice of supervisor or support staff	2	3	6
4	Problems with equipment within Building 18 – gas gun out of use, equipment being tested, etc.	Ability to continue but at a diminished rate for the period of equipment inactivity	Use alternative equipment until the item needed is repaired. Plan to start writing up during period of inactivity or equipment service	2	2	4

5	Problems with equipment on the small arms range or equipment being tested, etc.	Ability to continue but at a diminished rate for the period of equipment inactivity	Use alternative equipment until the item needed is repaired. Plan to start writing up during period of inactivity or equipment service	2	2	4
6	Inability to study during work time due to contract and other work commitments	Studying at a dimished Rate. Project could be delayed and an extension may be sought.	Agree with line manager and supervisor a suitable time to study during the working week (1 day a week). Inform customers of study time and arrange contracts accordingly.	2	2	4

The matrix used below is a guide to the risk rating given to the successful finish of this MSc project on time with minimal hassle.

Risk Matrix	Insignificant (1)	Minor (2)	Medium (3)	Major (4)	Catastrophic (5)
Almost Certain (5)					
Likely (4)					
Possible (3)					
Unlikely (2)					
Very Unlikely (1)					

Ethical Approval

Dear Andrew

Reference: CURES/1010/2016
Title: Dynamic bullet jacket removal

Your proposed research activity has been reviewed by CURES and you can now proceed with the research activities you have sought approval for.

Please remember that CURES occasionally conducts audits of projects. We may therefore contact you during or following execution of your fieldwork. Guidance on good practice is available on the research ethics intranet pages.

If you have any queries, please contact cures-support@cranfield.ac.uk

We wish you every success with your project.

Regards

CURES Team

May we remind you of the importance of addressing health and safety issues in your research. Templates and further guidance are available here.